UNIVERSITY OF OKLAHOMA

GRADUATE COLLEGE

A REGIONAL MODEL TO TEST THE CONCEPT OF GLOBAL EASTWARD MANTLE FLOW USING FINITE ELEMENTS

A DISSERTATION

SUBMITTED TO THE GRADUATE FACULTY

in partial fulfillment of the requirements of the

Degree of

DOCTOR OF PHILOSOPHY

By

PAUL MCCOLGAN
Norman, Oklahoma
2009

A REGIONAL MODEL TO TEST THE CONCEPT OF
GLOBAL EASTWARD MANTLE FLOW
USING FINITE ELEMENTS

A DISSERTATION APPROVED FOR THE
CONOCOPHILLIPS SCHOOL OF GEOLOGY AND GEOPHYSICS

Barry L. Weaver, Committee Chair

Richard D. Elmore

Dean S. Oliver

M. Charles Gilbert

Raymond L. Brown

DEDICATION

To my wife Nora

No words could possibly express my gratitude to your endless patience though this journey that took countless hours from our marriage other than:

“We both earned this”

With all my love

Paul

ACKNOWLEDGEMENTS

I would very much like to acknowledge the guidance of the doctoral committee for their willingness to participate and contribute to this dissertation through numerous comments and editorial suggestions to this paper such that I hope it will be both interesting to those that read it as well as make a significant contribution to the theory of plate tectonics and the drive mechanism behind it.

I would especially like to thank Dr. Barry Weaver for accepting the position of committee chairman on such short notice. In addition, while I consider myself to have very good technical skills, I must admit to having only fair writing skills. Dr. Weaver's extraordinary patience in both reading and editing this document is greatly appreciated! I also very much appreciate his moral support to keep me moving forward during times when I was ready to throw in the towel and just walk away from it all.

I would also like to thank Dr. Peter Bird for supplying the finite element program SHELLS used in this study, along with all of the supporting software and several input data volumes. In addition I would like to thank him for supplying numerous comments and ideas to improve the overall scientific merit of the study based on his expertise in both the subject matter and software utilization.

I would like to thank Dr. Elmore for addressing several of the complications that came up during the process of writing this dissertation. As a department head it is often easier to push difficult issues to the side than to deal with them directly.

Dr. Elmore has demonstrated to me that he is both a fair and just individual by making sure that both the needs of the student and the requirements of academic merit are met.

I would like to thank Donna Mullins for the countless number of times she assisted me in traversing the gauntlet of policies and procedures required by both the school of geology and geophysics and graduate college during the past eight years. I also very much appreciated all of her support during these years. As a part-time student, it is extraordinarily difficult to keep up with everything that is going on or needs to be done in order to graduate. However, I am just one student among many that Donna has looked after, and for that it has been an honor to know her.

I would like to thank Dr. Betty Britt for her council to Nora and I during some of the most trying times of our lives. We have learned much about ourselves and each other thanks to you.

I also have to recognize my faithful little companion Topaz (our cat) for the countless hours she spent by my side during these past eight years as I ran model upon model and typed the dissertation well into the morning hours. You know it's time to call it a night when your cat leaves you at 3 AM for a darker quieter room in the house.

TABLE OF CONTENTS **PAGE**

LIST OF TABLES

LIST OF FIGURES

LIST OF APPENDICES

ABSTRACT OF THE DISSERTATION

Computer modeling of tectonics involving the entire Caribbean and North Andes plates, as well as most of the Cocos plate and a portion of the Nazca plate, have been used to support the concept of a global eastward mantle flow beneath the region. The eastward flow is interpreted to be the results of a lithospheric rotation relative to the asthenosphere. The tectonic modeling has been used in combination with observations for the region to support a best fitting model that includes the global eastward flow.

The best fitting model to surface observations used parameters consisting of a due east asthenosphere flow at 100 mm/yr, a base of lithosphere temperature of 1380 K, and a fault friction coefficient of 0.12. The results from the best model demonstrate that a simple uniform eastward flow in the asthenosphere can account for the varying directions of movement and velocities on the surface for the tectonic plates in this region. The model was able to reproduce the simultaneous movements for the Caribbean plate, at nearly due east, the North Andes plate to the northeast, the Nazca plate due east, and the Cocos plate to the northeast. In addition, the best model was able to reproduce the large velocity contrasts between the Cocos plate at 70 plus mm/yr relative to the Caribbean plate at 20 mm/yr and the velocity contrast between the Nazca plate at 50 plus mm/yr and the North Andes plate at 10 mm/yr. These results demonstrate that simple uniform flow of the asthenosphere to the east in conjunction with plate to plate interaction can explain the complex movements that we observe for the tectonics of this region, and might serve as an overall global model.

1. INTRODUCTION

Plate tectonics is a well established theory in geoscience. The theory describes the lithosphere of the Earth as being broken up into approximately twelve major semi-rigid plates that float and move on the asthenosphere. However, the driving mechanism responsible for the movement of the lithospheric plates has yet to be fully understood. The two most popular models are the mantle drag mechanism and edge-force mechanism (figure 1).

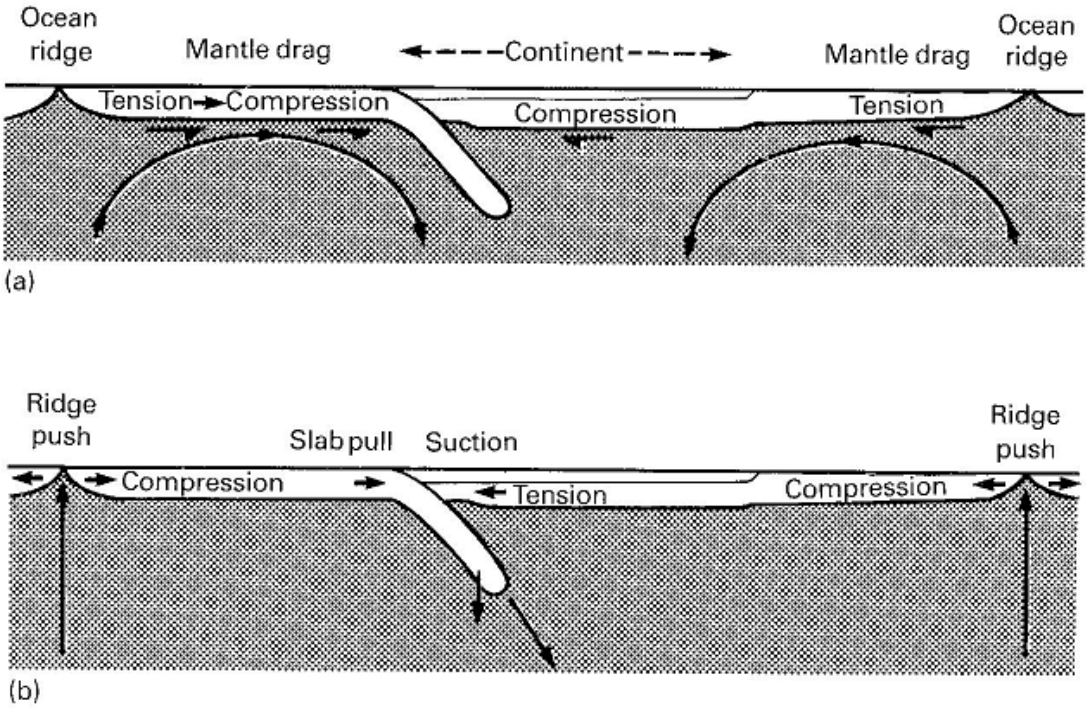

Figure 1. Two proposed models for the plate tectonic drive mechanism.: (a) cellular mantle convection; (b) ridge push - slab pull. (Figure taken from Kearey and Vine, 1996)

Early mantle drag models consisted of convection cells like those illustrated in figure 1a. Initially, convection cells of this geometry seemed to provide a simple explanation for both the rifting process and subsequent spreading. The vertical component of the cell would cause the lithosphere to split. Once split, the viscous

drag exerted to the base of the plate by the lateral portion of the cell would cause the plates to move away from each other. A major problem with this early convection model was the convection cell geometry itself. The simple cell geometry failed to explain the complex geometries of both the plate boundaries and direction of plate movement. In addition, they failed to explain the wide range of plate sizes; from as large as the Pacific plate to as small as the Juan de Fuca plate.

The edge-force model, figure 1b, consists of two force systems, ridge-push and slab-pull. A pushing force is believed to occur at the ridges where topographic highs develop as the plates pull apart. These topographic highs result in a hydrostatic imbalance that causes the plate to move away from the ridge as the forces try to equilibrate. The slab-pull model suggests that forces develop at subduction zones in response to the cold, dense slab descending into a hotter, less dense portion of the mantle whereby it pulls the rest of the plate with it. Bird (1998) demonstrated, through the use of finite element modeling, that neither of the forces from ridge-push or slab-pull were enough to move tectonic plates the size of the Pacific over a static mantle at rates consistent with the global kinematic model of NUVEL 1 (DeMets et al., 1990). The problem persisted even when the mantle was set to unreasonably high temperatures to lower the viscosity limit, and the fault friction coefficients along the transform faults were set to unreasonably low values to make the faults nearly frictionless. Doglioni et al. (2007) listed twenty two reasons why slab pull is not a suitable model for both initiating the subduction process as well as the movement of the plates thereafter. They found no correlation between the dip of the subducting slab relative to the age of the slab, whereas (Carlson et al., 1983) previously argued that

subduction is a function of negative buoyancy that develops within older, colder, and consequently denser oceanic lithosphere. However, for purposes of comparison to the model of interest, the slab pull model was also tested as part of the modeling efforts presented here.

Prior to the development of plate tectonic theory, Jardetzky (1948) proposed that the zonal rotation observed in the atmospheres of Jupiter, Saturn and the Sun may be part of the normal evolutionary process for planetary formation and therefore may exist within the Earth's interior. Zonal flow consists of cellular convection with both horizontal and vertical components. However, there are several major differences between the zonal flow convective model and the convection model originally proposed for plate tectonics. First, individual zonal flow cells (figure 2) span the entire circumference of the planet as a continuous cell. Second, the horizontal component of zonal flow assumes a predominantly eastward direction, following the rotation of the planet. Third, the velocity of the convection system is maximal at the equator and diminishes to a minimum at the poles. This pattern is best observed in the atmospheres of Jupiter and Saturn (figures 3 and 4).

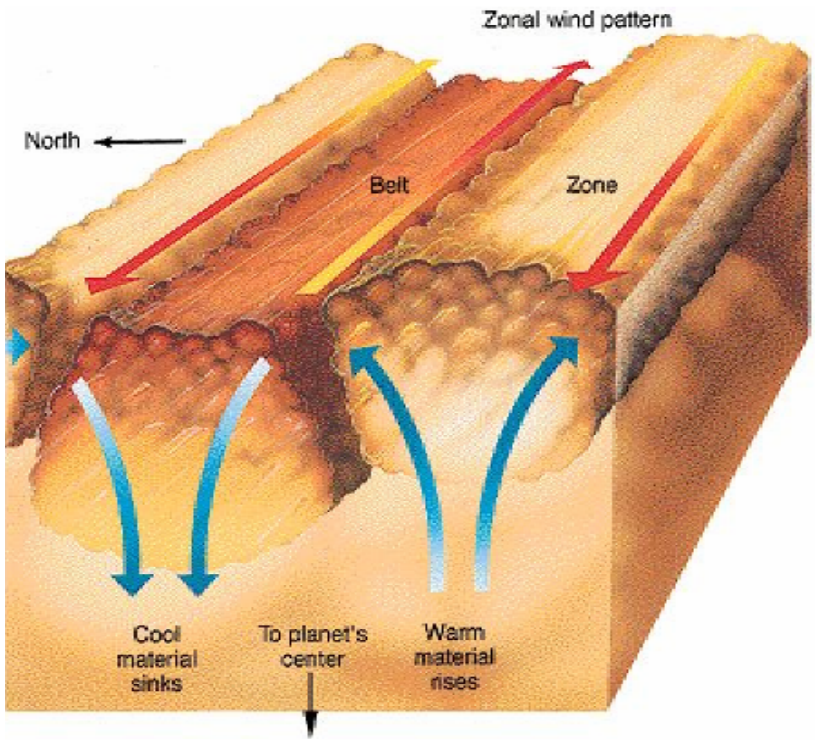

Figure 2. Zonal flow convection pattern. (Figure taken from Chasson and McMillan, 1993)

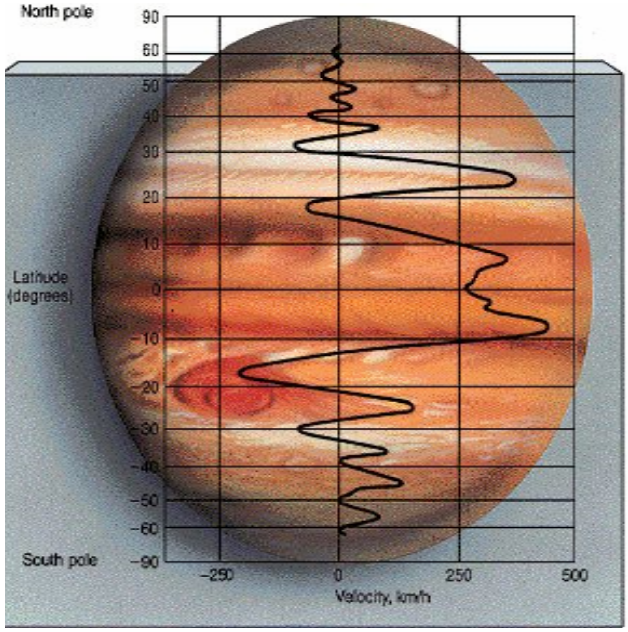

Figure 3. Zonal flow of Jupiter's atmosphere. (Figure taken from Chasson and McMillan, 1993)

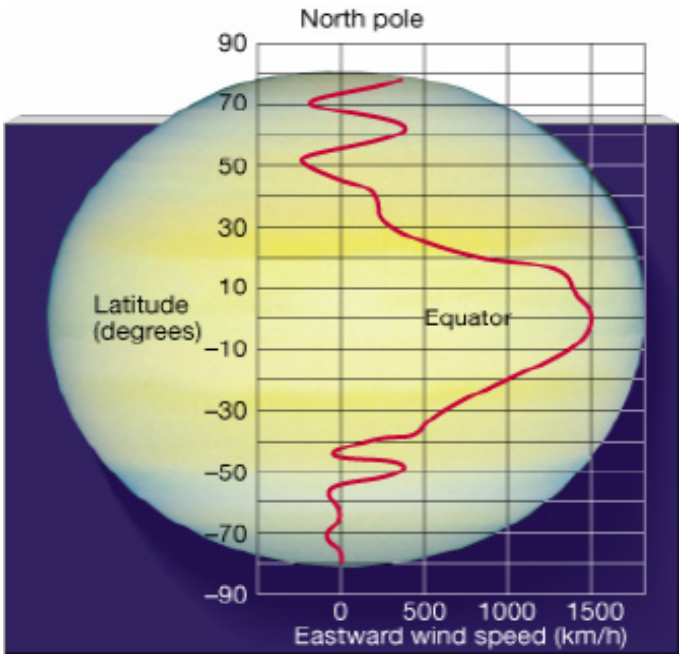

Figure 4. Zonal flow of Saturn's atmosphere. (Figure taken from Chasson and McMillan, 1993)

An eastward flowing mantle is the primary focus of this study, and while Jardetzky's model is rather dated and computer modeling has not supported the existence of this phenomena in the mantle (Schubert et al., 2001), there are more recent studies that do support eastward flow in the mantle. Doglioni et al. (2007) also propose a global eastward mantle flow based on geological, geophysical, and geodetic evidence. The flow pattern differs from Jardetzky's in that it follows an undulate path that makes an angle approximately 30° relative to the geographic equator (figure 5). It is Dr. Doglioni's belief that that the Earth's rotation is a driving mechanism of plate tectonics, which is based on the research he and his colleagues have carried out over the years (personal communication). Negredo et al. (2004) proposed eastward mantle flow beneath the Caribbean plate base on finite element modeling. Doglioni et al. (2003) modeled an eastward-migrating mantle beneath the East Pacific Rise, as did Hammond and Toomey (2003). An eastward mantle flow

beneath the Tyrrhenian Sea can be inferred from the study by Margheriti et al. (2003). In addition, eastward mantle flow beneath South America was proposed by Van Hunen et al. (2002) and beneath North America by Silver and Holt (2002). Russo and Silver (1994) proposed eastward mantle flow beneath the Nazca plate based on shear wave splitting analysis.

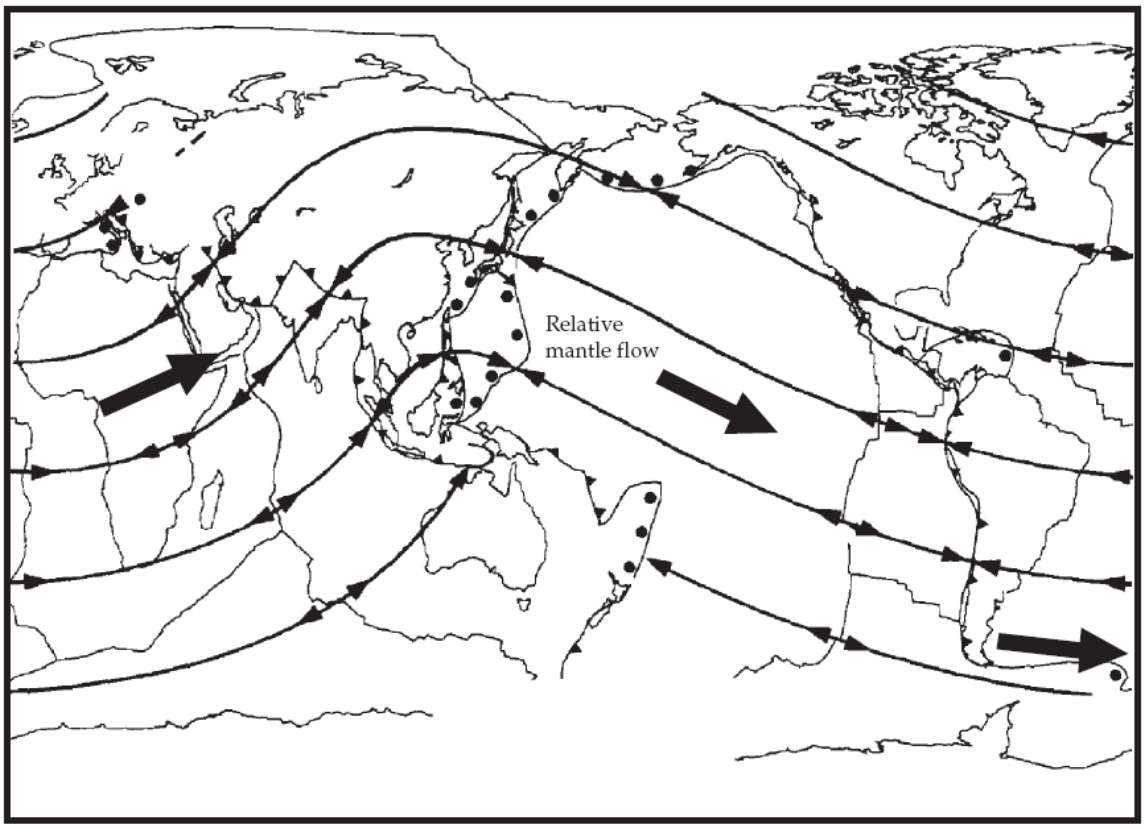

Figure 5. Global eastward mantle flow pattern proposed by Doglioni et al. (2007). (After Doglioni, 1993)

Jardetzky (1948) hypothesized that if a predominantly eastward flow does exist within the Earth's mantle, drag from this convection system could account for both the rifting of the continents as well as their subsequent movements. The movements of the continents would be in a predictable pattern. The continents would assume an easterly motion, with counterclockwise rotation in the northern hemisphere

and clockwise rotation in the southern hemisphere. To test the hypothesis, Jardetzky (1948) built a physical model composed of heated pitch to represent the mantle, and dried plaster or dough to represent the original supercontinent of Pangaea (figure 6). The model provided a means of generating a parabolic-like flow beneath a plate of dried plaster or dough, which floated on top of the pitch, in order to determine how that plate would break up under these conditions. The results were consistent with the hypothesis, whereby the initial block broke into several pieces demonstrating components of rifting, compression, and shearing (figure 7). Additionally, the results demonstrate that without prior knowledge of the underlying velocity field one could assume individual blocks move both east and west when in fact all of the blocks move to the east. The separation between blocks is simply a function of some blocks moving faster to the east *relative* to other blocks. A common analog to this phenomenon is that of an ice flow in a river where a combination of large and small, as well as geometrically irregularly shaped, blocks of ice move in response to both their interaction with each other and the simple flow pattern of water below that serves as the primary driving force.

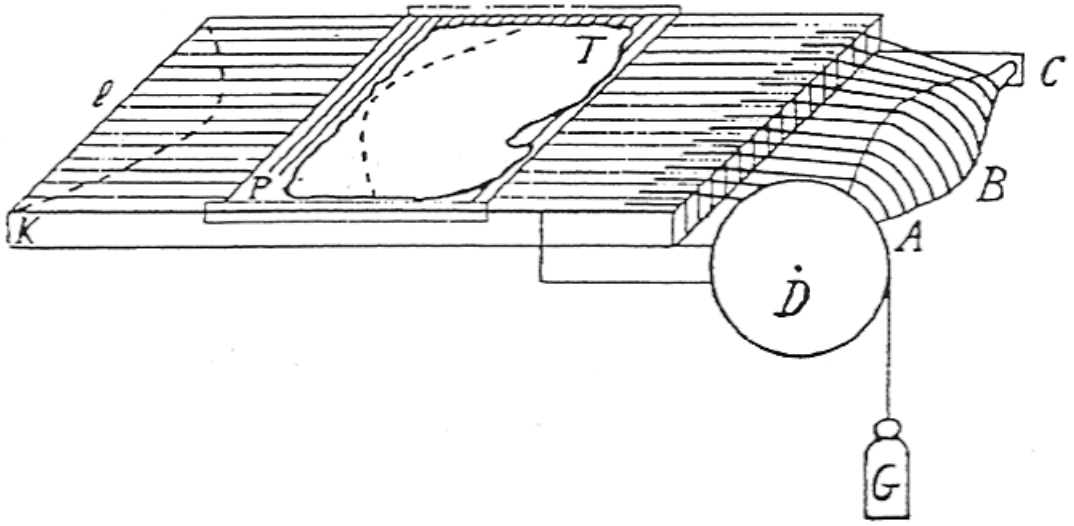

Figure 6. Schematic diagram of Jardetzky's (1948) zonal flow model. A box a pitch is heated to a temperature of 55 – 40° C and a dried layer of plaster or dough is placed on top. Strings, wrapped around a spindle in the shape of a parabola, are rotated to create a parabolic flow within the pitch from left to right (west to east). (Diagram taken from Jardetzky, 1948)

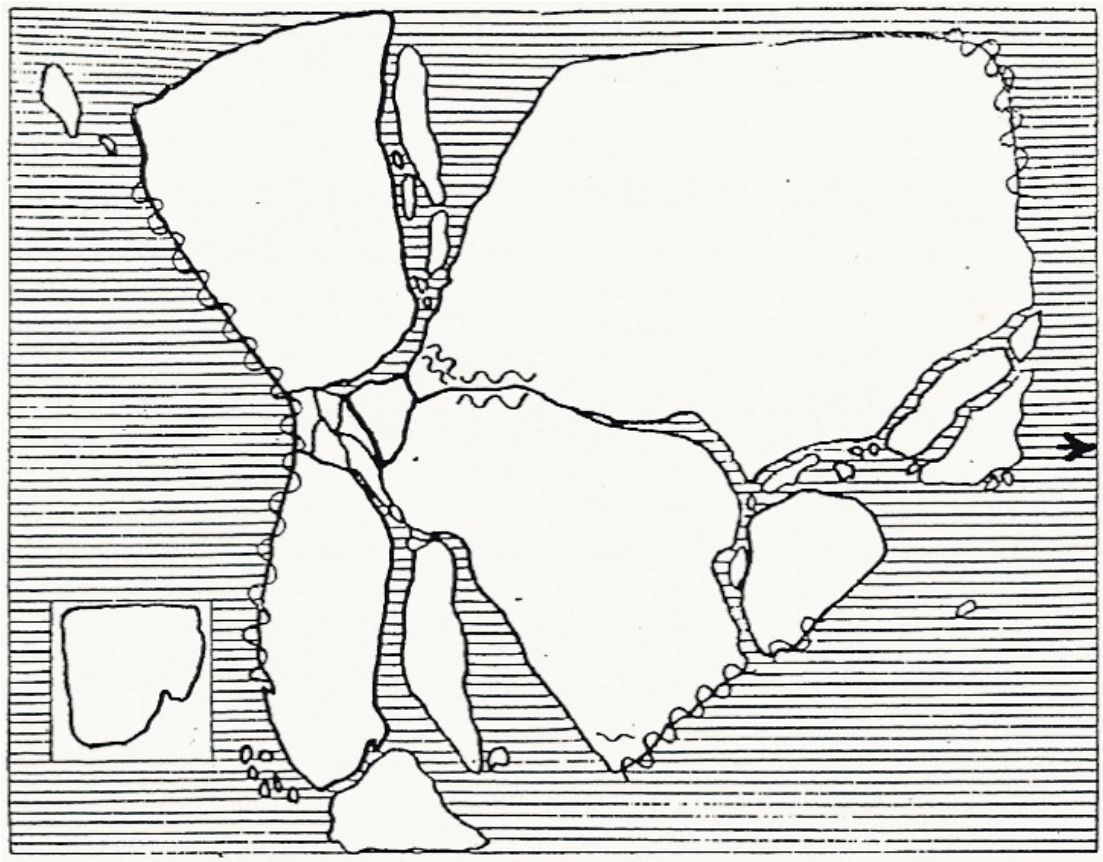

Figure 7. Example of a test result from Jardetzky's (1948) experimental apparatus. The shape of the velocity field in the pitch is that of parabola with maximum velocity in the center, and near zero velocities at the top and bottom. The inset is the original shape of the test plate. The results demonstrate rifting, compression and shear. More importantly, the results demonstrate that without prior knowledge of the underlying velocity field, one could assume the individual blocks moving in both east and west directions, when in fact all of the blocks are moving to the east. The separation between the blocks is a function of some blocks moving to the east faster than others. There is also a rotational component to the movement of the bocks that creates a differential velocity between bocks. (Diagram taken from Jardetzky, 1948)

When compared to today's technology, Jardetzky's (1948) physical model to demonstrate the possibility of an eastward mantle flow is now somewhat rudimentary. For example, it lacks the ability to account for the curvature of the Earth and the varying physical properties and geometries of the Earth's tectonic plates. In the present day the computer provides for much more robust modeling techniques. The answers to complex differential equations are now closely approximated though the use of numerical modeling methods such as finite element modeling, which can

account for a wide range of variables simultaneously. Finite element modeling is most often used for determining stresses and strains in mechanical systems such as buildings and bridges. In addition, it is frequently used for solving problems in heat transfer and fluid dynamics.

Finite element modeling has also been applied to the field of plate tectonics in several places around the globe where the principal contribution is related to earthquake hazard planning. Bird and Kong (1994) applied finite elements to the primary fault system of California. In addition to the faults, the model incorporated the variations in elevation, crustal thickness and heat flow of the region. Various parameters, primarily the coefficient of friction for the faults, were modified until model results closely approximated the published estimates of average fault slip rates, principal stress directions, and geodetic measurements. Wei et al. (2000) performed a similar study on the Chinese mainland where major regions of great earthquakes occur. Their models were able to reproduce stress concentrations in the ductile layer of the lithosphere that corresponded to the regions of great earthquakes. They determined that driving forces from the plate boundaries were responsible for the concentration of stress in these particular regions. Calibrated models such as these can be used as reasonable guides for estimating the earthquake hazard potential in other regions of the modeled area where observational data is limited.

Finite element modeling is used here to examine the hypothesis of a pervasive eastward flow in the mantle as a possible driving mechanism for plate tectonics. A regional model consisting of multiple plates with differing velocities and directions of

movement was selected as a scaled down representation of a global model in order to simplify the numerical experiment. The region of interest includes all of the Caribbean and North Andes plates, most of the Cocos plate, and a portion of the Nazca plate. There are a number of advantages to using this region to test the hypothesis. The first advantage is the conclusion from the finite element study by Negredo et al. (2004) that an eastward mantle velocity of 20 mm/yr beneath the Caribbean plate is necessary to explain the observed motions between North and South America. The region is also comprised of a system of plates that vary in size, geometry, age, and composition (continental *versus* oceanic crust). Most of the major tectonic features such as strike-slip faulting, thrust faulting, rifting, and subduction are also present. The region also has a wealth of geodetic information from which the model can be calibrated, and there exists a wide range of plate velocities and directions. During the entire testing process for the project, there were more than eight finite element grids constructed and over two thousand parameter tests.

2. METHOD

SHELLS is a finite element program that has been developed over a number of years by Peter Bird (Bird, 1999) and is freeware that can be download by ftp from http://peterbird.name/oldFTP/. SHELLS has previously been used to model the neotectonics of the Azores Region (Jimenez-Munt et al., 2001), North America (Liu and Bird, 2002), the Ibero-Maghrebian region (Negredo et al., 2002), New Zealand (Liu and Bird, 2002), Australia (Burbidge, 2004), Indo-Asia (Kong X. et al 1996), Caribbean plate (Negredo et al., 2004), and the whole globe (Bird, 1998; Bird and Liu, 1999). Additional supporting applications and data used to build the models are also provided. A slightly modified version of the SHELLS program is used for the purposes of this study.

The method assumes the lithosphere can be represented by a thin spherical shell (figure 8) and it can be applied to large regional models as well as global models. It also performs certain functions whereby it can be considered a pseudo three dimensional algorithm. The method uses a two-dimensional finite element grid in a manner that only the horizontal components of the momentum equation are solved and only the horizontal components of velocity are predicted; the inertia term in the momentum equation is ignored. The radial component of the momentum equation is represented by the isostatic approximation and the vertical normal stress at any point is assumed to be equal to the weight of overburden per unit area. The strength of the lithosphere is vertically integrated, and the velocity vectors are assumed to be independent of depth in the lithosphere. The total thickness of the shell is controlled by the user by entering the depth of the model into the parameter file

read by SHELLS. The value of 400 km is typically used as it is considered to be the base of the asthenosphere. The base of the lithosphere is defined as an isothermal surface that occurs at a transition point from a conductive to an adiabatic geotherm.

SHELLS allows for the use of faults, laterally varying elevation (topography/bathymetry), crust, lithosphere and mantle thickness, and heat flow. The program uses a set of initial conditions, such as asthenosphere temperature, velocity magnitude and direction, as well as realistic rheologies and densities (among other variables) to solve the equations of stress equilibrium and conservation of mass to predict plate velocities, stresses, and strain rates. These values can then be compared quantitatively to observed values within the modeled area, such as GPS measurements, in order to determine the validity of the model results. Additional details of the methodology can be found in Appendix A.

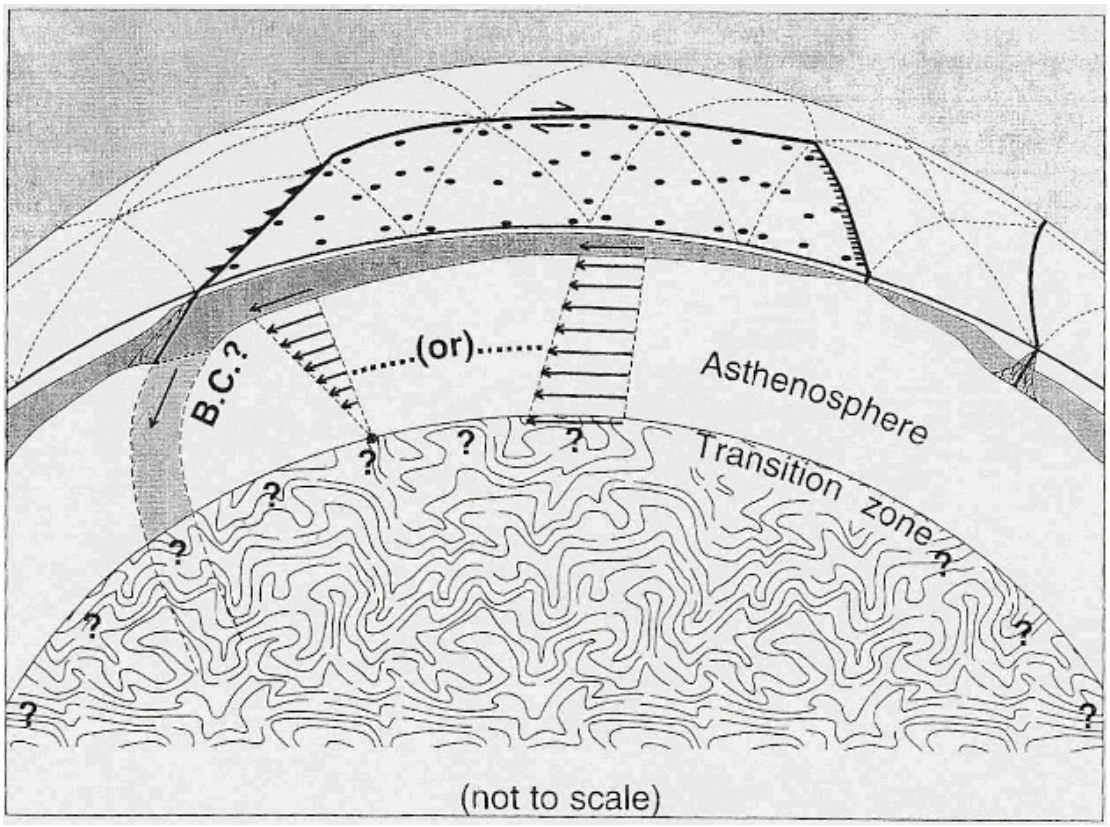

Figure 8. Cartoon of the geometry assumed in program SHELLS. Crust (white) is bonded to the mantle lithosphere (shaded) and their joint strength is represented by 2D grid of spherical triangles on surface. Within each triangle, vertical integrals of strength are performed at 7 Gauss integration points (black dots). Fault elements are used to represent plate boundaries. Because subducting slabs deeper than 100 km are not included in model, their 'cut' ends require boundary conditions (either velocity or traction specified.) Whether lower mantle is assumed to be fast-moving or sluggish, velocity differences between lower mantle and lithosphere cause simple shear in asthenosphere, which applies horizontal shear tractions to base of model. (Figure taken from Bird, 1999; Note: the required boundary conditions for subducting slabs refer to global models only and not regional models such as tested here.)

3. MODEL DEFINITION AND CONSTRUCTION

3.1. MODEL DEFINITION

The finite element model used for this study (figure 9) is an expansion of the model by Negredo et al. (2004) used to study the neotectonics of the Caribbean plate. The primary differences between the models are with respect to the western boundary and the North Andes plate. The western boundary in this study was extended to the

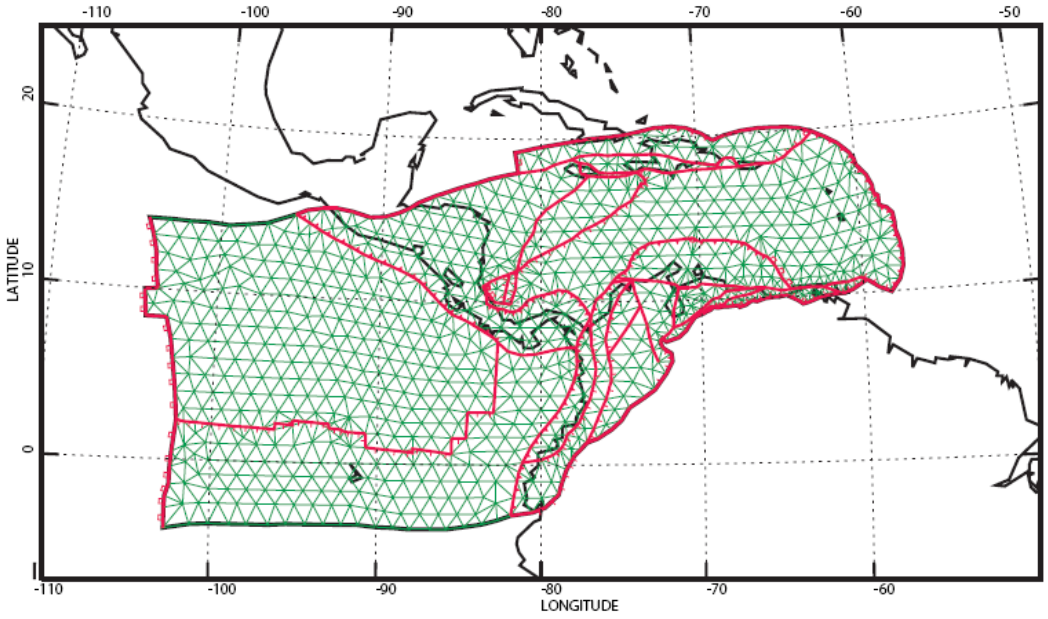

Figure 9. Finite element model consisting of: 1594 nodes, 1859 continuum elements, and 432 fault elements. This model is an expansion of that used by Negredo et al. (2004) to model the Caribbean plate. The additional areas added to the model include all of the North Andes plate, most of the Cocos plate, and a portion of the Nazca. An additional difference between this and the Negredo et al. (2004) model is that the subduction zone along Central and South America does not serve as a boundary condition.

East Pacific Rise (EPR) and comprised nearly all of the Cocos plate and a portion of the Nazca plate. This effectively removed the Middle America Trench (MAT) as a forced boundary condition which enabled the MAT to respond to the movements of the adjoining plates and the basal velocity field independently. An additional advantage of using the EPR as the western boundary is as a spreading ridge it can be

treated as a free boundary, whereas velocity conditions would have been imposed if the western boundary was a convergent boundary. This allows the Cocos and Nazca plates to respond primarily to the basal velocity field being tested. The northern boundary of the Cocos plate and the southern boundary of the Nazca plate were set as free boundaries. The North Andes plate was extended southward through Ecuador and the Gulf of Guayaquil, where it was tied into the subduction zone off the South American coast. Justification for this southern extension is based on the interpretation of the tectonic maps and earthquake fault plane solutions taken from the Harvard Centroid Moment Tensor (CMT) data base (figure 10).

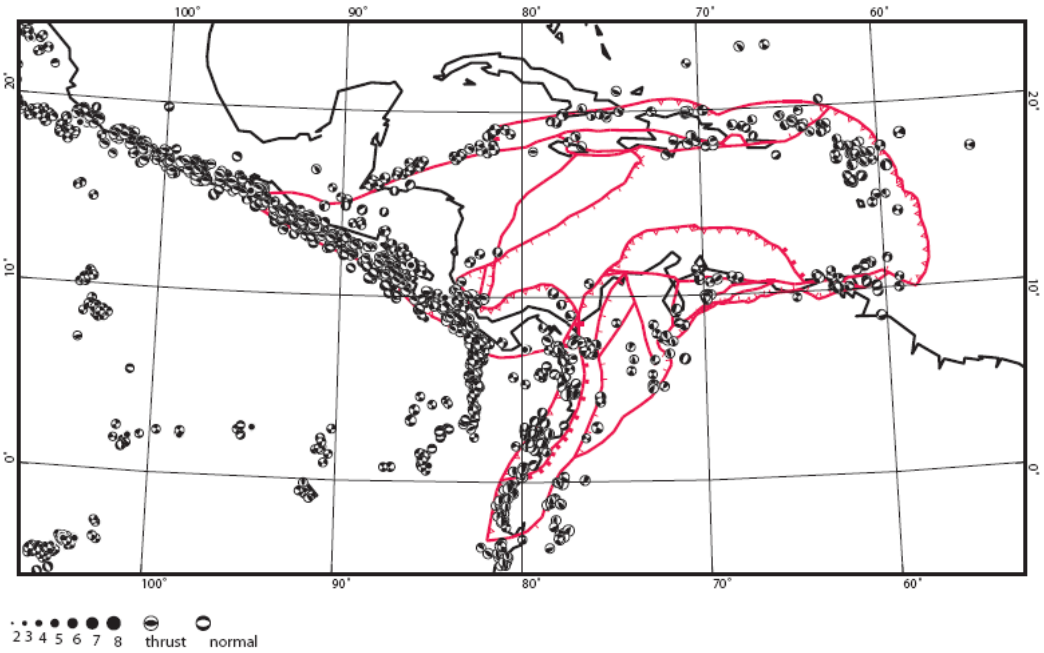

Figure 10. Fault plane solutions taken from Harvard Centroid Moment Tensor (CMT) database.

3.2. FINITE ELEMENT GRID CONSTRUCTION

Boundaries and faults in the grid construction were interpreted from the Tectonic Map of the World (AAPG, 1994) and the Tectonic Map of South America (1978). In several places within the model it was necessary to interpolate the position of faults where they were not clearly depicted on the maps. In addition, it was sometimes necessary to approximate fault dip values. Because the dip of a fault contributes directly to its resultant slip-rate in the model, a value of 45 or 65 degrees was initially assigned to faults of unknown dip based on simplified geologic assumptions. Faults illustrated on tectonic maps with both low relief and no indication of strike-slip motion may well be normal or reverse faults and were therefore assigned a dip value of 45 degrees to accommodate either slip direction. Based on the assumption that strike-slip motion is usually associated with high angle faulting, faults on tectonic maps with both thrust and strike-slip motion were assigned a dip of 65 degrees in the direction of thrust. In areas where such values resulted in initial poor slip rate results (e.g., too much or too little fault slip), these initial dip estimates were readjusted

A supporting program to SHELLS computes the structure of the lithosphere (thickness of the crust and upper mantle lithosphere) for each node in the model. It does so based on four assumptions: the base of the lithosphere is an isothermal surface; heat conduction though the lithosphere is in steady state; all lithosphere is isostatic with respect to the mid-ocean ridges; and the crust and mantle lithosphere are approximated as laterally homogeneous. The three primary variables the program uses to build the structure of the lithosphere are elevation (topography/bathymetry),

surface heat flow, and the mantle adiabat. Several other parameters, such as thermal conductivity and radioactive heat production are also incorporated in the process, but these are usually held constant. The topography/bathymetry data was taken from the ETOPO2v2 data set (National Geophysical Data Center, June 2006); whereas the heat-flow data were obtained from a 5°-mean compilation of Pollack et al. (1993) (figure 11). This differs slightly from the Negredo et al. (2004) model which used a 2°-mean global heat flow compilation which was not available for this study.

The total lithosphere thickness generated from these parameters can be seen in figure 12. One potential problem with respect to the heat flow data having a negative impact on the model concerns the relatively low heat flow values in the Cayman Trough spreading center. These low heat flow values can result in the creation of a more rigid lithosphere than what is normally expected along a spreading center. The increased rigidity, or lithosphere thickness, may cause the spreading center to experience higher resistance to spreading than normal.

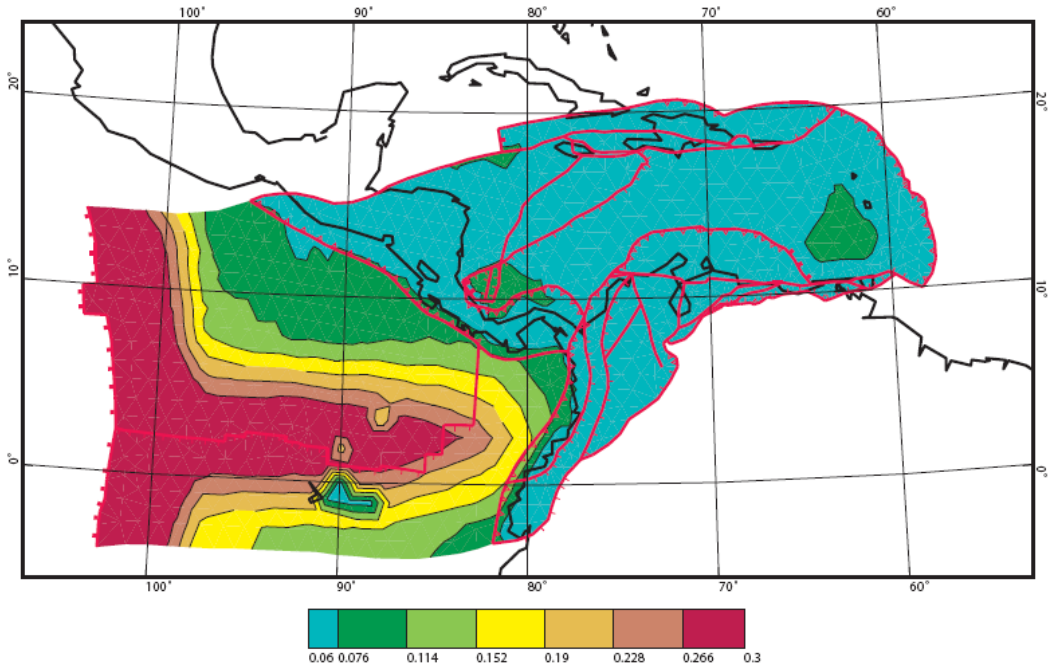

Figure 11. Illustration of heat flow data used as input into all three models based on the 5 degree heat flow data in SI units of (W/m^2) of Pollack et al. (1993). The data along the ridges were truncated at 0.3 W/m^2 to prevent artifacts.

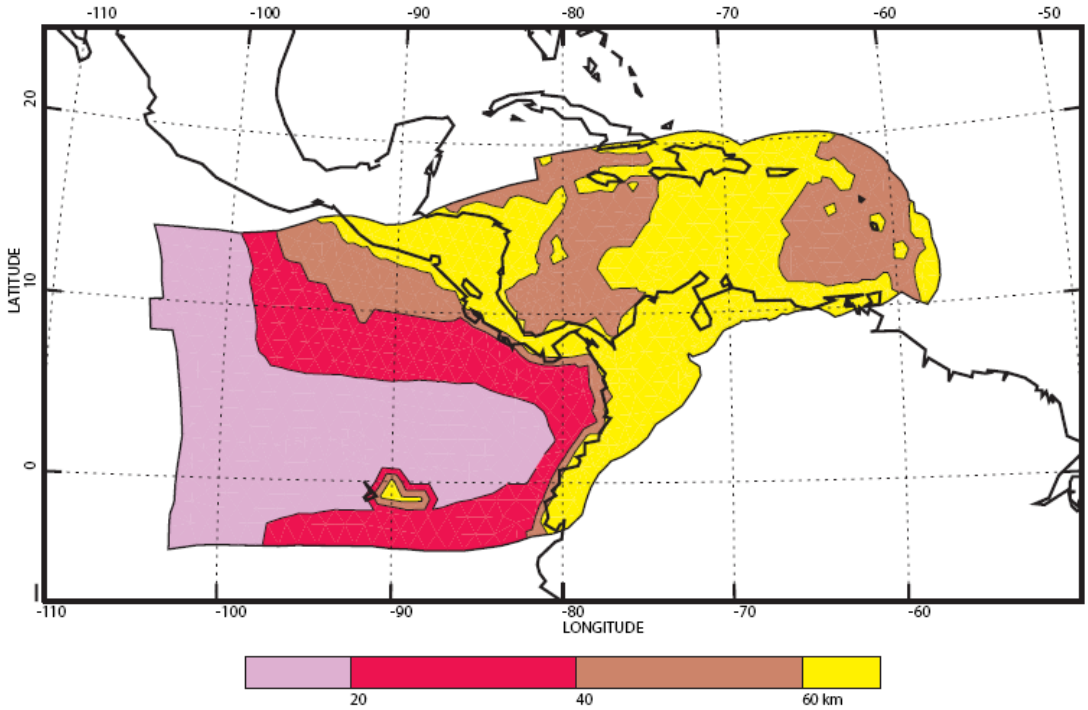

Figure 12. Total lithosphere thickness for the model. The thin area along the boundary between the Cocos and Nazca plates is attributed to the high surface velocities in this area because the asthenosphere, along with its velocity field, is closer to surface under these conditions. In this case, the basal velocity was 100 mm/yr whereas the surface velocity ranged between 80 and 90 mm/yr.

An attempt was made to simplify the boundary conditions of the model due to the number of individual tectonic plates within and adjacent to the model that move in various directions with respect to each other. All of the boundary nodes for the Cocos and Nazca plates were set as free (requiring no velocity). This allowed these plates to respond primarily to the basal velocity field being tested in the model. In addition, the velocity for the boundary nodes of the North and South American plates were set to zero such that these plates are fixed, leaving the Caribbean, North Andes, Cocos, and Nazca plates as the only plates permitted to move. This enabled the results from this portion of the model to be more a function of the basal velocity field being tested, and to a lesser extent, the boundary forces. It is acknowledged that setting the boundary nodes along North America to zero would still have an affect on the model; however, justification for setting these nodes to zero comes from the fact that the relative motion between these plates is small; between 10 and 20 mm/yr (Weber et al., 2001; DeMets et al., 2000; Kellog et al., 1996). Therefore, the assumption was made that results from models using these conditions, which fell close to the observed values, could be deemed reasonable approximations to the results of models where the boundary velocities from the adjacent plates had been applied. However, the model was also run with boundary conditions applied to the North America and the Nazca plates, relative to South America, in order to examine the significance of these boundary conditions on the model. This was particularly important with respect to the Nazca plate where only a portion of the plate was being used in the model and the influence of mantle drag on the excluded portion of the plate could not be accounted for.

The basal boundary condition consists of three primary parameters: the velocity magnitude, velocity direction, total depth of the model. The SHELLS program used for this project was a modified version of the 2002 version supplied by Bird such that the magnitude and direction of the basal velocity could be changed in order to test various mantle velocity models. With the exception of the outer boundary nodes, all interior basal nodes were assigned a velocity and direction that was dependent on the desired mantle velocity pattern being tested. The basal depth parameter for all models was set at 400 km. Additional details of model construction can be found in Appendix B.

4. METHODOLOGY FOR VALIDATING MODEL RESULTS

In general, models can be evaluated to a limited extent, “semi-quantitatively” with respect to relative velocity rates, stress directions, and spreading rates. The term semi-quantitative refers to the fact that all three analytical devices above have inherent errors. Plate velocities are constrained from geodetic measurements (GPS), which are commonly placed in tectonically active regions and are quite often subject to errors related to localized movements that obscure overall plate velocity measurements. Stress direction measurements suffer from a number of problems that affect their accuracy. Many of the data are derived from earthquake focal mechanism solutions (FMS) which can be considered more a measurement of strain than stress. Dr. Peter Bird (personal communication) suggests that because the majority of earthquakes occur along plate boundary faults, the faults tend to be weak and slip repeatedly along the same plane and therefore do not provide the comprehensive information needed to accurately determine the orientation of the principal stress axis. Therefore, stress values derived from FMS data along active fault planes are considered questionable. Other stress measurements are taken from boreholes often related to the oil and gas exploration and tend to be clustered in small specific areas of interest. Seafloor spreading rates are “estimated” velocity rates along spreading ridges that are determined from large time intervals related to magnetic reversals on the seafloor that are not always sharply defined. In addition, they don’t necessarily account for the possibility of asymmetric spreading on the ridge. However, the acceptance of these errors in all three data types provides enough information to semi-quantitatively evaluate model results.

A supporting software application called ORBSCORE is supplied with SHELLS to simplify the means of comparing the results output by SHELLS to published field data like those described above. To do this, the field data must have positional information such as longitude and latitude. With this information, the program locates the element within the model that falls closest to the field data point and calculates the misfit between the model result and the field data. The mean and root-mean-square are the primary values calculated for the misfits between these two values. An area weighting factor is also incorporated into the calculation in order to account for the clustering of field data. Clustering of data typically occurs in focused regions of geologic interest, such as major active faults and volcanoes, and can therefore bias field data. The weighting factor adjusts for this bias by treating individual data points within a cluster as fractional representations of the total area, where the sum of all fractions represent the unit area.

The source for the geodetic data used for this project was the Global Strain Rate Map project (GSRM), (Kreemer et al., 2003; http://gsrm.unavco.org/data/). An important aspect of the project is that it provides several versions of geodetic data rotated to various reference frames. South America serves a fixed boundary of significant length in the model being tested here. Therefore, the geodetic data set rotated to the South American reference frame was selected for this project (figure 13). The database used to calculate seafloor spreading rate misfits was taken from the global compilation of horizontal spreading rates along the normal faults at mid-oceanic ridges (DeMets et al., 1990). Two data sets of stress were used for this project; both data sets were obtained from the World Stress Map database

(Heidbach et al., 2008; www.world-stress-map.org). The first data set (figure 14) contained 285 values that fell within the model area, and was comprised predominantly of single focal mechanism solutions with a quality factor of "C" (the data quality ranking is based on the method developed by Zoback and Zoback (1989), and Sperner et al., (2003)). Dr. Bird created a filtered version of the world stress data due to the problems related to FMS data stated above. The selection criteria for this data set was primarily based on the premise that data points located within plate interiors are considered to be more representative of intra-plate stress than data points along plate boundaries. This data set is made available for download from the ftp site http://peterbird.name/oldFTP/ and was used for this project. A total of 16 data points fell within the model area using the edited version of the world stress map data (figure 15). Bird (1998) also indicated that since the stress discrepancy can not exceed 90 degrees at any point, a misfit in azimuth between field data and model results equal to 45 degrees would be indicative of a model where the stress results are uncorrelated to the field data. In addition, a misfit of azimuth between field data and model results greater than 45 degrees would be indicative of a model where the stress results are anti-correlated to the field data. However, Kong (1995) and Bird (1998) also statistically examined the stress data available at the time and determined that the field data had an internal discrepancy such that no model is likely to have a mean azimuthal misfit of less than ~25 degrees. Therefore, a good model result would be one where the azimuthal difference between the field data and model results are

closer to 25 degrees, whereas a poor model result would be one where the azimuthal difference between field data and model results would be closer to, or exceed, 45 degrees.

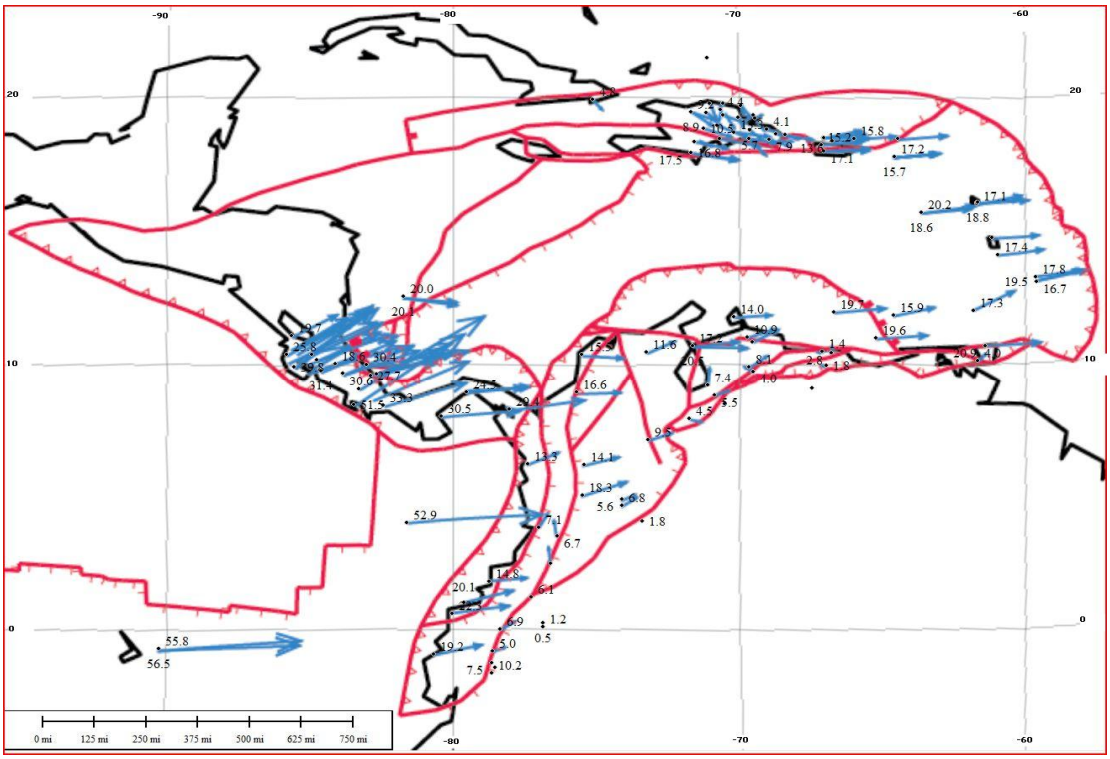

Figure 13. Geodetic velocities used to calibrate the model. The frame of reference is South America. (Data source: GSRM project Kreemer et al., 2003)

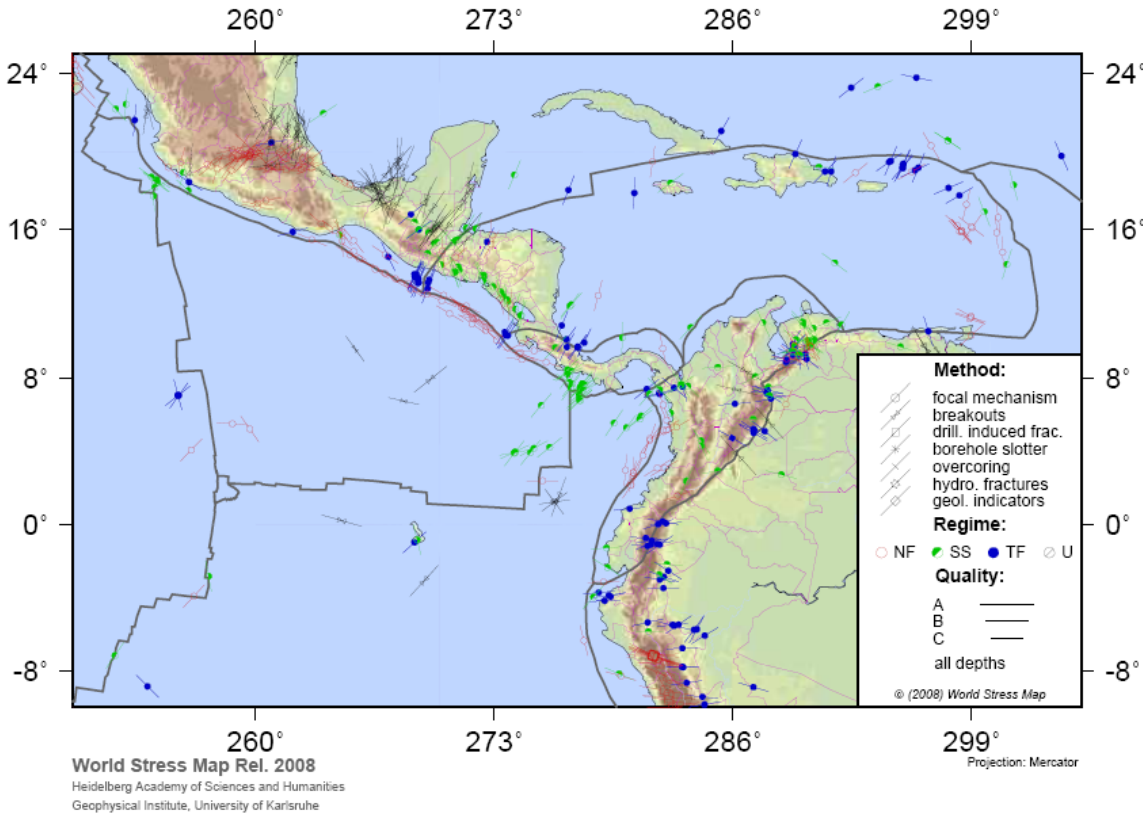

Figure 14. Stress data within the project area. A total of 285 data points fell inside the model area. (Source: World Stress Map data base Heidbach et al., 2008; www.world-stress-map.org)

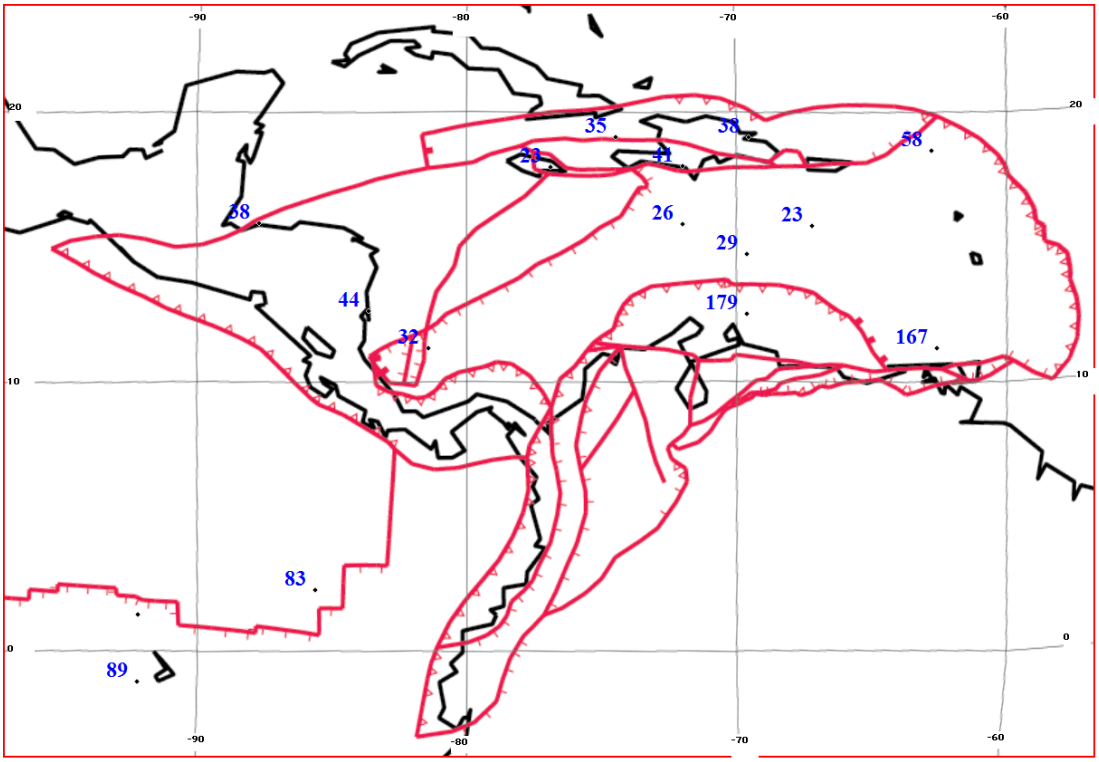

Figure 15. An edited version of the World Stress Map data (in degrees) provided by Peter Bird (http://peterbird.name/oldFTP/) based on the premise that data points located within plate interiors are considered to be more representative of intra-plate stress than data points along plate boundaries.

Preliminary testing of ORBSORE yielded anomalously low velocity misfits in the summary report between the geodic velocities and model velocities. Investigation of this problem revealed a subroutine within the program, called ADJUST, that makes an assumption that the geodetic data is not in the same reference frame as the model velocity data and attempts to resolve the problem by computing a pole of rotation that is used to minimize the weighted RMS of the magnitude of the velocity differences. The early test results quite often calculated a correction pole of rotation with a rotation velocity equivalent to the velocity of the basal velocity field being tested. This subroutine was deactivated in the program because there was a high level of certainty that the geodetic data and model velocities were in the same reference

frame. This was based on the fact that the geodetic data was exported in South American reference frame, and model boundaries adjacent to South America were set to zero such that South America was fixed in the model.

Upon removal of the subroutine ADJUST, another problem with velocity misfits in the summary report appeared. ORBSCORE outputs a table that provides the location of each geodetic measurement, the geodetic velocity, the velocity result from the model closest to the geodetic location, and the misfit between the two values. The average misfit calculated manually from the table was more than double the average misfit in the geodetic summary report. The geodetic velocities in the table were confirmed at various GPS locations via manual velocity calculations using published poles of rotation (DeMets et al., 2000; Weber et al., 2001). It was determined that the discrepancy was related to the area weighting factor applied to the results. The weighting was taken out of the program with the knowledge and acceptance that the resultant average will contain the affects of clustered data. However, upon removal of the weighting factor, the average misfit dropped by nearly half in most tests.

The removal of these two functions from ORBSCORE may create uncertainties in the summary results between geodetic velocities and model velocities provided by the program. However, there are 131 geodetic measurements within the model and over 125 model configurations were tested. Therefore, the use of ORBSCORE was necessary to process this vast amount of data. A detailed manual evaluation of model velocities was carried out once a model was selected from the results of ORBSCORE that was considered to bear the most promising overall results.

The manual evaluation focused on singular points within the model that were spread throughout various locations of the Caribbean and North Andes plates in order to account for data clustering that may have affected the misfit evaluation by ORBSCORE.

5. SENSITIVITY ANALYSES

5.1 PARAMETERS TESTED USING EASTWARD BASAL FLOW ONLY

A large number of parameter tests were carried out on the finite element grid. Five models of 50 degree isothermal increments, representing the base of the lithosphere, were constructed with the following temperatures: 1323 K, 1373 K, 1423 K, 1473 K, 1523 K. The temperature selection was based on bracketing on either side of 1423 K, the temperature used by Negredo et al. (2004) to model the neotectonics of the Caribbean plate. For each temperature condition, models were run with five increments of 20 mm/yr basal velocities: 20, 40, 60, 80, and 100 mm/yr. Selection of the velocity values were based on bracketing between the highest geological-based estimated velocity values within the model, which occur along the spreading ridge of the EPR at nearly 100 mm/yr (Kreemer et al., 2003), and the slower GPS-based measurements of Caribbean plate at 20 mm/yr (DeMets et al., 2000; Weber et al., 2001) . All of the velocity fields were assigned a due east direction. An example of the due east basal velocity field can be seen in figure 16. The Caribbean plate model of Negredo et al. (2004) deemed to be most successful used a fault friction coefficient of 0.03. This value is geologically reasonable and is supported by the experimental results of Hickman (1991) and the numerical modeling results of Hassani et al. (1997), Bird (1998), and Sobolev and Babeyko (2005). In addition, a range of fault friction coefficients between 0.17 and 0.25 was used successfully in numerical modeling of the neotectonics of California (Bird and Kong, 1994). Based

on the above studies, a range of five intervals of fault friction coefficients were used to test this model: 0.04, 0.08, 0.12, 0.16, and 0.20. The velocity boundary conditions for all models were set to zero.

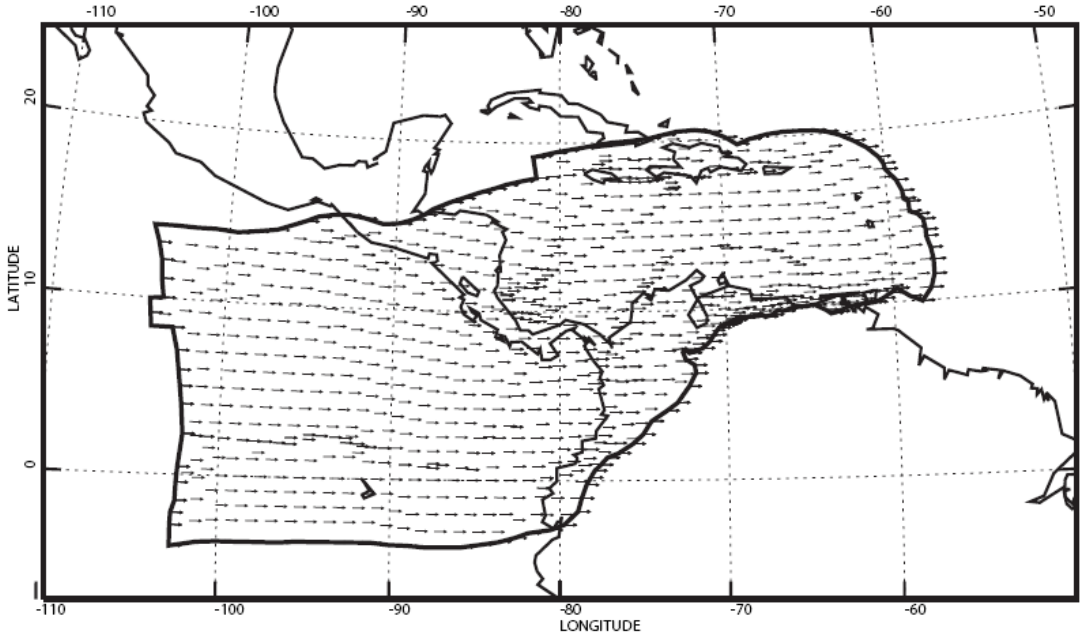

Figure 16. An example of a basal velocity field for the model that was set due east for all runs. The apparent change in direction of the vectors is an optical illusion due to the geometric orientation of the nodes with respect to the triangular shape of the elements and the map projection.

5.1.1. SENSITIVITY ANALYSIS OF EASTWARD PARAMETERS

Portions of the misfit results determined from ORBSCORE for both models can be seen in Tables 1A & 1B. Table 1A shows results from the model where the boundary conditions for both NA and SA were set to zero and NZ was free. Table 1B shows results from the model where the boundary conditions for NA and the bottom boundary of NZ were set relative to SA. Both data sets are sorted based on the model with the smallest geodetic misfit. In general, the models using boundary conditions for NA and NZ relative to SA were slightly poorer in an overall context. However, velocity errors in the Nazca plate were significantly reduced in the model where

boundary conditions were applied. The complete set of results for the model with a fixed North and South America are presented in Appendices D and E, both sorted and unsorted. The results for the model where boundary conditions were applied to both the North American and Nazca plates relative to South America are presented in appendices F and G. In addition, the misfits for models 1 through 125 are presented in chart form in figures 17 through 21.

RUN No.	TEMP K	TEMP ℃	VEL MM/YR	FRIC COEFF.	VEL MISFIT MM/YR	CAYMAN TROUGH SPREADING MISFIT	STRESS MISFIT °	MAT SUBDUCTION RATE	MAT SUBDUCTION ANGLE MISFIT
8	1323	1050	40	0.12	8.4	2.0	29.5	14.2	48.5
37	1373	1100	60	0.08	8.5	4.9	29.2	28.8	47.8
15	1323	1050	60	0.02	8.5	3.4	27.9	31.4	51.7
42	1373	1100	80	0.08	8.9	1.5	29.9	37.1	49.1
14	1323	1050	60	0.16	8.9	1.6	28.6	25.6	51.1
43	1373	1100	80	0.12	9.3	6.8	29.2	44.3	49.5
48	1373	1100	100	0.12	9.3	2.7	28.9	55.6	50.6
9	1323	1050	40	0.16	9.7	6.2	28.0	18.7	49.6
49	1373	1100	100	0.16	10.3	8.7	28.1	61.8	50.7
38	1373	1100	60	0.12	11.1	10.1	28.4	32.6	48.1

Table 1A. Top 10 test results based on lowest velocity misfit where the boundary conditions for NA and SA were set to zero and bottom boundary of NZ was free. The models with temperatures in the 1373 K range with a basal velocity of 100 mm/yr offer the best combination of lowest overall velocity misfit along with reasonable velocities towards the Middle America Trench (MAT) based on plate kinematic model of Kreemer et al. (2003).

RUN No.	TEMP K	TEMP ℃	VEL MM/YR	FRIC COEFF.	VEL MISFIT MM/YR	CAYMAN TROUGH SPREADING MISFIT	STRESS MISFIT °	MAT SUBDUCTION RATE	MAT SUBDUCTION ANGLE MISFIT
139	1323	1050	60	0.16	8.7	0.1	37.5	30.9	43.4
132	1323	1050	40	0.08	8.7	2.9	40.1	14.0	32.7
167	1373	1100	80	0.08	8.9	0.9	35.8	40.0	43.3
162	1373	1100	60	0.08	9.0	5.6	36.0	33.0	40.9
140	1323	1050	60	0.20	9.2	5.6	30.4	36.8	45.0
173	1373	1100	100	0.12	9.2	4.3	31.3	58.1	46.0
168	1373	1100	80	0.12	10.0	8.1	29.0	47.8	44.6
145	1323	1050	80	0.20	10.2	1.2	32.9	44.7	47.0
134	1323	1050	40	0.16	10.5	8.0	31.5	24.4	40.0
174	1373	1100	100	0.16	11.1	10.6	28.7	64.7	46.5

Table 1B. Top 10 test results based on lowest velocity misfit where the boundary condition for NA and the bottom boundary of NZ were set relative to SA. The models with temperatures in the 1373 K range with a basal velocity of 100 mm/yr offer the best combination of lowest overall velocity misfit along with reasonable velocities towards the Middle America Trench (MAT) based on plate kinematic model of Kreemer et al., 2003.

A notable anomaly that the charts do not clearly indicate is that, of the 250 models tested, only ten converged using a fault friction coefficient value of 0.04. All five models that did converge using this value were associated with models where the base of lithosphere temperature was 1523 K. In addition, several models using a fault friction coefficient value of 0.08 did not converge; these were more widely spread among models of varying temperature for the base of lithosphere. Examination of the failed velocity fields that used the fault friction coefficient of 0.04 revealed that the failure consistently occurred along the far western boundary of the model where the boundary conditions of the Cocos and Nazca plates were set to free and the faults were set at 45 degrees. The low friction coefficient value applied to these faults resulted in landslides that exceeded 20 “meters”/yr, and in one case 128 “meters”/yr. These values substantially exceed even the largest basal velocity field applied to the model of 100 mm/yr.

The geodetic misfits from all models using the combination of all three variables, base of lithosphere temperature, basal velocity, and coefficient of friction are illustrated in figure 17. The results indicate the model to be particularly sensitive to a base of lithosphere temperature greater than 1373 K; above this temperature the geodetic misfit increases dramatically. The results also indicate that multiple combinations of the three variables can lead to similar velocity misfits. For example, an increase in temperature theoretically reduces the shear component in the model, thus reducing the transfer of velocity from the base of the model to the surface. However, this can be compensated for by an increase in basal velocity. This lack of uniqueness diminishes the use of the geodetic misfits as a guide for determining the optimum parameters for a successful model. In addition, the results are somewhat incomplete as there are no geodetic measurements within the Cocos plate which comprises nearly one third of the model.

The misfits for the rate of subduction and angle of convergence along the Middle America Trench from all models using all three variables are illustrated in figure 18a and 18b respectively. The subduction rate is compared to the plate kinematic model of Kreemer et al. (2003) and suggests that subduction of the Cocos plate is clearly dependant on a particular combination of all three variables. The most successful results are with a lithosphere basal temperature of 1373 K, a basal velocity of 100 mm/yr, and a fault friction coefficient of 0.20. The sensitivity of the subduction rate of the Cocos plate to all three parameters significantly narrows the range of parameters that produce a model with the least overall misfits to field observations.

The misfit for the angle of convergence of the Cocos plate towards the MAT was determined by comparing only the Harvard CMT data used by DeMets et al. (1990) for slip rates between the Cocos and Caribbean plate (26.6° azimuth). The trend suggests the error in the angle of convergence with the trench increases with decreasing basal temperature and increasing basal velocity, and that the better results are with models with high basal temperatures with low basal velocity. However, the models with the least error also have the lowest subduction rates as reported in figure 18a and are therefore unlikely to be considered successful models. In general the fit of the convergence angle was poor for most models where the geodetic and MAT subduction rate misfits were low. Further analysis regarding these poor results is addressed later in the discussion section of this paper.

Spreading rate misfits along the Cayman trough (figure 19) are very similar to the geodetic misfits. The results are most sensitive to the base of lithosphere temperature, and even more so than the geodetic misfits. They provide no particular insight as to what combination of variables would produce a model with the least overall misfits to field observations.

The misfits of stress direction for the two data sets consisting of 16 and 285 data points can be seen in figures 20 and 21 respectively. The smaller data set appears more sensitive to the coefficient of friction, whereas the larger data set appears more sensitive to the temperature at the base of the lithosphere. The most striking observation is not which variable each data set is most sensitive to, but the magnitude of difference between the two data sets and their azimuthal misfit range relative to the

model results. There was an azimuthal misfit range between 25.3 and 31.3 degrees in stress direction using the data set containing 16 data points, whereas there was an azimuthal misfit range between 38.2 and 47.6 degrees in stress direction when using the 285 data points. The misfit range of the smaller data set indicates it to be the better of the two data sets to use for model comparison based on the previous discussion where good model results are where the azimuthal difference between the field data and model results are closer to 25 degrees, and poor model results would be where the azimuthal difference between the field data and model results are equal to, or in excess of, 45 degrees.

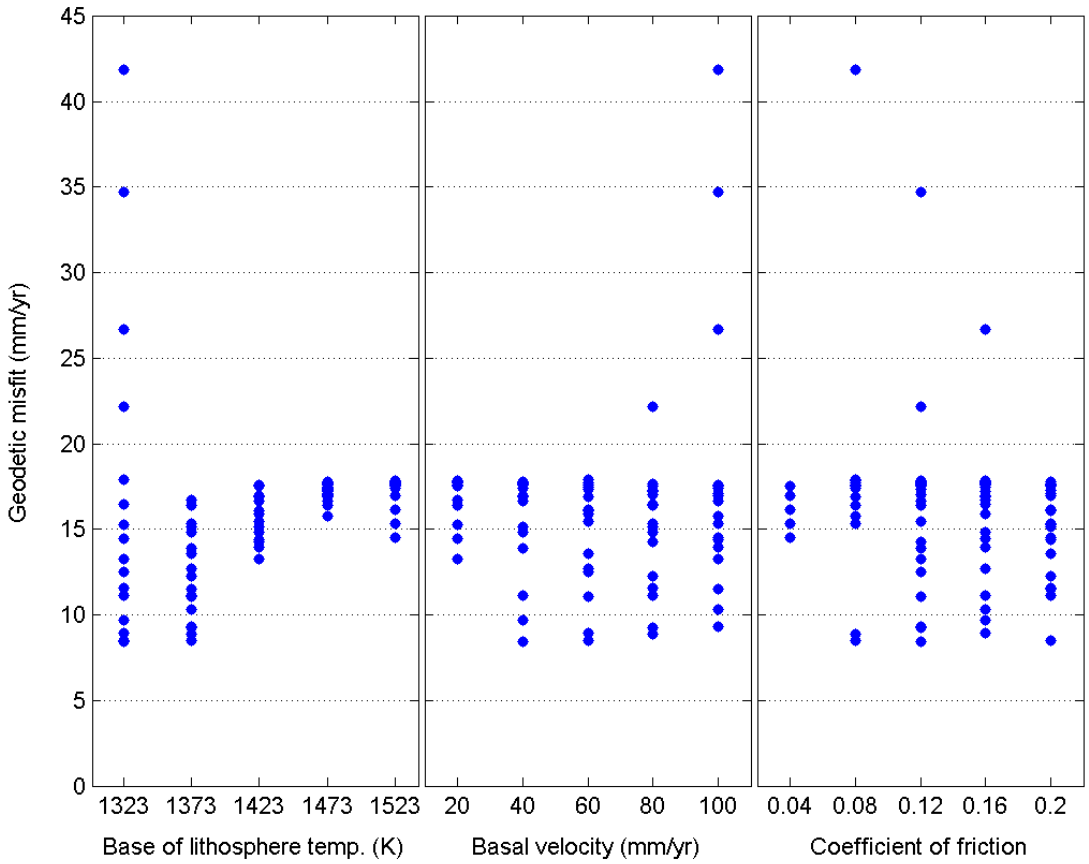

Figure 17. Geodetic misfits from all models based on the combination of all three variables: base of lithosphere temperature, basal velocity, and coefficient of friction. The results indicate the model to be most sensitive to base of lithosphere temperature. The results also reveal that there are a multiple combinations of the three variables that can result in similar low misfits of velocity, which indicates a level of non-uniqueness in the model parameters. However, the results are somewhat incomplete as there are no geodetic measurements within the Cocos plate which comprises nearly one third of the model.

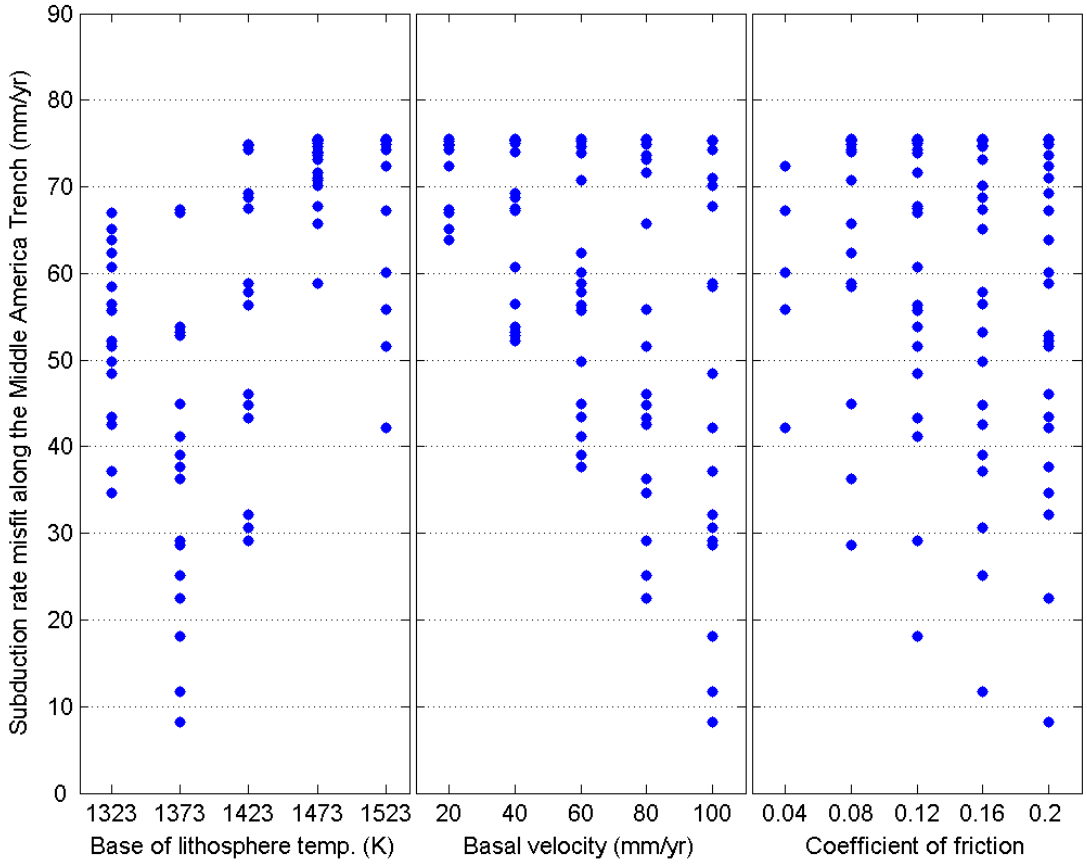

Figure 18A. Subduction rate misfit along the Middle America Trench from all models based on the combination of all three variables: base of lithosphere temperature, basal velocity, and coefficient of friction. The subduction rate of the Cocos plate is clearly dependant on all three variables. The most successful results appear consistent with a lithosphere basal temperature of 1373 K and basal velocity and fault coefficient of friction of 100 mm/yr and 0.2 respectively (compared to plate kinematic model of Kreemer et al., 2003).

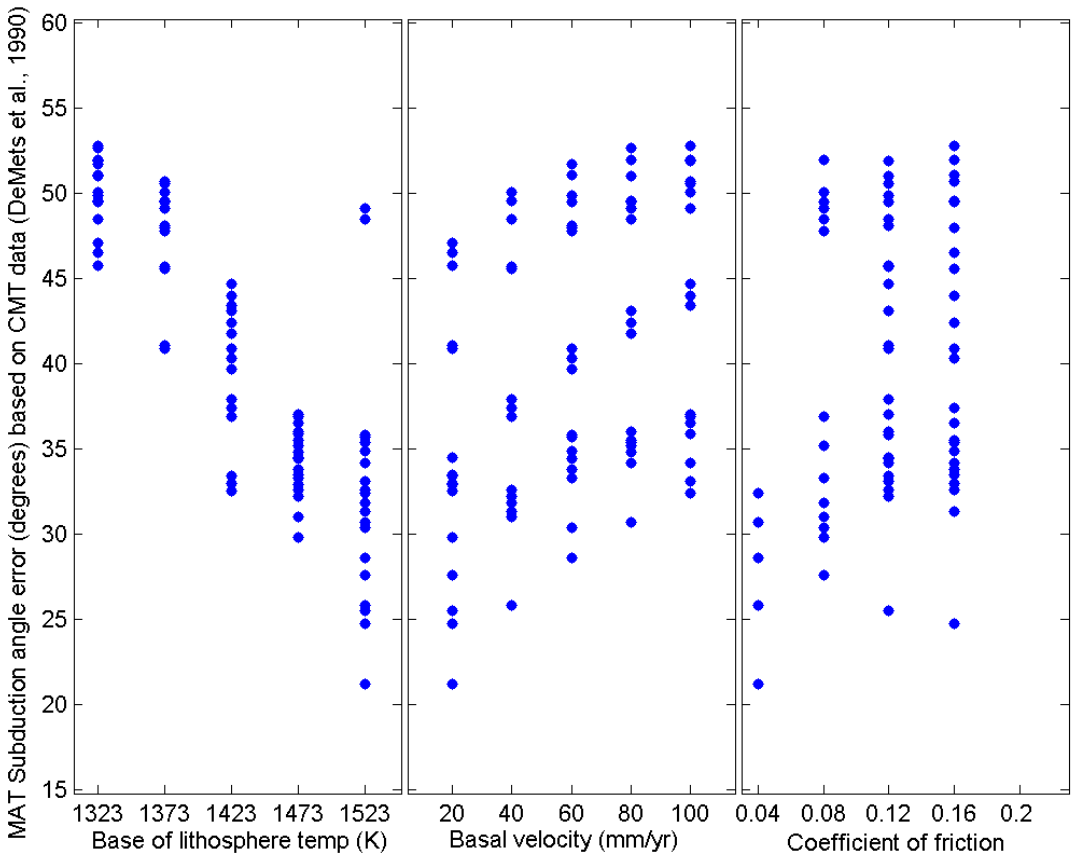

Figure 18B. Subduction angle misfit along the Middle America Trench from all models based on the combination of all three variables: base of lithosphere temperature, basal velocity, and coefficient of friction (compared to Harvard CMT data used by DeMets et al., 1990, for slip rates between Cocos and Caribbean plates).

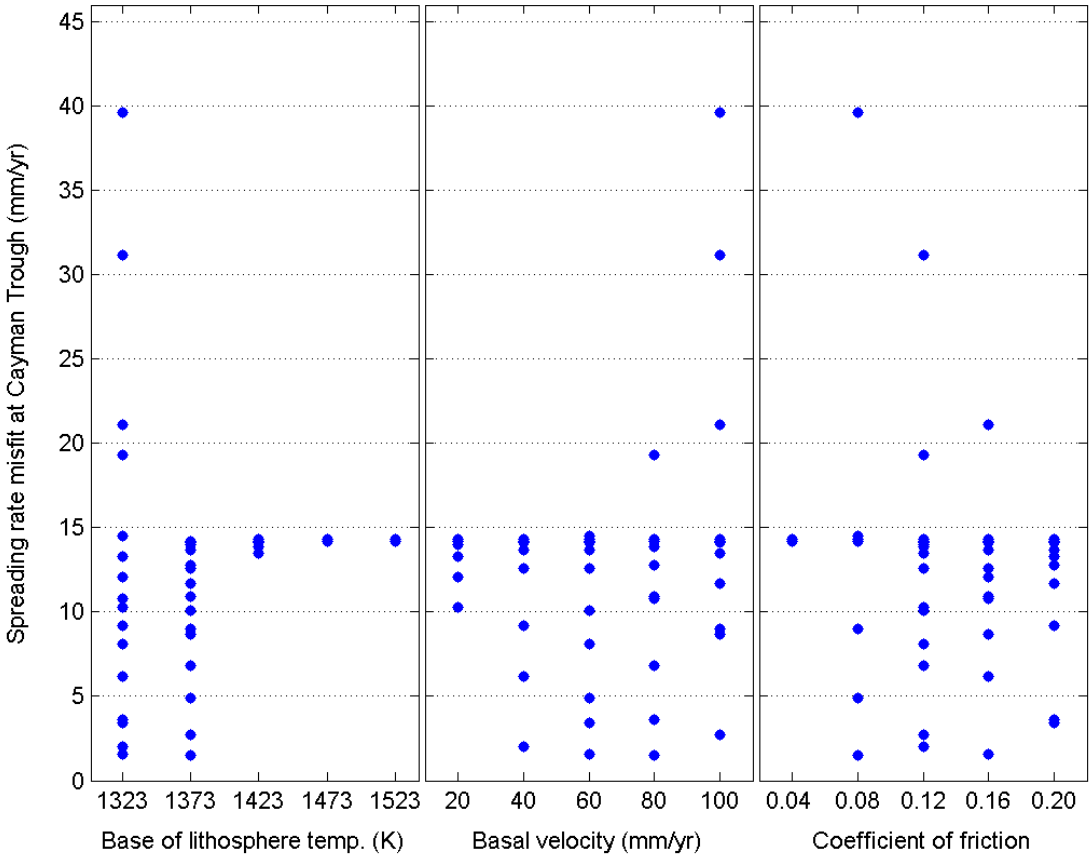

Figure 19. Spreading rate misfit from all models based on the combination of all three variables: base of lithosphere temperature, basal velocity, and coefficient of friction. The results are very similar to the geodetic misfits, in that the results are most sensitive to base of lithosphere temperature.

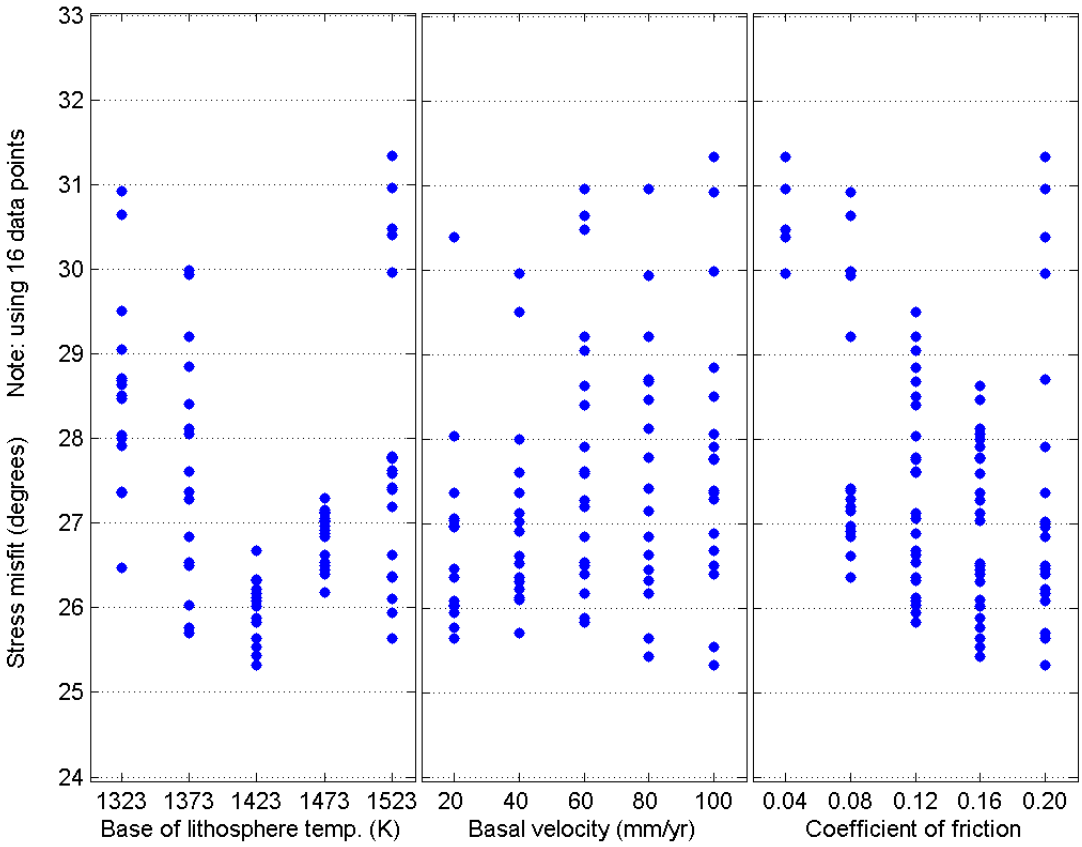

Figure 20. Stress direction misfits based on the 16 stress data points from the World Stress Map project that fell primarily within the interior portions of the model and away from plate boundaries. The results appear most sensitive to the coefficient of friction. This could be due to the fact that while most of the sixteen points fall within the plate interior, many still reside in close proximity to faults as illustrated in figure 15.

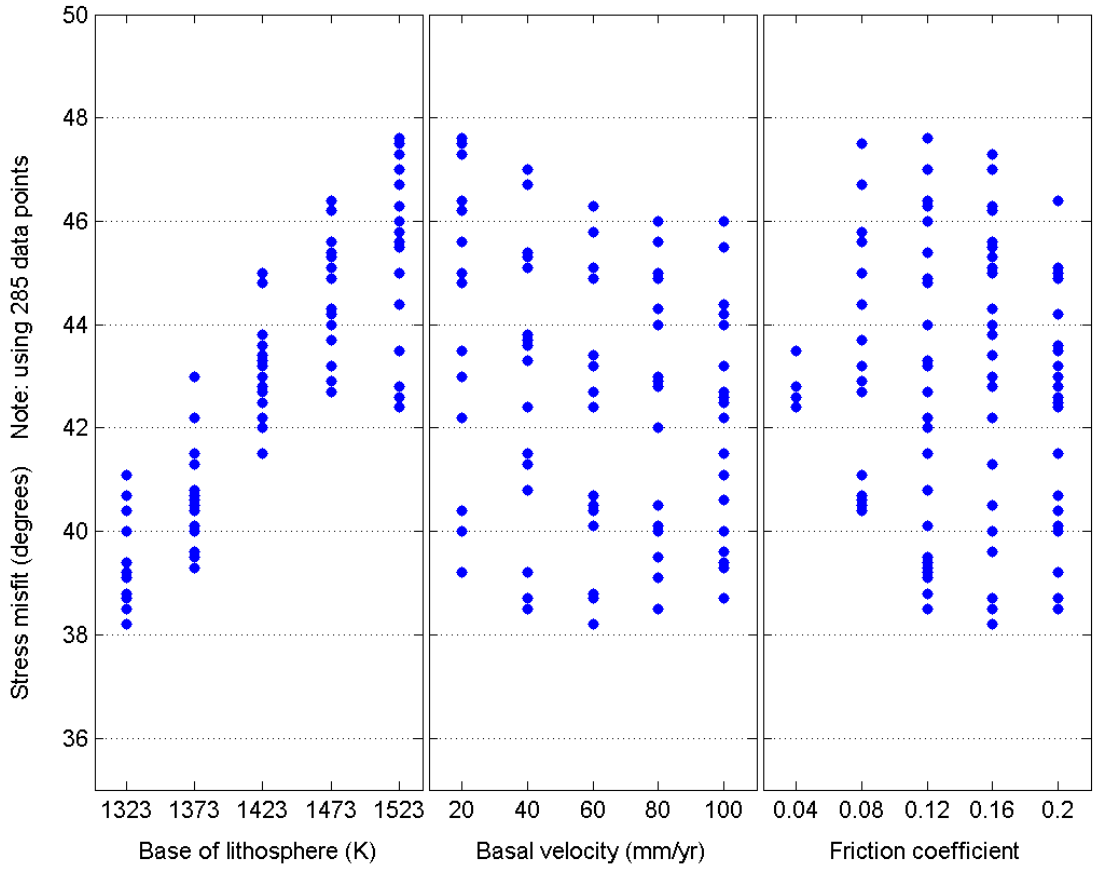

Figure 21. Stress direction misfits based on the 285 stress data points from the World Stress Map project that were scattered widely throughout the entire model area as seen in figure 14 . These misfits are significantly larger than those derived using the 16 interior data points.

5.1.2. SENSITIVITY OF MODEL TO DIRECTION OF BASAL VELOCITY

To test the sensitivity of the model to basal flow direction, it was necessary to create a model where the basal velocity field had a direction other than due east. To make the test as meaningful as possible, a velocity direction had to be chosen that varied considerably from due east, but was also consistent with a velocity that occurs within the model area. The chosen velocity field was that of the surface velocity of the Cocos plate which comprises roughly one third of the model. The Cocos plate moves 80 mm/yr in a direction 30 degrees east of north relative to the Caribbean plate (Kreemer et al., 2003; figure 22). The predominant northward movement of the

Cocos plate provided a sixty degree differential in direction, relative to the models tested with the due east basal velocity field. This difference in basal velocity direction was considered sufficient to determine the importance of mantle flow direction on the model. Only one model using these velocity parameters was tested. The other two parameters for this model, base of lithosphere temperature and fault friction coefficient, were set at 1373 K and 0.12 respectively. These parameters were selected based on the results of due east basal velocity models described above that had the smallest overall misfit.

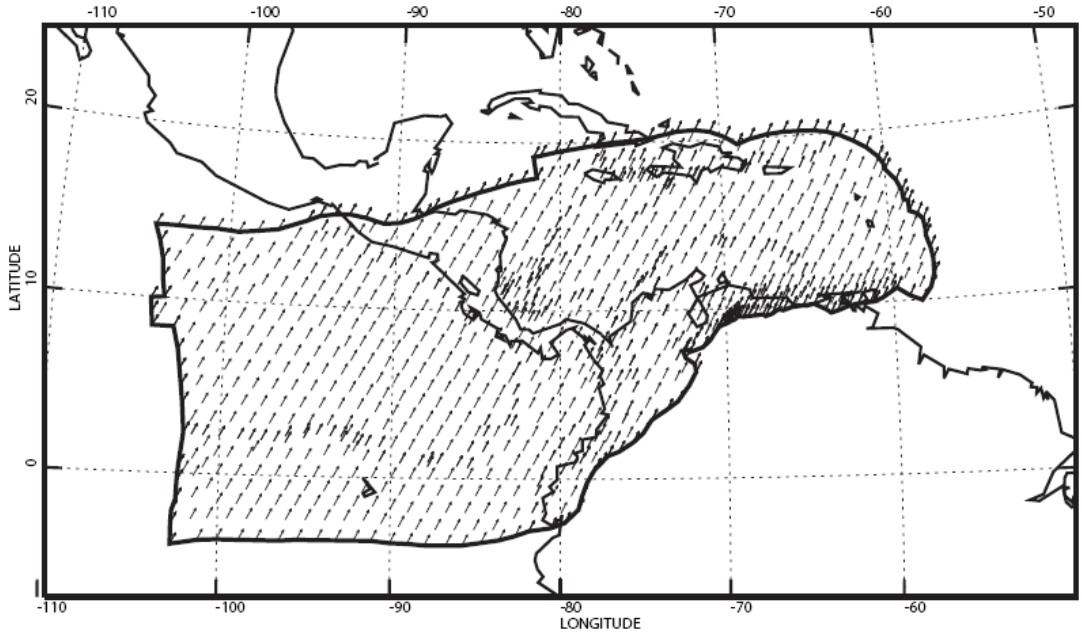

Figure 22. Basal velocity field based on the relative motion of the Cocos plate relative to the Caribbean plate as determined by the GSRM model (Kreemer et al., 2003). The velocity is constant throughout the model and flows at 80 mm/yr in a direction 30 degrees east of north.

The misfit results, shown in table 2, from the model using the parameters described above for a Cocos basal velocity field are compared to the smallest overall misfit results for an eastward basal velocity model. The geodetic and stress direction misfits between the two models are relatively close. The primary differences between

the misfits of the two models are with respect the spreading rate of the Cayman trough and the subduction rate along the MAT. The Cocos basal velocity model yielded a spreading rate misfit along the Cayman trough of 11.3 mm/yr too slow, whereas the eastward basal velocity model yielded a spreading rate misfit along the Cayman trough of 2.7 mm/yr too fast. The significantly slow spreading rate along the Cayman trough given by the Cocos basal velocity field model suggests that, under these conditions, very little eastward movement occurs along the east-west oriented transform faults that form the spreading center. This most likely suggests that the strong northern component of the Cocos basal velocity field inhibits motion along these faults, and that a stronger eastward velocity component is necessary to move these faults at their observed rates.

TEMP K	BASAL VELOCITY DIRECTION	BASAL VELOCITY MM/YR	FRIC. COEFF.	AVERAGE GEODETIC MISFIT MM/YR	SPREADING MISFIT OF CAYMAN TROUGH	STRESS MISFIT (DEGREES)	MAT SUBDUCTION MISFIT
1373	Due East	100	0.12	9.3	2.7	28.8	18.0
1373	Cocos 30 degrees from north	80	0.12	10.4	11.3	30.1	1.7

Table 2. Comparison between lowest overall misfit results for eastward directed basal velocity flow and a basal velocity flow based on the surface velocity of the Cocos plate relative to the Caribbean plate (compared to plate kinematic model of Kreemer et al., 2003).

While the Cocos basal velocity model yielded poor results for the Cayman trough spreading rate in the Caribbean, it provided a very good subduction rate result along the MAT, with a misfit of only 1.7 mm/yr, whereas the subduction rate result from the eastward basal velocity model gave a misfit result of 18 mm/yr. The low subduction rate misfit for the Cocos basal velocity model supports the possibility that a mantle velocity based on the surface velocity of the Cocos plate “is appropriate for

the Cocos plate". However, it may not be suitable for the Caribbean plate as indicated by the large spreading rate misfit in the Cayman trough discussed above. This is further supported when the misfits relative to the MAT and Cayman trough are normalized. The subduction rate misfit along the MAT for the eastward basal velocity field is only ~23% too slow, whereas the spreading rate misfit along the Cayman trough for the Cocos based velocity field is ~80 % too slow. Additional analyses of these models are discussed in the following results section, and provide additional contrast between the results of the two models.

6. RESULTS

6.1 RESULTS BASED ON LOWEST AVERAGE VELOCITY MISFIT USING ONLY A DUE EAST BASAL VELOCITY FIELD

The model parameters with the lowest overall velocity misfit were for a temperature of 1323 K, a basal velocity of 40 mm/yr, and a fault friction coefficient of 0.12. This yielded an overall velocity misfit of 8.4 mm/yr, a spreading misfit at the Cayman trough of only 2 mm/yr, and a reasonable stress direction misfit of 29.5 degrees. The surface velocity for this model is shown in figure 23. However the subduction misfit along the MAT was significant, at over 60 mm/yr. This implies that very little subduction occurs along the MAT with these test parameters (figure 24). The geodetic misfits of this model are illustrated in figure 25.

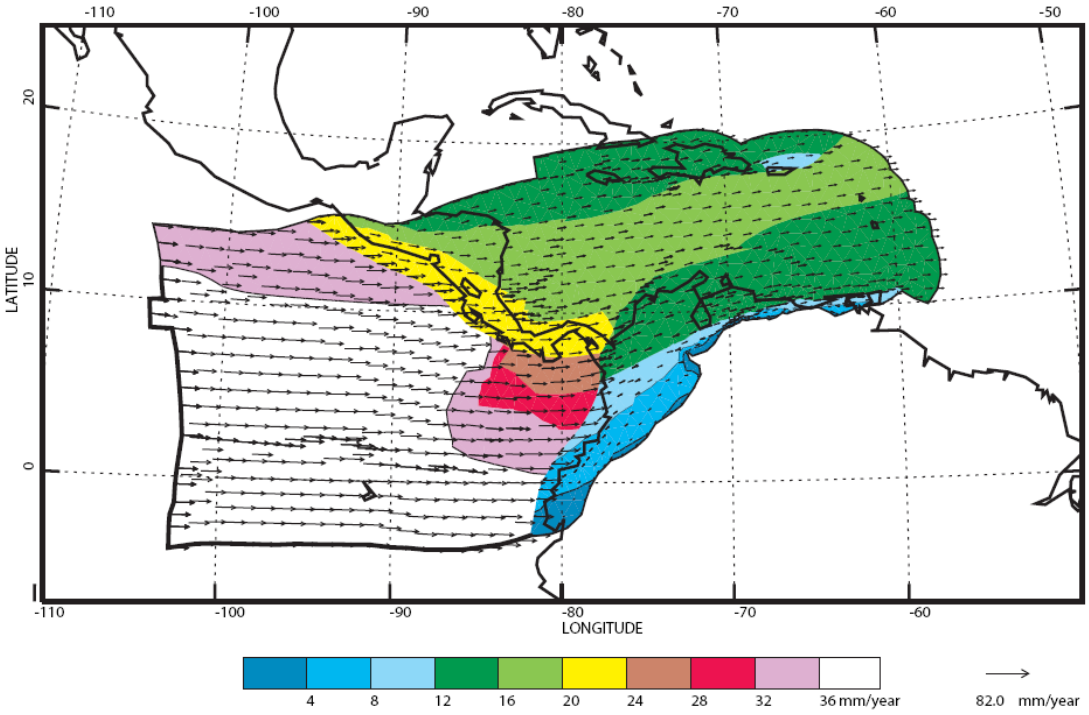

Figure 23. Surface velocity for the lowest average velocity misfit model with parameters of 1323 K, 40 mm/yr basal velocity, and a fault friction coefficient of 0.12.

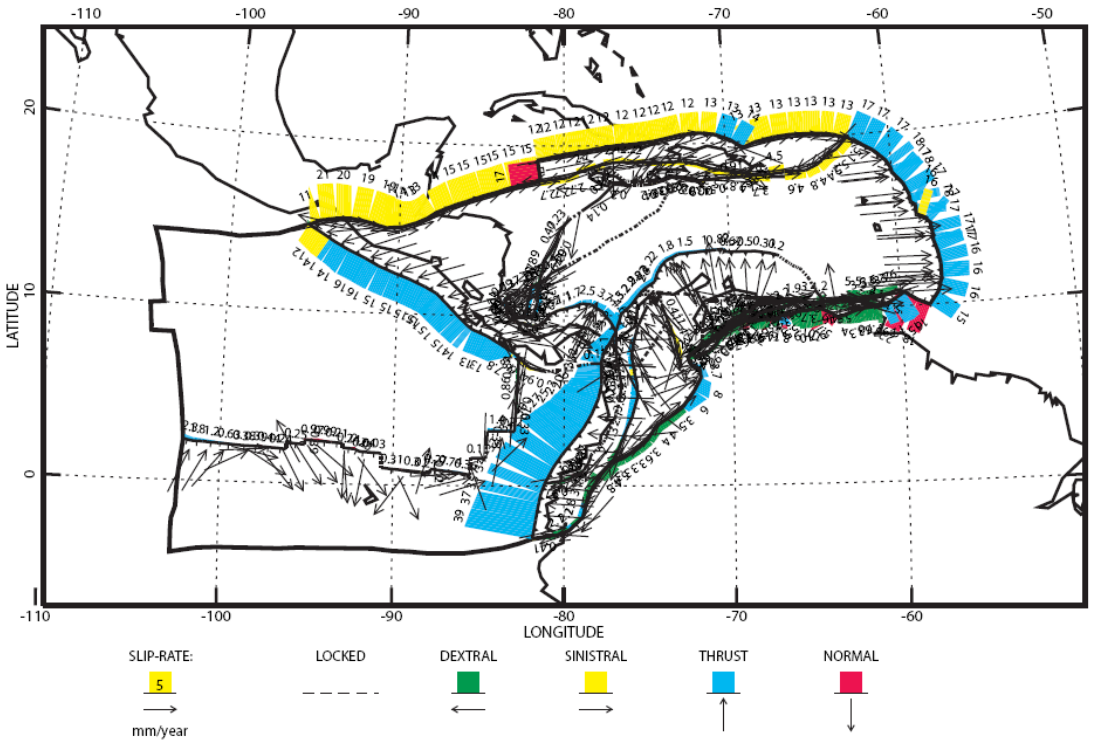

Figure 24. Fault slip rates for the lowest overall velocity misfit model with parameters of 1323 K, 40 mm/yr basal velocity, and a fault friction coefficient of 0.12. However, the subduction misfit is significant along the MAT, with only 15 mm/yr subduction instead of the estimated average rate of ~75 mm/yr relative to the Caribbean, based on the GSRM project (Kreemer, et al., 2003).

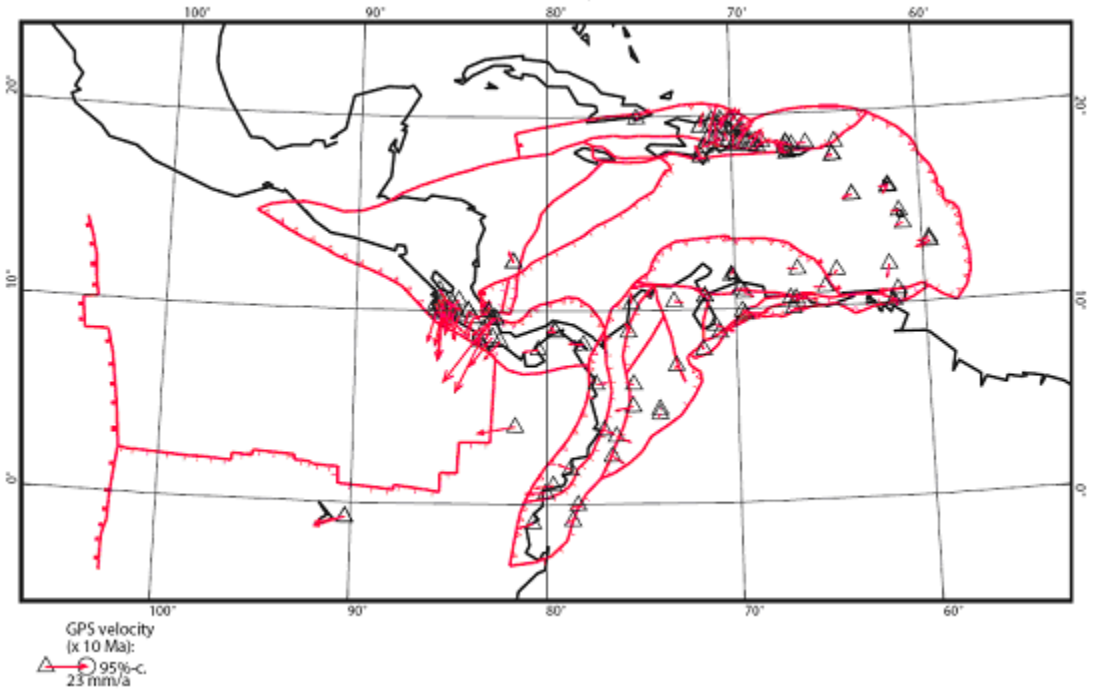

Figure 25. Geodetic misfits for the lowest average velocity misfit model with parameters of 1323 K, 40 mm/yr basal velocity, and a fault friction coefficient of 0.12.

6.2 RESULTS USING VELOCITY AND DIRECTION OF COCOS PLATE

The surface velocity results using a basal velocity field derived from the velocity of the Cocos plate relative to the Caribbean (Kreemer et al., 2003) are presented in figure 26. The average surface velocity of the Cocos and Nazca plates range between 40 and 80 mm/yr. The high velocities of these plates are largely a function of their thin lithosphere, allowing the basal velocity field of the model to be closer to the surface. A more significant observation from these results is the single digit velocities for the Caribbean plate. These low velocity values are likely a function of two controlling variables. The first is the thicker lithosphere of this plate and the consequent deeper basal velocity field. The second variable is likely related to the eastward component of the basal velocity vector, which in this case is weaker due to the stronger northward component of the basal velocity field that moves thirty degrees east of north. This would suggest that, in order for the Caribbean plate to move faster to the east, a stronger eastward component of the basal velocity field is required. The velocity misfits of the model relative to the geodetic measurements can be seen in figure 27. The most prominent feature is the large northward misfit for the Nazca plate. This misfit suggests that while the thirty degree east of north basal velocity field may be appropriate for the Cocos plate, it is clearly unsatisfactory for the Nazca plate.

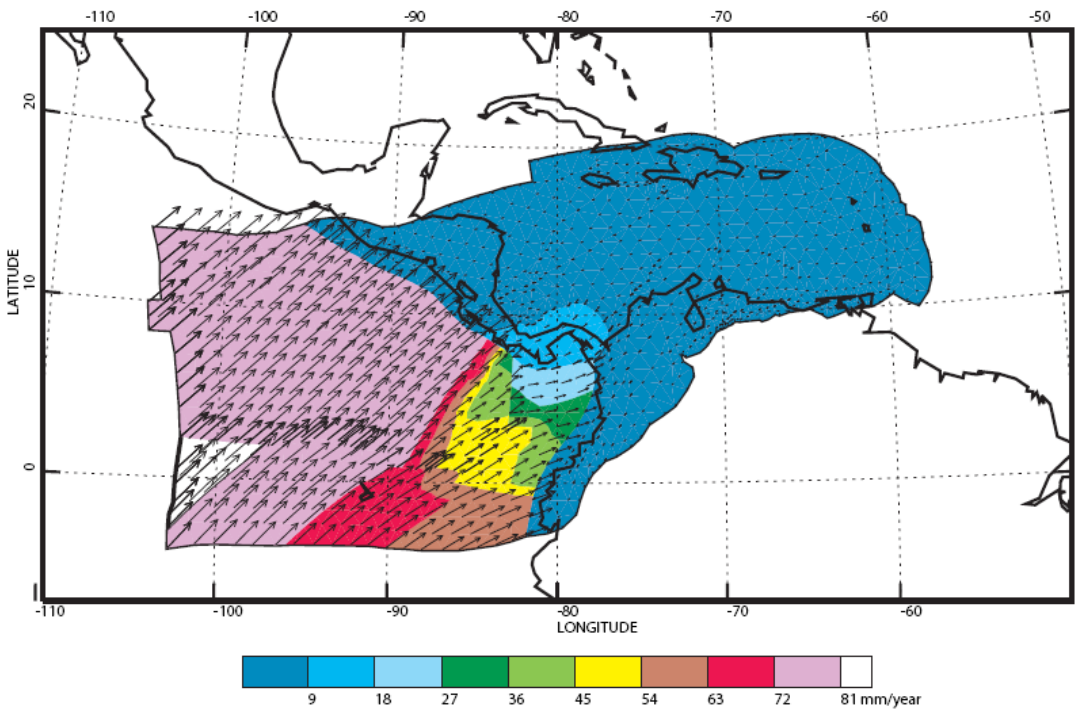

Figure 26. Most of the Cocos and Nazca plates have surface velocities between 40 and 80 mm/yr, whereas velocities in the Caribbean plate are in the single digits. The large velocity contrast between the Cocos and Caribbean plates results in the high subduction rates along the Middle America Trench observed in figure 28. However, the lack of contrast along the boundary between the Cocos and Nazca plates is equally responsible for the lack of fault extension here. These results would also appear to suggest that in order for the Caribbean plate to move there must be a more eastward component to the basal velocity field; otherwise the plate will not move.

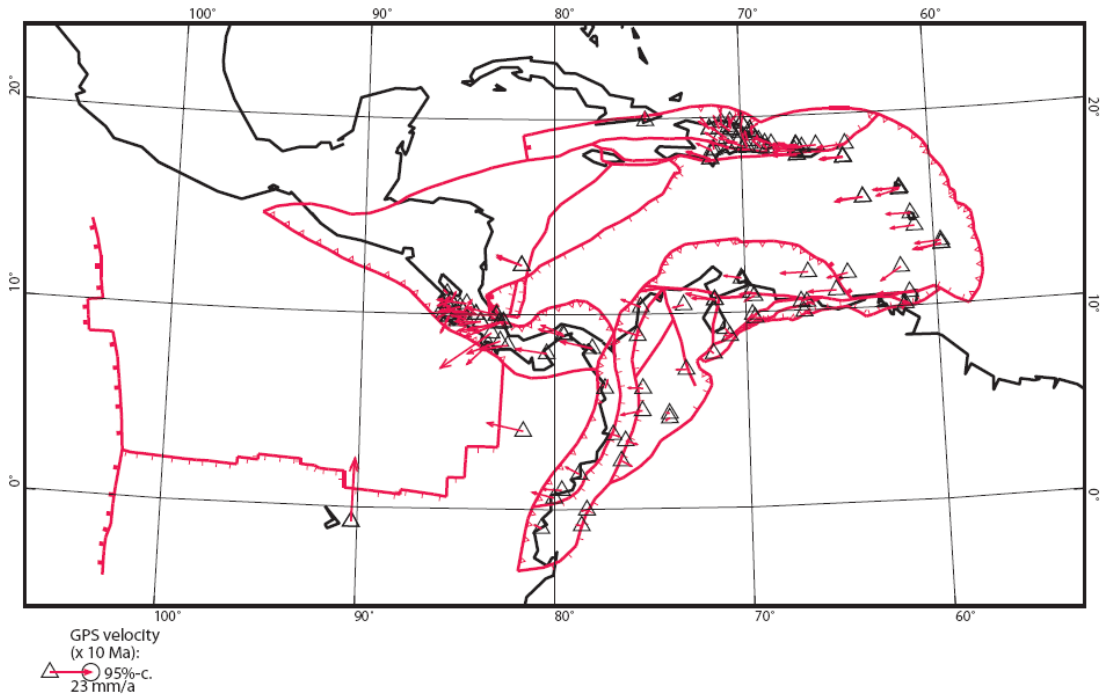

Figure 27. Geodetic misfits from a model using a Cocos plate velocity of 80 mm/yr in a direction 30 degrees east of North. The isothermal temperature was set at 1373 K and the coefficient of friction for the faults was set at 0.12. The most notable misfit is with respect to the Galapagos, which indicates that the Nazca plate in the model moves northward instead of eastward. In addition, the geodetic misfits suggest that the eastern Caribbean is not moving fast enough to the east.

The fault slip rates from the model are illustrated in figure 28. The slip rates are very poor with the exception of the MAT, where subduction occurs at a rate very close to the average rate of 75.5 mm/yr estimated by Kreemer et al. (2003). Subduction also occurs along the boundary between the Nazca and South American plates, but approximately 20 mm/yr slower than the 55.8 mm/yr estimated by Kreemer et al. (2003). The slip rates along the northern, eastern, and southern boundaries of the Caribbean plate are in the single digits, and spreading within the Cayman Trough is nearly non-existent. In addition, many of the faults within the North Andes plate and the northern Caribbean plate are locked. There is accurate prediction of right-lateral motion along the Panama Fracture to the north, which

indicates northward motion of the Cocos plate; however, the extensional faulting between the Cocos and Nazca plates is much smaller than the maximum of 60 mm/yr estimated by Kreemer et al. (2003).

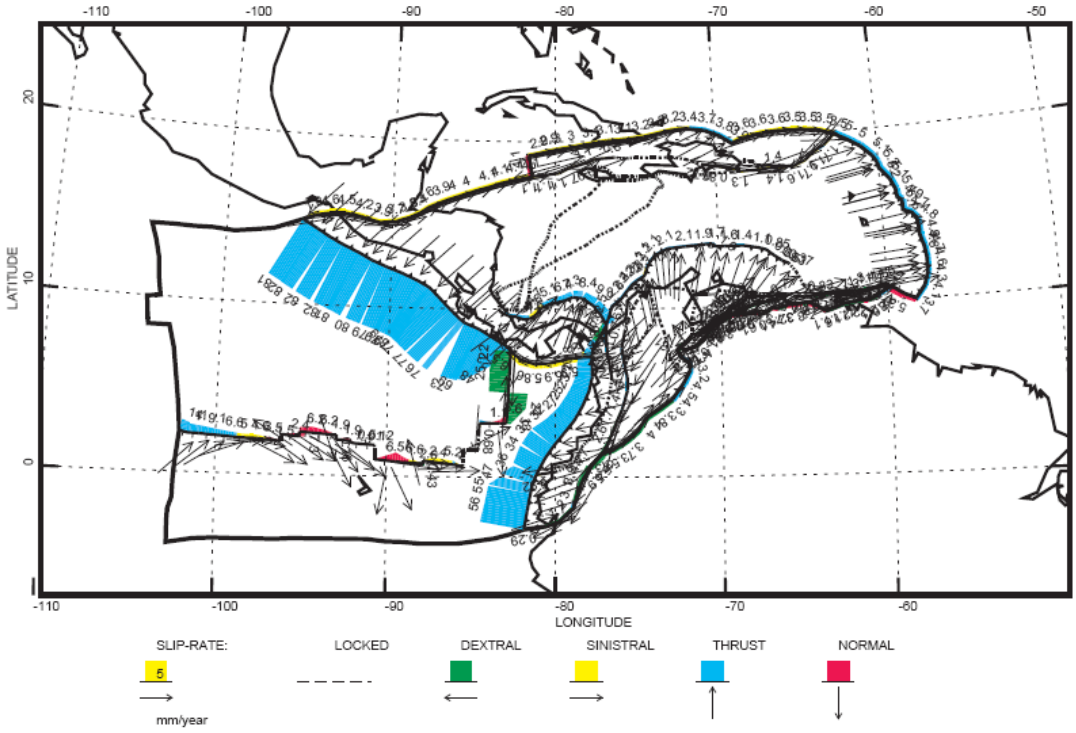

Figure 28. Fault slip rate results for a model with a basal velocity field of 80 mm/yr at 30 degrees east of north, which is consistent with the closing rate between the Cocos and Caribbean plates as determined by the GSRM model (Kreemer et al., 2003). The results are very poor with the exception of the subduction rate along the Middle America Trench. One surprising result is the very low extension rate between the Cocos and Nazca plates, which might suggest a problem with the model at this location as the entire Nazca plate was not included in the model.

The direction of the maximum horizontal principal stress of this model is presented in figure 29. The pervasive extensional features along the boundary between the Caribbean and South American plates, along Venezuela, are contrary to the thrust and strike-slip faults that make up the majority of the tectonic features along this boundary. In addition, the strong compressive features that are perpendicular to the strike-slip faults along the northern boundary of the Caribbean

plate, adjacent to the Cayman trough, are contrary to the tectonic features of this region. These observations, along with the number of locked faults that occur in the Caribbean, may suggest that the Cocos plate based basal velocity field may have too strong of a northern component, such that it moves the Caribbean plate more to the north than to the east.

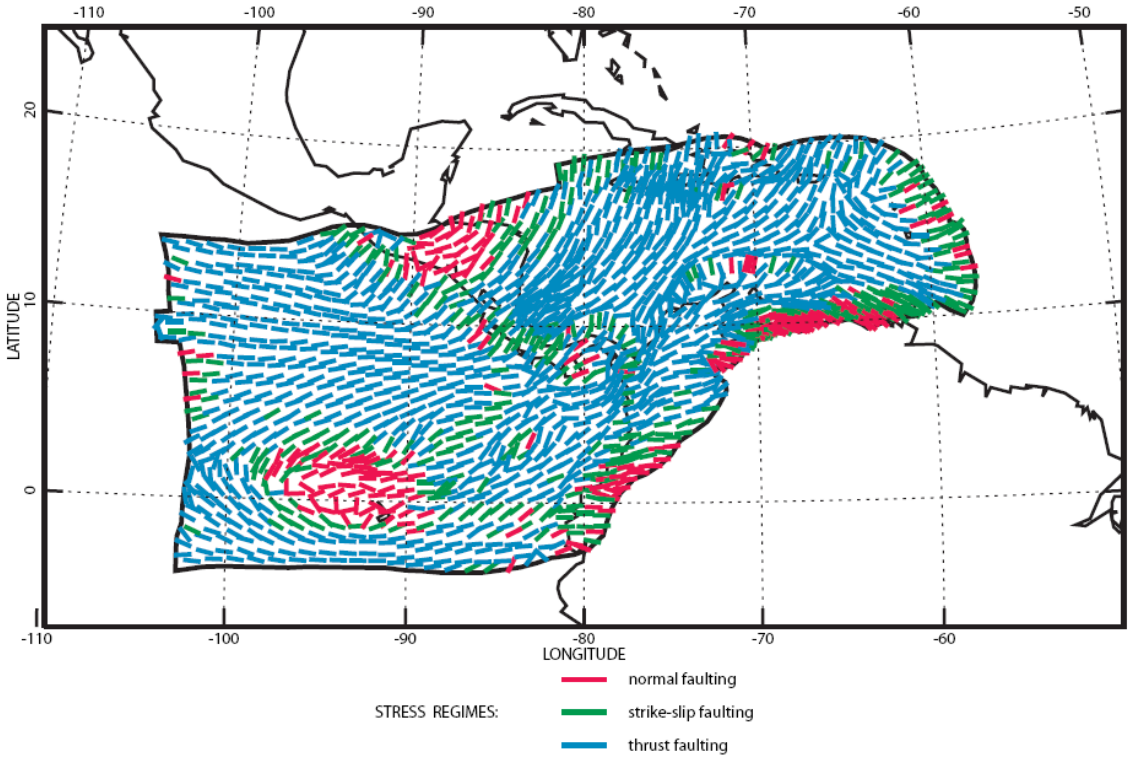

Figure. 29 Direction of the maximum horizontal principal stress calculated in the model using a basal velocity field based on the surface velocity of the Cocos plate relative to the Caribbean plate.

In summary, a basal velocity field similar to that of the surface velocity of the Cocos plate yielded overall poor results when the full model was reviewed with respect to surface velocity, fault-slip rates, and maximum horizontal principal stress directions. In particular, the number of locked faults provides the strongest evidence that this particular basal velocity field is incapable of moving the plates in the correct direction.

6.3 RESULTS OF EASTWARD MODEL WITH REFINED PARAMETERS

The model parameters consisting of a temperature of 1373 K, a basal velocity of 100 mm/yr, and a fault friction coefficient of 0.12 had the lowest overall misfit and the best fit to the MAT subduction zone. This model had an average velocity misfit of 9.3 mm/yr, a spreading misfit at the Cayman trough of 2.7 mm/yr, a stress direction misfit of 28.9 degrees, and a relatively lower subduction misfit of 18.1 mm/yr. Additional parameter testing was carried out to further refine the model. The parameters of 1380 K, a basal velocity of 100 mm/yr, and a fault friction coefficient of 0.10 yielded the optimum results based on a combination of the minimum velocity misfit, minimum spreading misfit for the Cayman trough, and minimum subduction misfit along the MAT. Using these values, the average velocity misfit was 9.1 mm/yr, a spreading rate misfit along the Cayman Trough of 1.6 mm/yr, a stress direction misfit of 28.1 degrees, and a subduction rate misfit of 20.5 mm/yr along the MAT. The slight increase in subduction misfit along the MAT was expected due to the slight increase in temperature which reduced basal shear in the model.

6.3.1 QUALITATIVE REVIEW OF EASTWARD BASAL MODELS

A qualitative review of the results using the refined parameters above starts with the surface velocity rates and directions illustrated in figure 30. The most striking result is the large velocity contrast between the Cocos plate and the entire western boundary of the Caribbean plate. The velocities abruptly transition from a range between 70 to 100 mm/yr in the Cocos plate to a range between a few mm/yr and 30 mm/yr in the Caribbean plate. The majority of the surface velocity within the Nazca and Cocos plates point predominantly due east, whereas the surface velocities

within the Caribbean plate vary from east to northeast. The second most important observation is with respect to the velocity vectors of the North Andes plate. The velocity vectors point to the northeast in the southern portion of the plate and gradually “roll over” the northwest tip of South America and ultimately point due east adjacent to Venezuela.

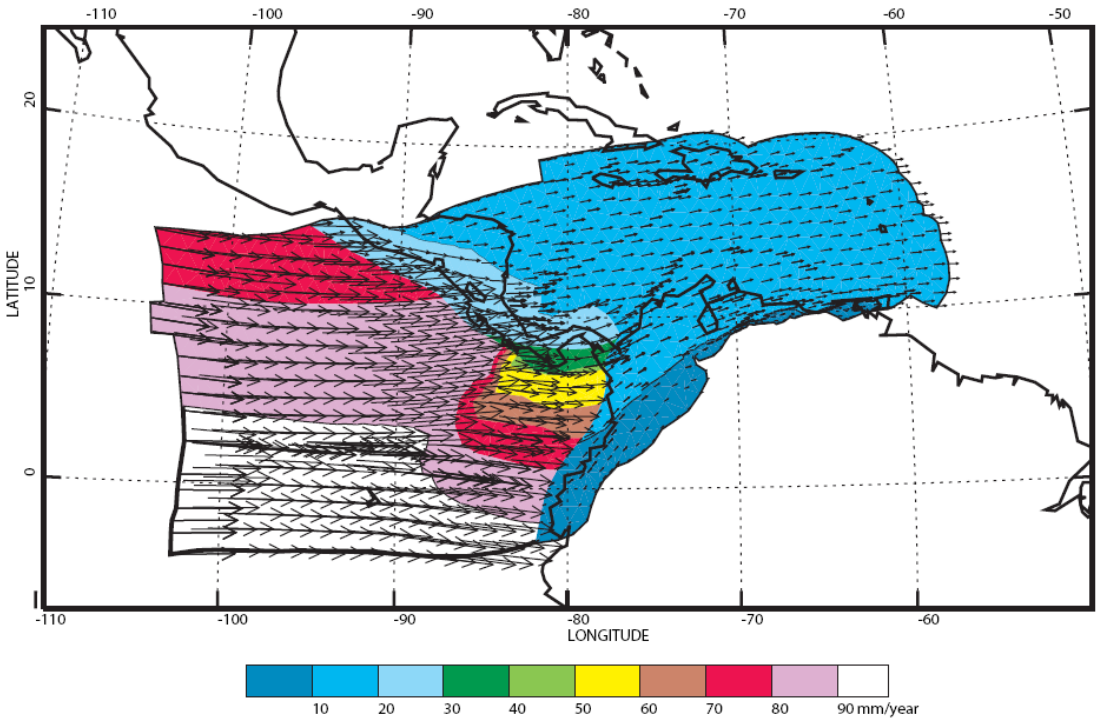

Figure 30. Surface velocity results using the revised parameters of 1380 K, a basal velocity of 100 mm/yr, and a fault friction coefficient of 0.10. The most notable feature is large velocity contrast between the Cocos and Nazca plates and the entire western boundary of the Caribbean plate. The second important observation is with respect to the velocity vectors of the North Andes block. The vectors have a strong north-north-east component in the south of the block and rotate eastward over the tip of northwest South America where they ultimately point predominantly due east in eastern Venezuela. Both features are significant due to the fact that the basal velocity model was held constant at 100 mm/yr due east.

The highest surface velocities in the model occur along the boundary between the Cocos and Nazca plates. This is likely a function of the surface heat flow values used to build the model in this area. The high heat flow in this region (figure 11)

likely produced an underestimation of the total lithosphere thickness. In places where the lithosphere is thin the asthenosphere is closer to the surface, and therefore the basal velocity field is also close to the surface. In this particular region, the surface velocity ranges between 80 and 90 mm/yr, and is close to the basal velocity of 100 mm/yr applied to the model. This is a major drawback of using heat flow data to build the physical characteristics of the model, but it is the best method currently available. Several modifications of the heat flow values of the grid in the problematic region were made in attempt to alleviate the problem. However, the results from these modified values were typically an order of magnitude worse than the original model results. The failure of the heat flow modifications to yield better results is likely related to the fact that the calculation of the total lithosphere thickness is based on a computational relationship between heat flow and elevation. Therefore, arbitrary modifications of either of these values will likely lead to unreliable calculations of the total lithosphere thickness. Another potential reason for this error can be related to the fact that only a small portion of the Nazca plate is included in the model and therefore may not be modeled properly. Boundary conditions were added to the southern boundary of the Nazca plate in half of the models run to address this problem, which did result in a reduction of this velocity error, but did not remove it entirely.

The fault slip rates in the model are presented in figure 31. In general, the fault slip directions are in good agreement with the observed fault slip directions of the region. Left-lateral strike-slip predominantly occurs along the northern boundary with the North American plate, whereas extension occurs along the Cayman trough at approximately 18 mm/yr, well within the observed range of 12 to 20 mm/yr

(Macdonald & Holcombe, 1978; Rosencrantz & Sclater, 1986; Leroy et al., 2000). Right-lateral strike-slip, with minor extension, is the predominant feature along the southeast boundary of the model region with South America. Right-lateral strike-slip is also the predominant feature along the southwest boundary of the model region where the North Andes plate abuts the South American plate.

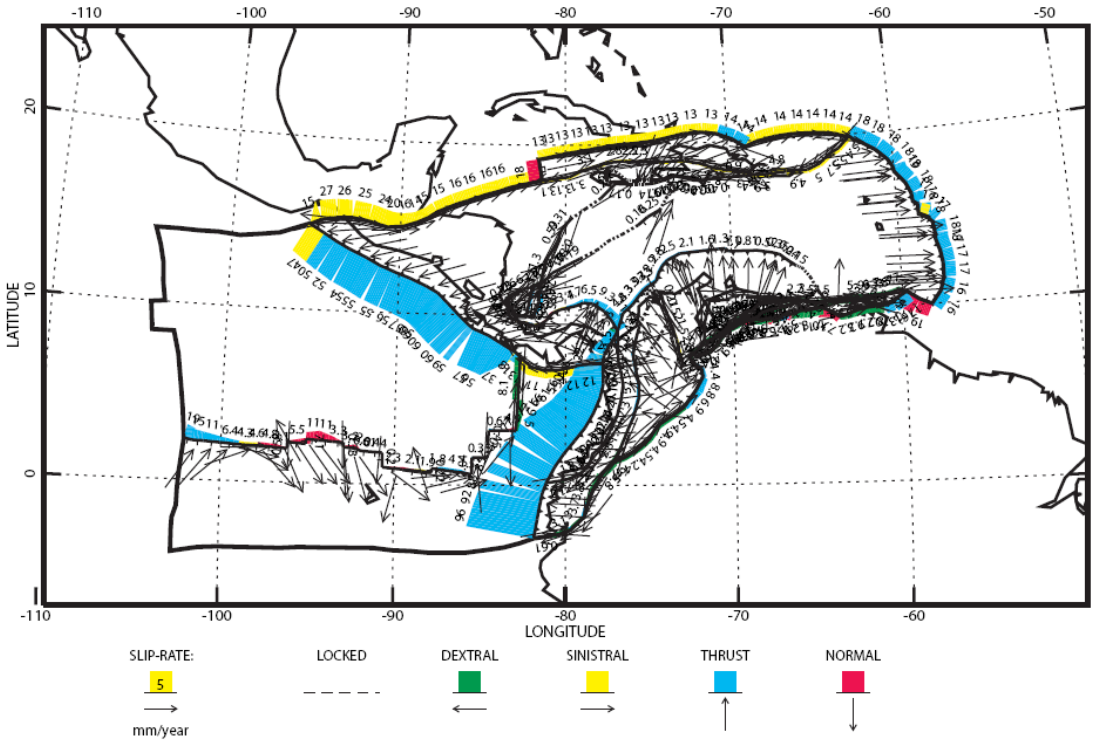

Figure 31. Fault slip rates using the revised parameters of 1380 K, a basal velocity of 100 mm/yr, and a fault friction coefficient of 0.10. The spreading rate of the Cayman Trough is 18 mm/yr, which is consistent with the 12 to 20 mm/yr estimated rates (Macdonald & Holcombe, 1978; Rosencrantz & Sclater, 1986; Leroy et al., 2000). Subduction occurs along the MAT but at a slightly slower rate than that predicted by the global plate model GSRM (Kreemer et al., 2003). Subduction occurs along the boundary between the Nazca and South America plates, but at a slightly higher rate than that predicted by the same global model. Spreading also occurs along the boundary between the Cocos and Nazca plates, but also at a rate slower than estimated by the global plate model.

Within the North Andes plate (figure 32) minor left-lateral strike-slip occurs along the Santa Marta Bucaramanga fault, thrusting occurs along the Central Cordillera, and the Western Cordillera is locked. The Oca fault is also locked, which

is the case for most of the models examined. There is subduction north of Panama and left-lateral strike-slip south of Panama. Northeastward subduction also occurs along the MAT, whereas near due east subduction occurs at the boundary between the Nazca and South America plates. The high rate of subduction between the South American and the Nazca plates is likely due to the excessive velocity of the Nazca plate as discussed above. The majority of these results are in good agreement with respect to the observed fault types and direction of slip. However, they vary in agreement with respect to the observed slip rates.

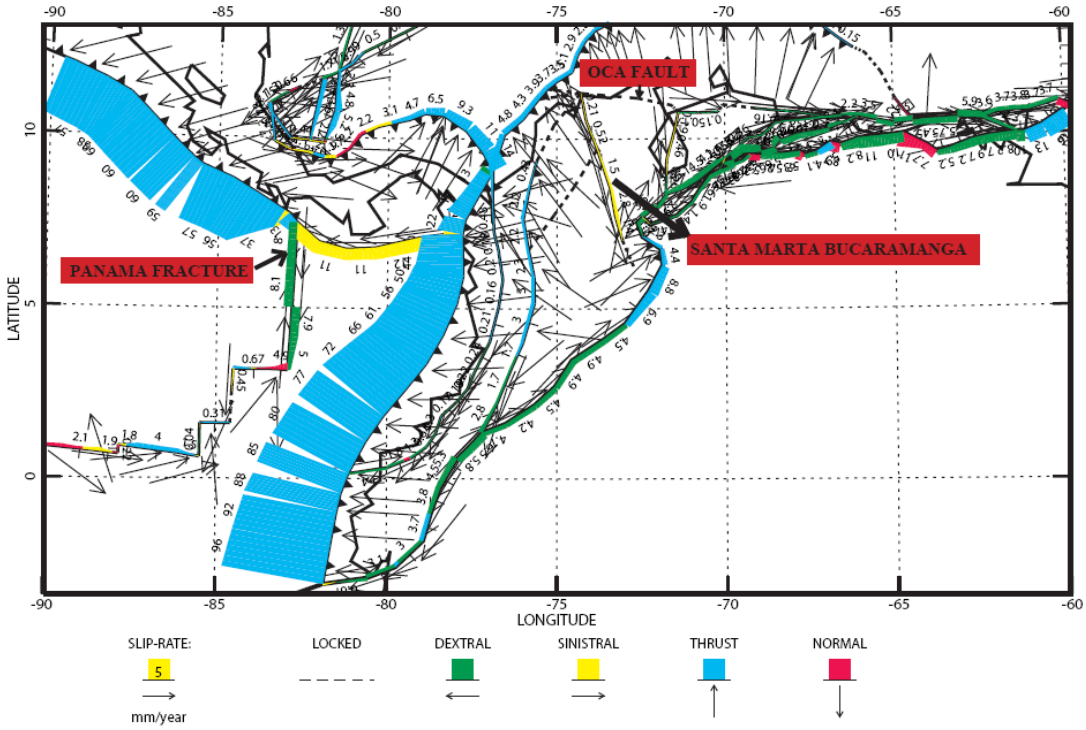

Figure 32. Close-up view of North Andes and Panama Fracture fault slip results using the model parameters of 1380 K, a basal velocity of 100 mm/yr, and a fault friction coefficient of 0.10. A key observation is the north-south right-lateral slip of the Panama Fracture which is perpendicular to the underlying due east basal velocity field of the model. While the slip rate is significantly slower than the global model estimates, it clearly demonstrates that plate motions observed on the surface do not necessarily represent the underlying flow pattern that drives the plate.

One of the more important observations of figure 32 is with respect to the north-south right-lateral slip motion of the Panama Fracture. It is significant because the fault essentially moves perpendicular to the underlying eastward basal velocity field of the model. Admittedly, the slip rate is much slower then the estimated rate of 50 mm/yr or greater (Cowan, 1998). However, the movement of this fault, and that of the North Andes plate, clearly demonstrates the concept that surface velocities of tectonic plates may not necessarily correspond to the underlying flow pattern that drives their surface motion.

A greater degree of complexity is further revealed by the direction of the maximum horizontal principal stress results of the model in figure 33, which indicate that most of the Caribbean plate is in a state of compression in varying directions. A notable exception to this is the large area of extension in Guatemala, Honduras, and Nicaragua, which continues into the continental shelf along the Nicaragua Rise to the Cayman trough. There are other smaller regions of extension directly adjacent to Venezuela as well. The extensional features in Guatemala and Honduras are consistent with the tectonics of the region (Caceres et al., 2005; figures 34 & 35), as are the extensional features in Nicaragua, the Nicaragua Rise, and the Cayman trough (figure 36). In addition, the extensional features observed along the southeast boundary of the model region appear geologically reasonable as they occur in proximity to the Los Roques Canyon just north of Venezuela, which is bounded by a series of normal faults (figure 37). The isolated segment of extensional stress in the far southeast of the model region between the North Andes block and South America is likely a function of gravitational slide. At this location, the boundary fault lies

directly on a topographic high along the Andes. The combination of the boundary being a fault, together with the massive change in relief over a span of less then three degrees between the mountain high and the ocean low, likely produces a landslide affect in the model. Another notable area of extension occurs at the boundary between the Cocos and Nazca plates. However, in this case, the orientation of extension is in the east-west direction, which is contrary to the north-south extension that actually occurs along this spreading ridge. This is the largest misfit in the model with respect to most compressive stress axis results. One explanation for this misfit may be related to the fact that only a small portion of the Nazca plate is included in the model.

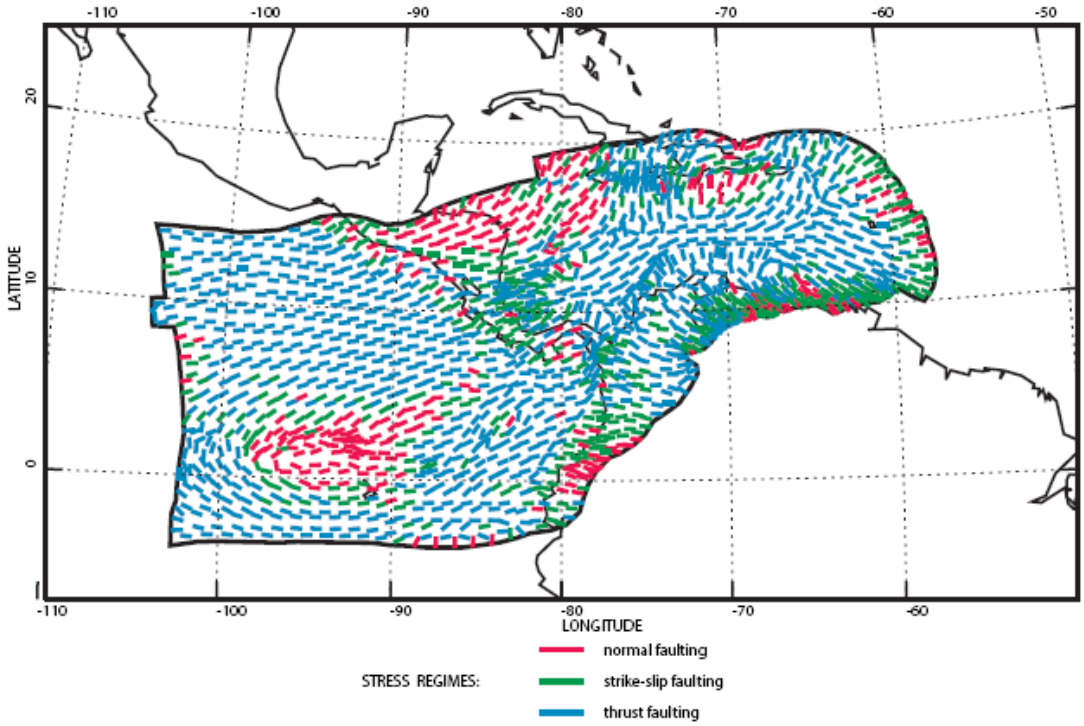

Figure 33. Direction of the maximum horizontal principal stress calculated in the model using the parameters of 1380 K, a basal velocity of 100 mm/yr, and a fault friction coefficient of 0.10. Most of the model is in a state of compression with several areas of extension. The only extension within the Nazca plate is along its boundary with the Cocos plate. The axial direction is variable, with some axis being oriented northeast-southwest and others east-west. With respect to the Caribbean plate, the largest area of extension is located in Guatemala and Honduras, which is consistent with several of the previous models. The extensional features north of Venezuela are mixed with a large percentage of shear stress, which would seem consistent with a large strike-slip fault system. The segment of extension in the far south segment of the southeast boundary of the model, between the North Andes block and South America, is likely an artifact of gravitational slide in the model due to the boundary being a fault with a massive change of relief over a span of less then three degrees.

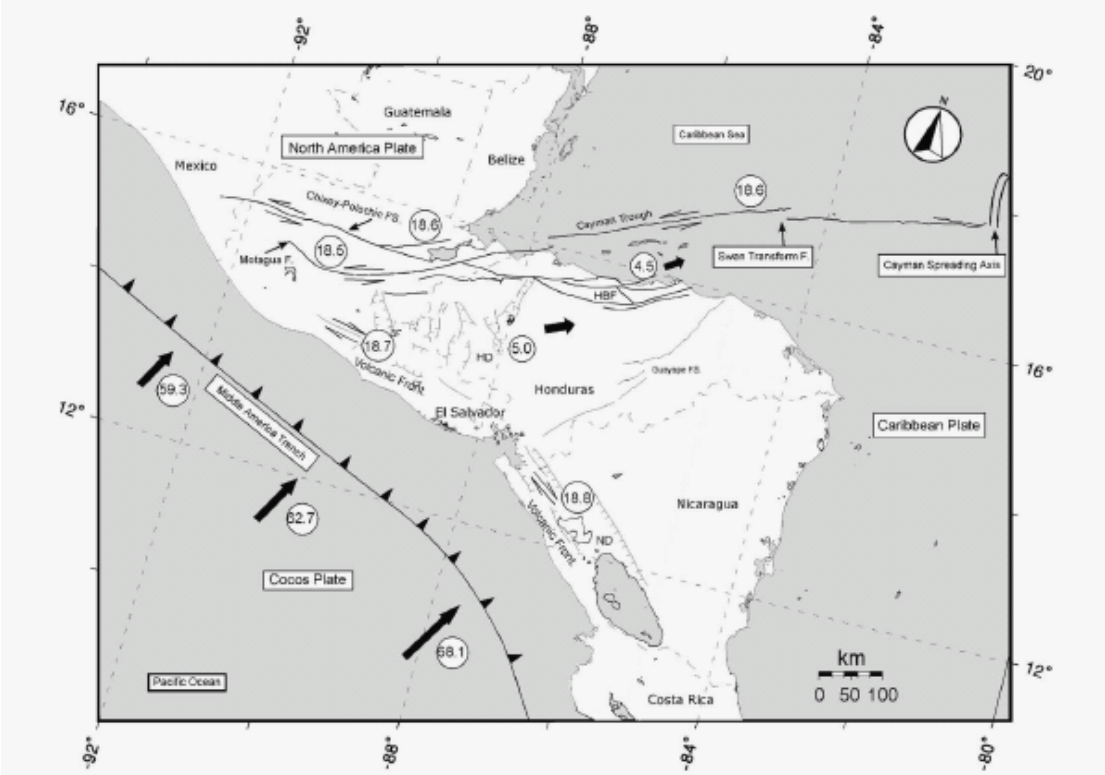

Figure 34. Tectonic setting of northern Central America. FS is fault system, HD is the Honduras depression, ND is the Nicaragua depression. Values and arrows indicate relative plate velocities (mm/yr) with respect to North American plate from NUVEL-1A in DeMets et al. (1990). Values for the Middle America Trench are from McNally and Minister (1981). Values for the North American-Caribbean plate Boundary from DeMets et al. (2000). (Figure taken from D. Caceres et al., 2005)

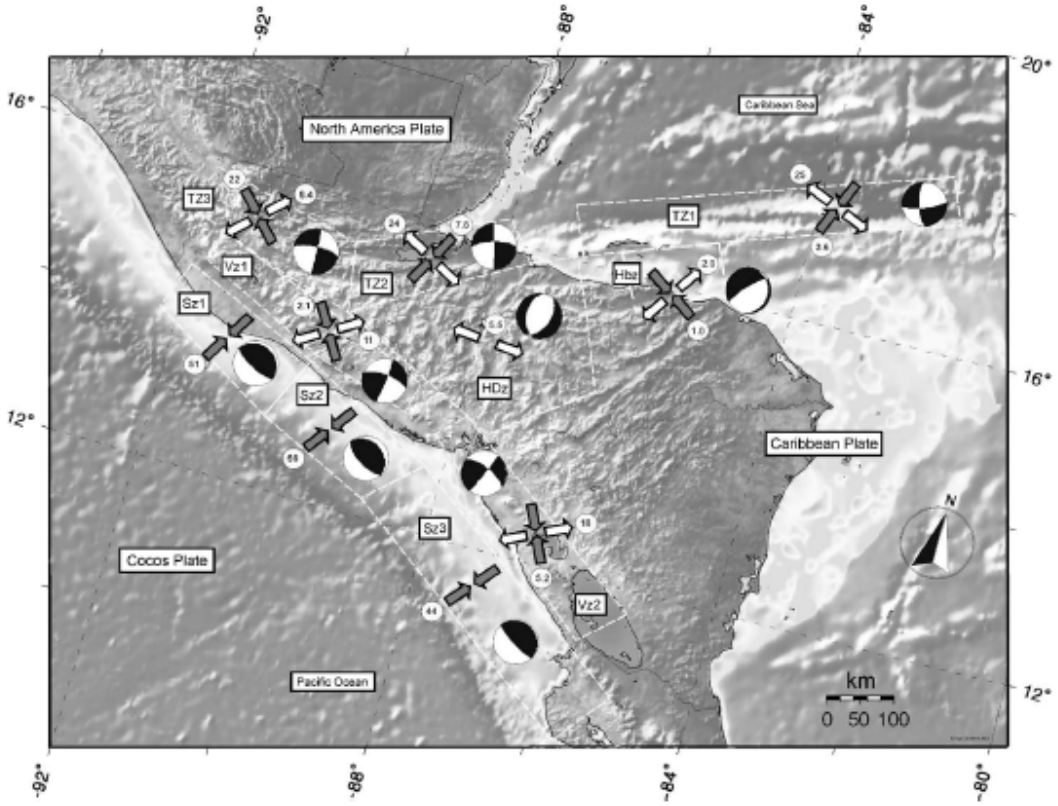

Figure 35. Topography map and distribution of deformation velocities for seismogenic zones into which northern Central America is divided. Values in circles are in mm/yr. Gray arrows indicate compression, white arrows extension. Focal spheres represent the average focal mechanism for each zone (Figure taken from D. Caceres et al., 2005).

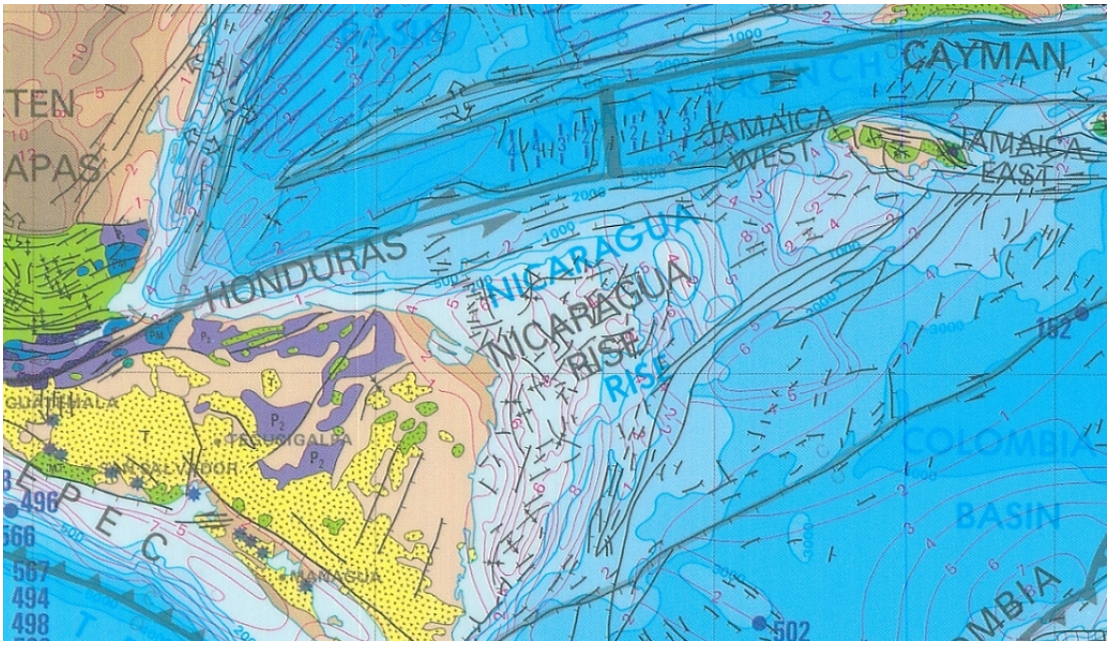

Figure 36. Extensional features of Nicaragua, the Nicaragua Rise, and the Cayman Trough, which are consistent with the extensional features indicated by the most compressive stress axes results of the model (Figure taken from Tectonic Map of the World; AAPG, 1994).

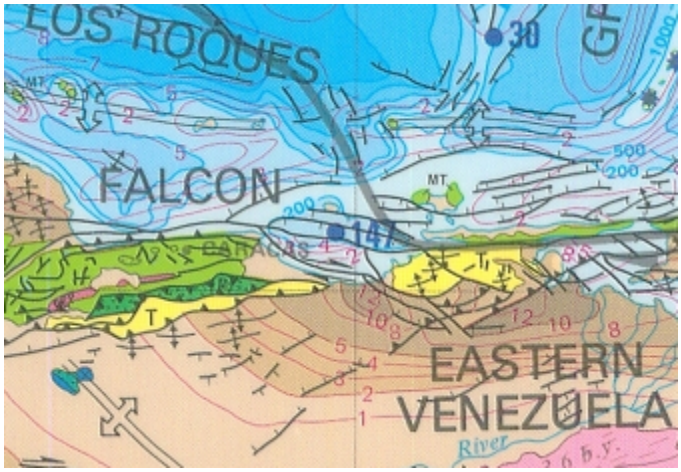

Figure 37. Significant extensional features just north of Eastern Venezuela that appear consistent with the extensional features indicated by the most compressive stress axes results of the model (Figure taken from Tectonic Map of the World; AAPG, 1994).

6.3.2 QUANTITATIVE REVIEW OF MODEL RESULTS

Two methods were used to quantitatively examine the result from the finite element modeling. A supporting program to SHELLS, called ORBSCORE, was used to evaluate the entire model using 131 geodetic measurements, 16 stress direction measurements, and 16 seafloor spreading rate measurements that fell within the model. In addition, a detailed velocity analysis was done for the Caribbean and North Andes plates. This method involved using the seven GPS stations examined by Weber et al. (2001) to determine the most recent Euler pole of rotation between the South American and the Caribbean plates. During construction of the model, seven nodes were placed in the model that corresponded to these GPS stations. The North Andes plate was evaluated by comparing the results for seven nodes within the plate to the estimated plate velocity determined by Kellogg et al. (1985), Freymueller et al. (1993), Kellogg and Vega (1995), Kellogg et al. (1996), and Trenkamp et al. (1996). In all cases, the velocity misfits presented are with respect to a fixed South American plate.

6.3.3 EVALUATION OF ENTIRE MODEL USING ORBSCORE

Using ORBSCORE, the model had an average velocity misfit of 9.1 mm/yr, and a worst single misfit of 66.3 mm/yr. A graphical representation of the velocity misfits over a 10 million year period is presented in figure 38. The errors for the Caribbean and North Andes plate are quite small. The results from the model have the Galapagos moving toward South America at a rate of 95 mm/yr (close to the basal velocity condition) in a direction of 95.7 degrees from east of north. The GSRM global plate model (Kreemer et al., 2003) predicts the Galapagos to move toward

South America at a rate of 55.8 mm/yr in a direction of 87.7 degrees from east of north. This is a misfit of nearly 40 mm/yr too fast. However, it is important to note that the misfit in direction is only 8 degrees. The velocity misfit in this region was significantly lower for the model where velocities relative to South America were applied to the lower boundary of the incomplete segment of the Nazca plate that made up the model.

The errors in heat flow data for the Cocos and Nazca plate portions of the model may also explain the fault slip rate misfits observed along the major subduction zones on the western side of the model. The rate of subduction for the MAT averages 55 mm/yr, which is approximately 20 mm/yr too slow relative to the predicted rate of 75.5 mm/yr taken from global plate model GSRM (Kreemer et al., 2003). In addition, the subduction in the model between the Nazca and South American plates averages 86 mm/yr, which is 20 mm/yr to fast with respect to the estimated values of GSRM. Spreading between the Cocos and Nazca plates occurs in the model at a maximum rate of 11 mm/yr, which is considerably lower than the 60 mm/yr rate estimated by GSRM. However, the spreading rate between the Cocos and Nazca plates did not improve in the model where velocity boundary conditions along the southern boundary of the Nazca plate were applied relative to South America.

An evaluation of the 16 stress measurements that fell within the model gave a mean azimuthal misfit of 28.2 degrees. These results are rather good based on the discussion above, where good model results are considered to be those where the

azimuthal difference between the field data and model results are close to 25 degrees. Had the model results been poor, the azimuthal difference between the field data and model results would have been closer to 45 degrees.

While there were sixteen seafloor spreading data points available for use by ORBSCORE, only the spreading ridge of the Cayman Trough was closely examined. The spreading rate misfits between the Cocos and Nazca plates were discussed above and the spreading rate along the EPR was very close to the predicted rate by GSRM; this is expected as the basal velocity field was set to approximate the spreading rate of the EPR. The spreading rate of the Cayman Trough was approximately 18 mm/yr, which yielded a very low spreading rate misfit of only 1.6 mm/yr.

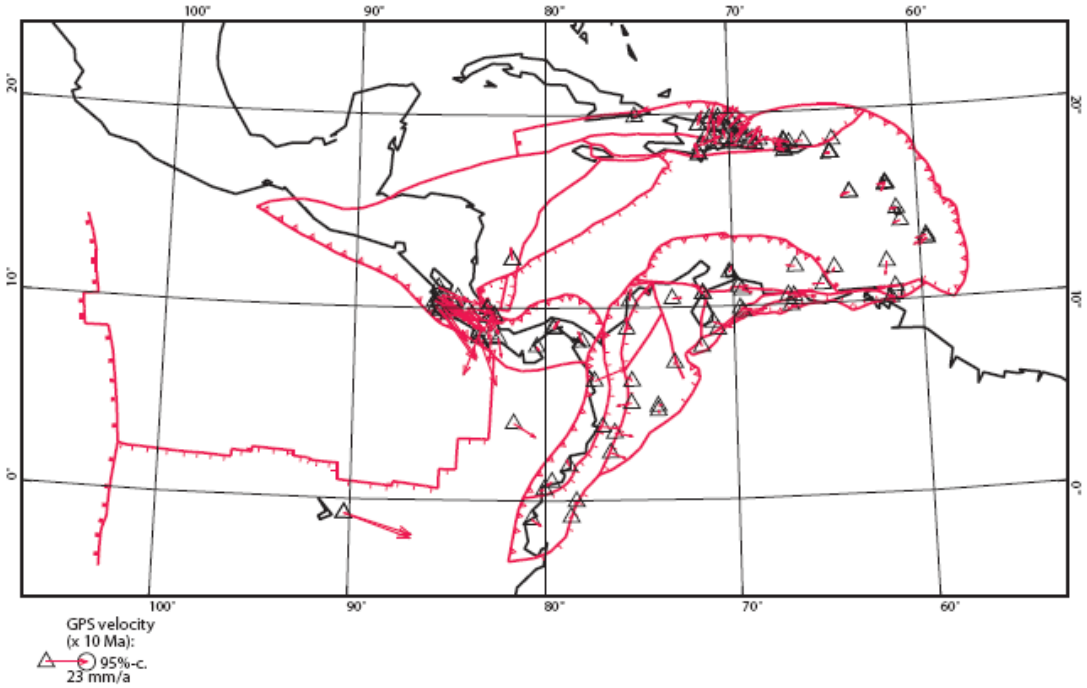

Figure 38. Model geodetic misfits over a 10 Ma period using the model parameters of 1380 K, a basal velocity of 100 mm/yr, and a fault friction coefficient of 0.10. The arrows represent the velocity "misfit" of the model, and point in the direction where the model is either moving too fast or to slow with respect to South America. The arrows indicate a very good fit between the geodetic data and model results for the Caribbean and North Andes plates. The largest misfit occurs in the Nazca plate at the Galapagose GPS site which gave a velocity magnitude misfit close to 40 mm/yr too fast, but a velocity directional misfit of only 8 degrees (Kreemer et al., 2003). The velocity magnitude misfit is most likely a consequence of an error in the physical model that can not be resolved at this time.

6.3.4 DETAILED EXAMINATION OF CARIBBEAN PLATE RESULTS USING INDIVIDUAL GPS STATION DATA WITHIN THE PLATE

Nodes were place in the model at the exact locations of the seven GPS stations used by Weber et al. (2001) to determine the most recent Euler pole of rotation between the South American and the Caribbean plates. This was done to limit some of the bias in the clustering of the geodetic measurements within the model that may not have been handled as well by ORBSCORE. The velocity and directional results of these seven nodes, with respect to South America, are presented in table 3. The average velocity for these nodes, as determined from the Euler pole, should be 19.4 mm/yr. The average from the model was 16.0 mm/yr. This gives a mean misfit of 3.6 mm/yr, which is a further reduction of the velocity misfit calculated by ORBSCORE. The mean direction of the seven GPS stations, as determined from the Euler pole, should be 91.4 degrees from North. The results from the model yielded an average of 84.0 degrees. This gives a median directional misfit for the model of 6.9 degrees relative to the Euler pole. The largest directional misfit is with respect to the San Andres Islands, which appeared to be a consistent misfit in other model runs, and is the reason the median, instead of the average, was used to evaluate the directional misfit.

	OBSERVED	OBSERVED	MODEL	
GPS Stations (Weber et al., 2001)	**DIRECTION**	**VELOCITY**	**DIRECTION**	**VELOCITY**
Aves Island	91.4	27.8	84.5	16.6
Barbados	83.9	18.7	88.4	15.9
St. Croix	88.7	16.6	83.9	16.9
Puerto Rico	91.5	16.3	79.1	12.0
Dominican Republic	96.6	16.7	78.4	16.4
San Andres Islands	105.1	19.7	80.5	18.6
Trinidad	85.9	19.6	86.6	14.9
MEAN VALUE	**91.4**	**19.4**	**83.9**	**16.0**
ABSOLUTE DIFFERENCE BETWEEN NODES				
Aves Island			6.8	11.2
Barbados			4.5	2.8
St. Croix			4.7	0.2
Puerto Rico			12.3	4.3
Dominican Republic			18.2	0.3
San Andres Islands			24.6	1.0
Trinidad			0.6	4.7
	MISFIT SUMMARY			
	MEAN MISFIT			**3.5**
	MEDIAN MISFIT		**6.8**	

TABLE 3. Comparison of model results to the 7 GPS stations examined by Weber et al. (2001).

6.3.5 DETAILED EXAMINATION OF NORTH ANDES PLATE RESULTS

A similar method of model calibration was performed for the North Andes plate (table 4). The nodes selected were taken from north to south in such a manner that they give a fair representation of the individual fault blocks that comprise the North Andes plate. In addition, the nodes were selected such that they represent the interior of the individual fault blocks, and thus were not associated with any fault elements. The results in table 4 are compared to the estimated movement of the North Andes plate based on both geologic and geodetic information (Kellogg et al., 1985; Freymueller et al., 1993; Kellogg and Vega (1995), Kellogg et al. (1996); Trenkamp et al., 1996). The plate is estimated to move at a rate of 10 mm/yr at an angle of 55 degrees to the northeast. The mean was taken for the velocities, whereas the median

was taken for the directional values. The average velocity of the block for the model was 9.2 mm/yr, resulting in a difference of 0.8 mm/yr from the observed. The average direction for the model results was 55.5 degrees. The velocity and directional results are therefore in very good agreement with the observed data.

NODE NUMBER FROM MODEL	MODEL RESULTS	MODEL RESULTS
	DIRECTION DEGREES FROM NORTH	Velocity mm/yr
878	67.2	15.6
845	64.0	10.3
767	59.1	11.0
764	48.5	6.3
561	44.4	9.4
630	42.2	7.3
523	56.1	4.1
MEAN VELOCITY		**9.1**
MEAN DIRECTION	**55.5**	

TABLE 4. North Andes plate velocity analysis using directions and velocities of 7 nodes within the plate which were unassociated with any fault nodes. The North Andes plate is estimated to move at a velocity of 10 mm/yr in a direction of 55 degrees from north (Kellogg et al., 1985; Freymueller et al., 1993; Kellogg and Vega (1995), Kellogg et al. (1996); Trenkamp et al., 1996).

6.4 SLAB PULL MODEL

While the focus of this study is primarily on an eastward mantle drag model, three additional simulations based on the slab pull model were run on the same finite element grid for comparative purposes. The boundary conditions along the North American portion of the model and the lower boundary of the Nazca plate were set relative to South America in all three models. In addition, the basal temperature and was set to 1380 K and coefficient of friction for the faults were set to 0.12 applied to all models.

The first of these models (SUB1) consisted of applying velocities to only those nodes in the finite element grid that occupied subduction zone boundaries along Central and South America. In addition, the model was run such that the base of the lithosphere was free from traction. The velocities for the subduction zone nodes were calculated based on the Euler poles of the Cocos and Nazca plates relative to South America. The parameters of the second model (SUB2) were nearly the same as SUB1 with the exception of the addition of velocities to the nodes along the subduction zone in the Caribbean adjacent to the North Andes plate. The velocities were determined using the Euler pole of rotation for the Caribbean plate relative to South America. The third model (SUB3) was identical to SUB2 with the exception that basal traction was applied to the model. The basal velocity field for all models was set to zero.

6.4.1 SUB1 RESULTS

The surface velocity results for SUB1 are shown in figure 39 with the geodetic errors presented in figure 40 and fault slip rates displayed in figure 41. One of the basic goals of running SUB1 was to determine if the forces from the subducting slabs of the Cocos and Nazca plates were significant enough to be responsible for the movements of Caribbean and North Andes plates. A review of the surface velocity results, geodetic error results, and fault slip rates for this model suggest this to be unlikely. The average geodetic error for the model was 12.8 mm/yr. The stress direction error was error very good at 25.5 degrees. However, close examination of the fault slip rates in figure 41 reveal that all of the faults within the Caribbean plate were locked. In addition, the interior velocities of the nodes within the Caribbean plate had velocities of less than 1 mm/yr. With respect to the Cocos

and Nazca plates, the magnitude and direction of the surface velocity field, and fault slip rates, appear “reasonable” based on both GPS measurements and the global plate model of Kreemer et al. (2003). On the other hand, it is noteworthy that the geodetic error related to the Galapagos was 14.6 mm/yr, which is surprisingly high considering that boundary conditions were applied to the base of the Nazca plate as well as along the subduction zone between the Nazca and South American plates. In general, the results for SUB1 were reasonable for the Cocos and Nazca plates, but were very poor for both the Caribbean and North Andes plates. One additional noteworthy result that points to this being an unsuccessful model can be seen in the direction of the maximum horizontal principal stress along the southeast boundary of the model between the Caribbean and South American plates (figure 42). The stress results here would suggest a high concentration of normal faulting, which is contrary to the actual tectonic features at this location which are predominantly associated with thrust and strike-slip faulting.

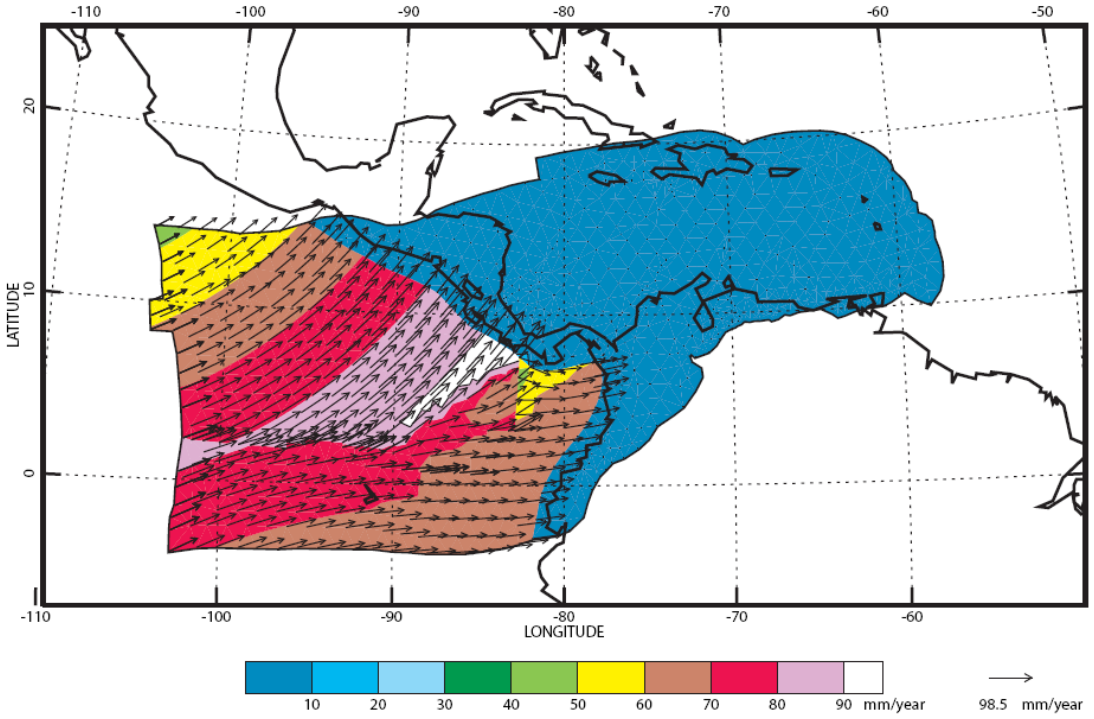

Figure 39. Surface velocity results of SUB1 using velocities assigned to nodes along the subduction zones adjacent to Central and South America; relative to SA. The basal velocity field was set to zero, and the base of the lithosphere was traction free. The basal temperature was set to 1380 K, and a fault friction of 0.12.

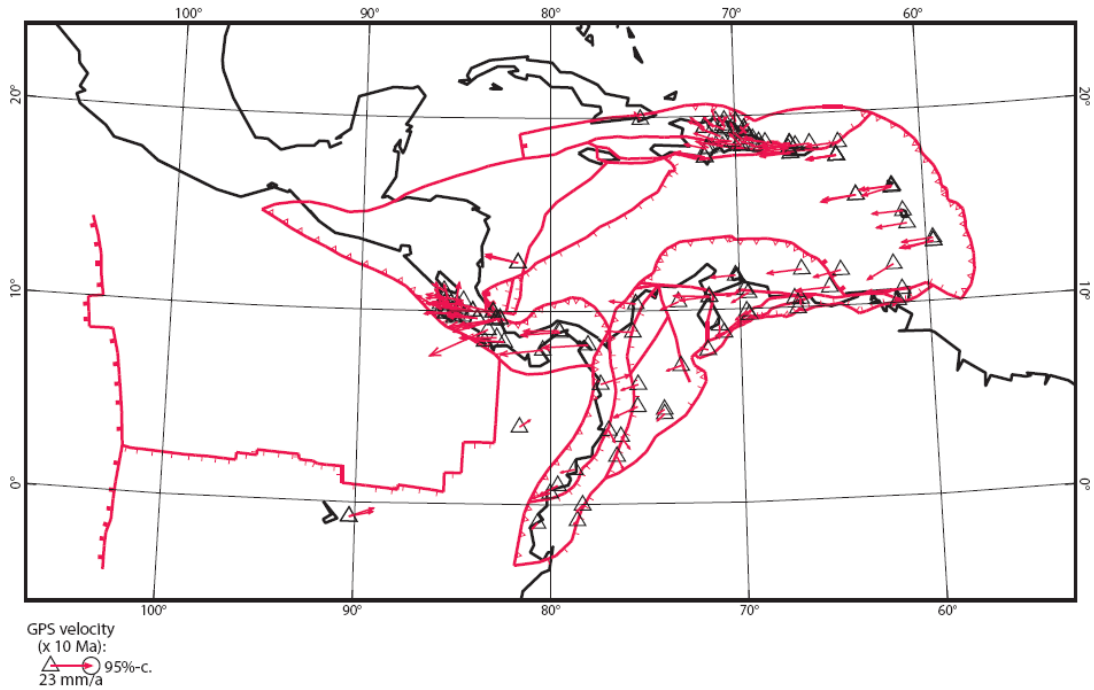

Figure 40. Geodetic errors for model SUB1.

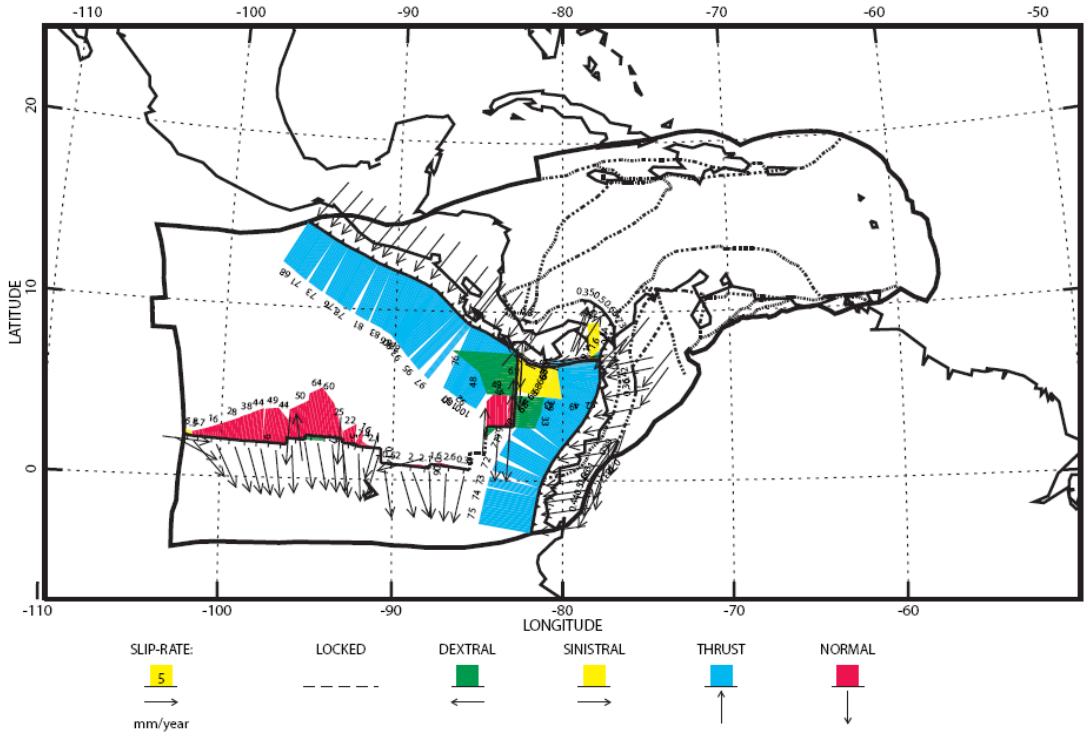

Figure 41. Fault slip rates for model SUB1.

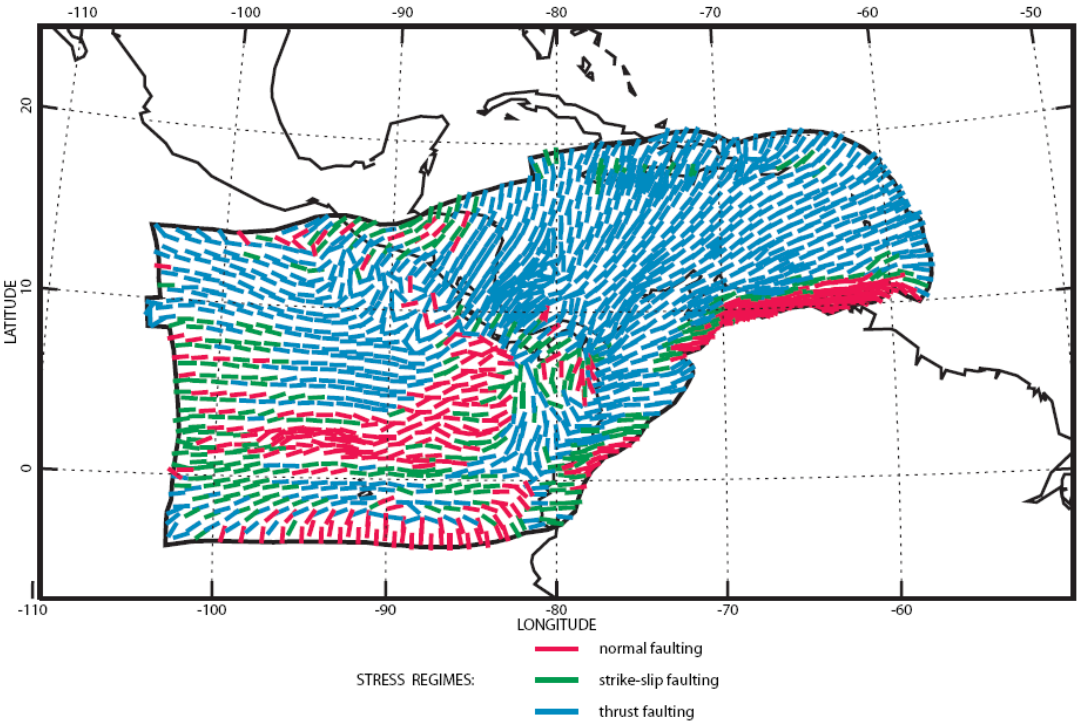

Figure 42. Direction of the maximum horizontal principal stress for model SUB1 using velocities assigned to nodes along the subduction zones adjacent to Central and South America; relative to SA. The basal velocity field was set to zero, and the base of the lithosphere was traction free. The basal temperature was set to 1380 K, and a fault friction of 0.12. The most notable feature is the concentration of normal faulting along the southeast boundary which is contrary to the actual tectonics at this location which is predominantly thrust and strike-slip faulting.

6.4.2 SUB2 RESULTS

The surface velocity results for SUB2 are shown in figure 43 with the geodetic errors presented in figure 44 and fault slip rates displayed in figure 45. The direction of the maximum horizontal principal stress is presented in figure 46. The average geodetic error for the model was 8.5 mm/yr, whereas the spreading error along the Cayman Trough was 13 mm/yr too slow. The average stress direction error for the model was rather good at 28.2 degrees.

There are several noteworthy observations that pertain particularly to the surface velocity field and fault slip rates for model SUB2. Unlike model SUB1, the Caribbean plate does move faster. However, the western portion of the Caribbean plate moves predominantly to the south-southeast, directly towards the subduction zone (dashed red line) where the nodes were assigned velocity values consistent with the motion of the Caribbean plate relative to South America. This is inconsistent with the geodetic measurements of the Caribbean which indicate a predominantly east to slightly northeast motion (Mann et al., 2002; Weber et al., 2001). Also, the surface velocities abruptly change to a nearly due east direction just beyond the subduction zone, but at velocities nearly 10 mm/yr too slow. In addition, examination of the fault slip rates along the northern boundary of the Caribbean plate with North America indicate slip rates in the single digits rather than in a range between 18-20 ±3 mm/yr (DeMets et al., 2000). With respect to the Cocos and Nazca plates, the velocity magnitude and direction were consistent with those for model SUB1 with the exception that the geodetic error for Galapagos was slightly lower at 11.3 mm/yr.

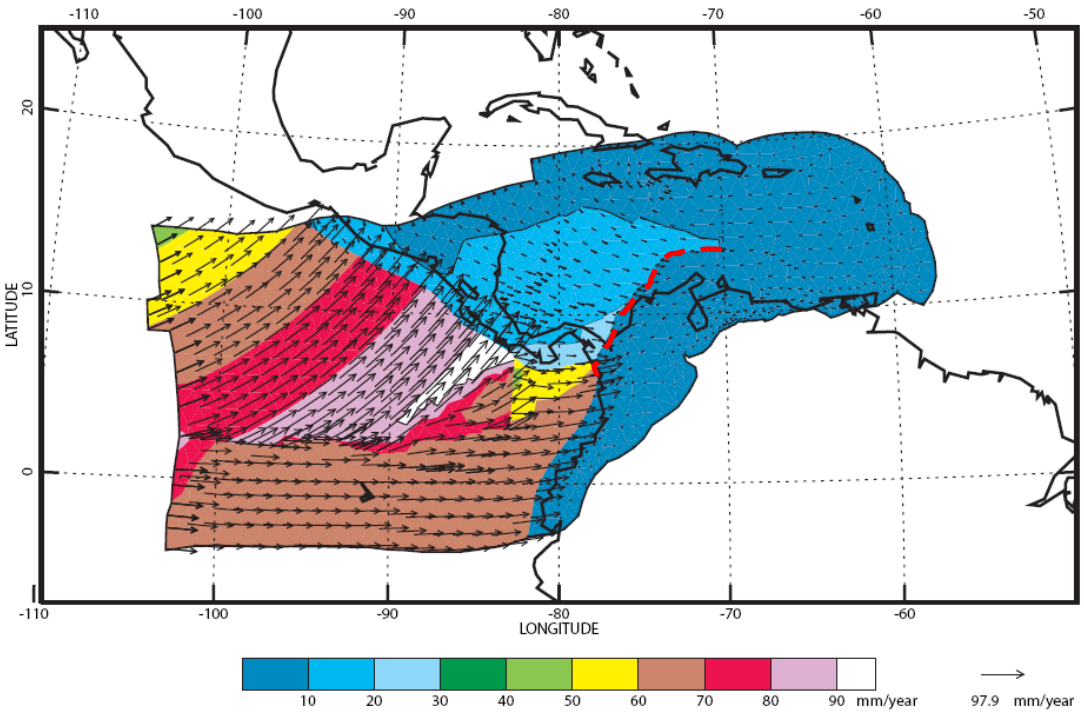

Figure 43. Surface velocity results of SUB2 using velocities assigned to nodes along the subduction zones adjacent to Central and South America as well as the subduction zone in the Caribbean adjacent the North Andes plate (dashed red line); relative to SA. The basal velocity field was set to zero, and the base of the lithosphere was traction free. The basal temperature was set to 1380 K, and a fault friction of 0.12.

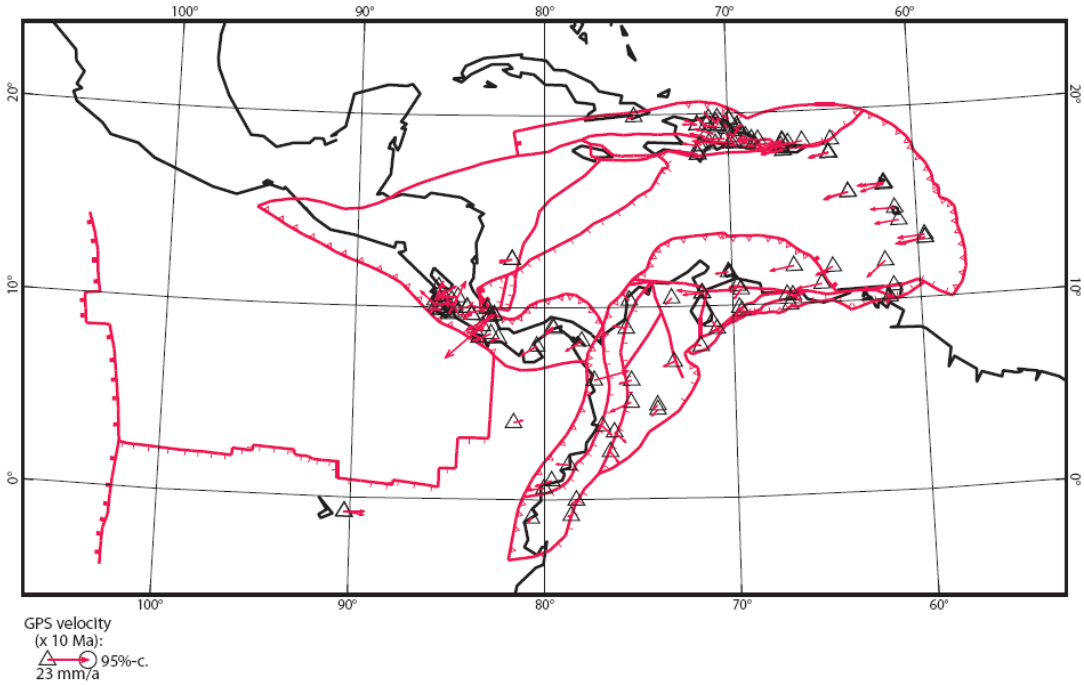

Figure 44. Geodetic errors for model SUB2.

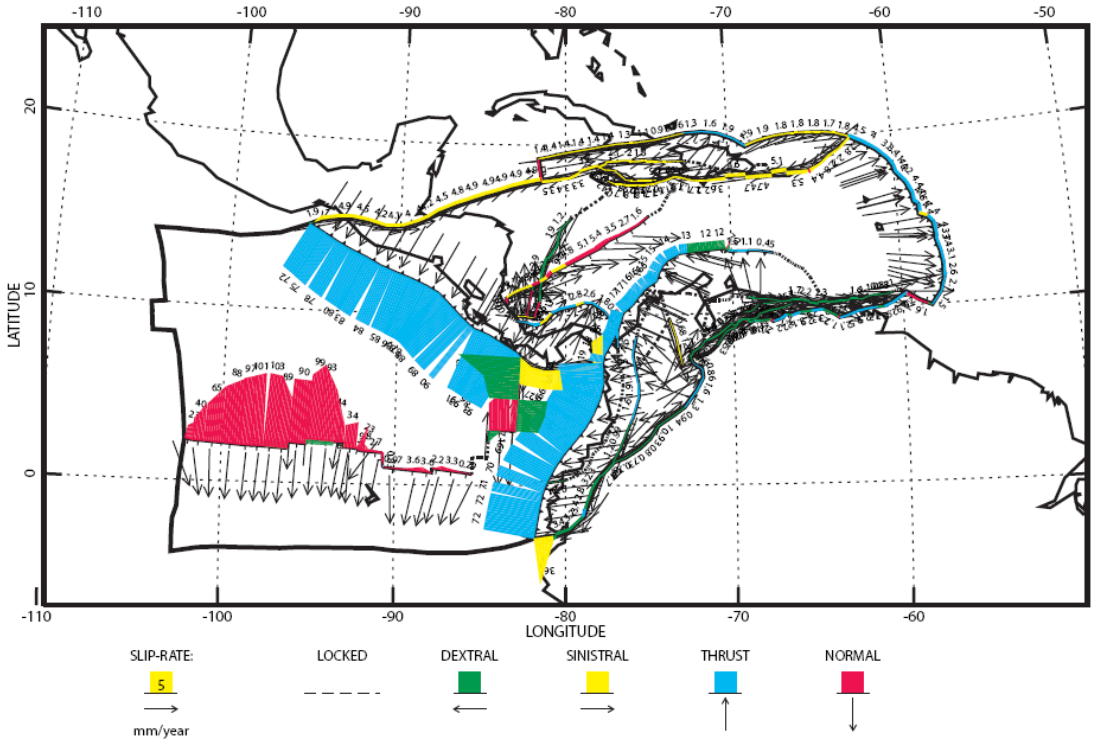

Figure 45. Fault slip rates for model SUB2.

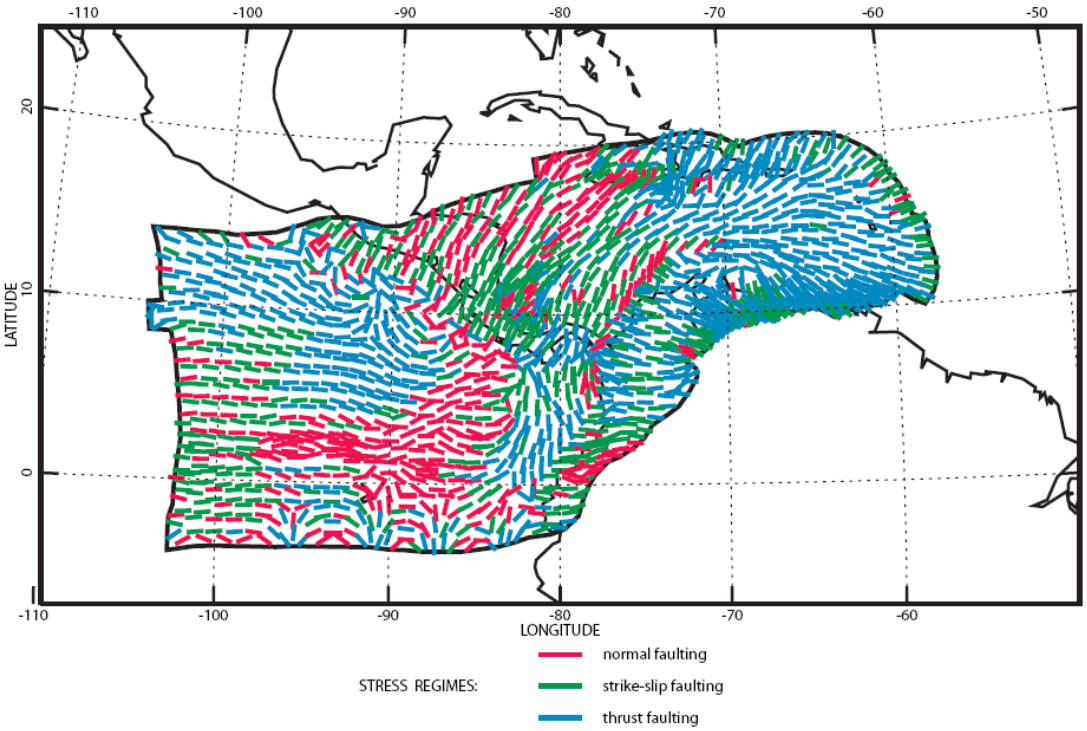

Figure 46. Direction of the maximum horizontal principal stress for model SUB2 using velocities assigned to nodes along the subduction zones adjacent to Central and South America as well as the subduction zone in the Caribbean adjacent the North Andes plate (dashed red line); relative to SA. The basal velocity field was set to zero, and the base of the lithosphere was traction free. The basal temperature was set to 1380 K, and a fault friction of 0.12. Unlike model SUB1, these results are more consistent with the tectonic features seen throughout the modeled region.

6.4.3 SUB3 RESULTS

The surface velocity results for SUB3 are shown in figure 47 with the direction of maximum horizontal principal stress illustrated in figure 48, geodetic errors presented in figure 49 and fault slip rates displayed in figure 50. The average geodetic error for the model was 9.8 mm/yr, whereas the spreading error along the Cayman Trough was 13.6 mm/yr too slow. The average stress direction error for the model was rather poor at 36.8 degrees. All of these values are higher than the results for model SUB2, which it is nearly identical to, with the exception of the addition of basal drag.

The surface velocity results in the Caribbean are nearly identical to SUB2 with respect to direction and velocity, with only a slight decrease in overall velocity. The primary difference in the velocity field between SUB3 and SUB2 is with respect to the Cocos and Nazca plates. Unlike in model SUB2, the velocities in SUB3 rapidly decrease away from the subduction zones where the velocity conditions were applied. This created two predominant features not seen in SUB2, where basal traction was not applied. The first is with respect to the direction of maximum horizontal principal stresses. The stress field in the Cocos and Nazca plates for SUB2 is predominantly compressional, whereas in SUB3 the stress field in the Cocos and Nazca plates is predominantly extensional, which is inconsistent with the overall tectonics of that region. The second notable feature is that the fault slip rate between the Cocos and Nazca plates was significantly lower than those observed in models SUB1 and SUB2. The surface velocity field results within the Caribbean plate were consistent with those observed in SUB2 such that they predominantly moved towards the south-southeast in the western portion of the plate, which is inconsistent with the general east to north-east trend determined by GPS measurements (Mann et al., 2002; Weber et al., 2001). The fault slip rates were also consistent with the results of SUB2 such that they were significantly slower along the boundary with North America.

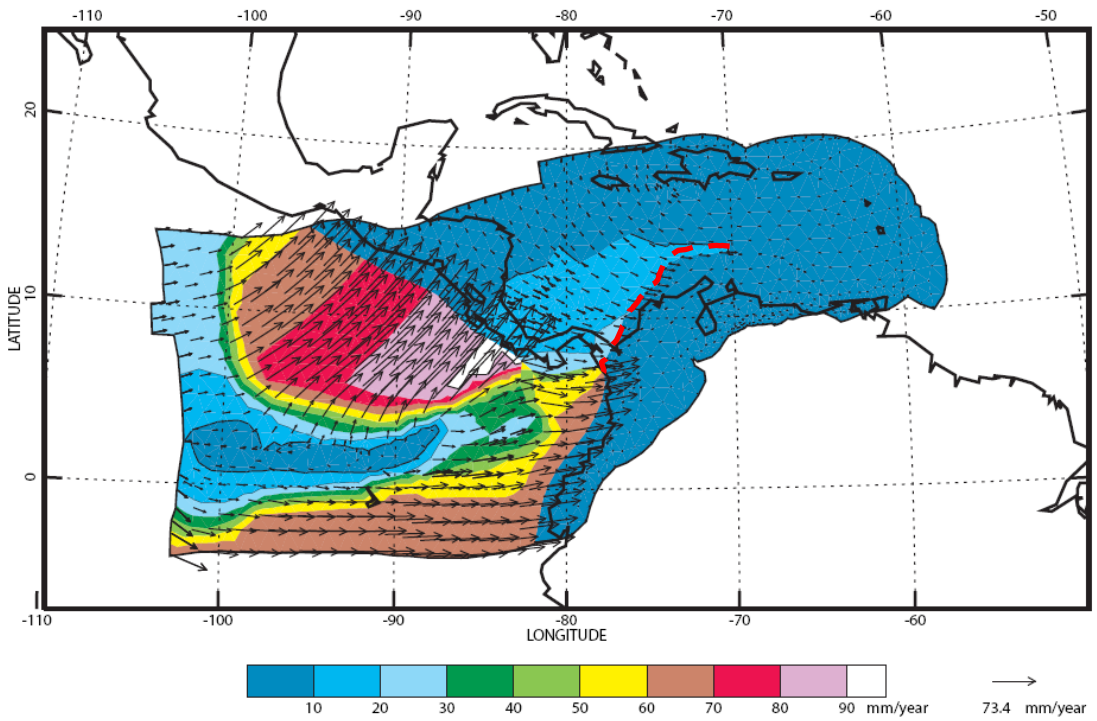

Figure 47. Surface velocity results of SUB3 using velocities assigned to nodes along the subduction zones adjacent to Central and South America as well as the subduction zone in the Caribbean adjacent the North Andes plate (dashed red line); relative to SA. The basal velocity field was set to zero. Traction was applied to the base of the lithosphere. The basal temperature was set to 1380 K, and a fault friction of 0.12.

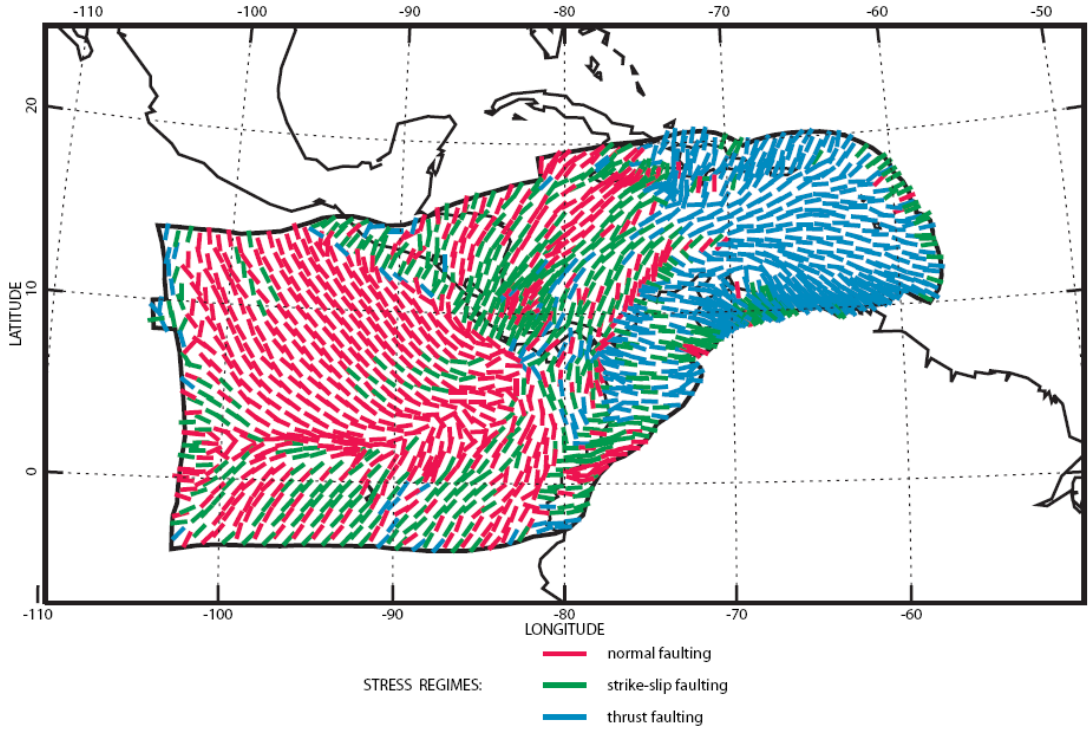

Figure 48. Direction of the maximum horizontal principal stress for model SUB3 calculated in the model using velocities assigned to nodes along the subduction zones adjacent to Central and South America as well as the subduction zone in the Caribbean adjacent the North Andes plate (dashed red line); relative to SA. The basal velocity field was set to zero. Traction was applied to the base of the lithosphere. The basal temperature was set to 1380 K, and a fault friction of 0.12. Under these conditions, the Cocos and Nazca plates would demonstrate extensive normal faulting throughout both plates; something that is not observed.

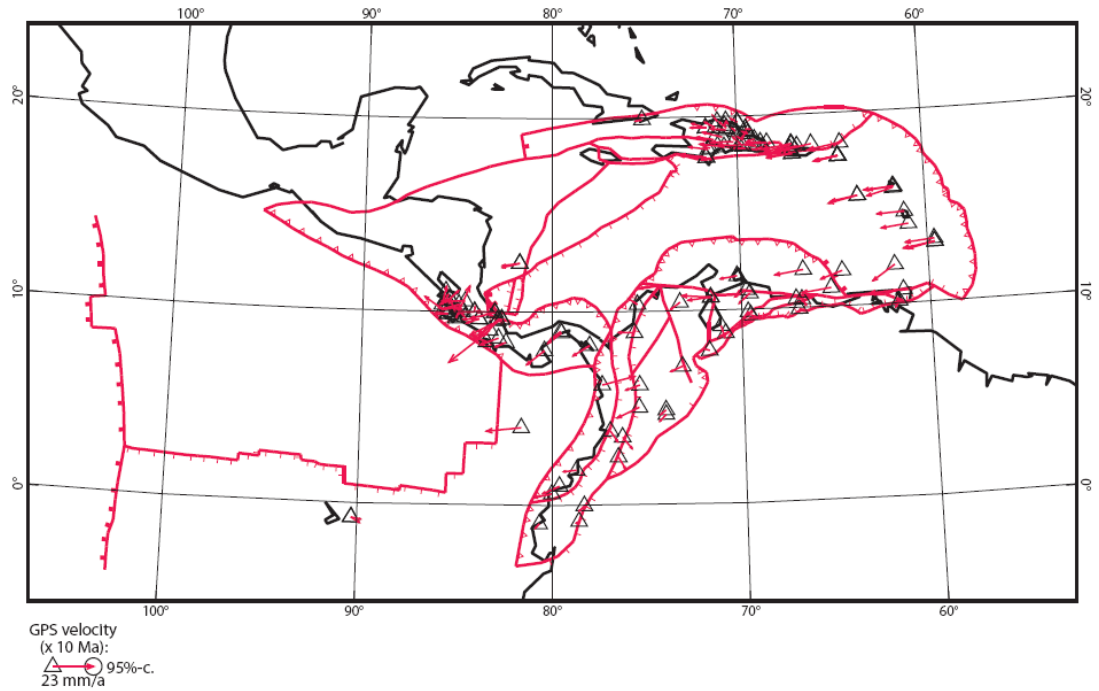

Figure 49. Geodetic errors for model SUB3.

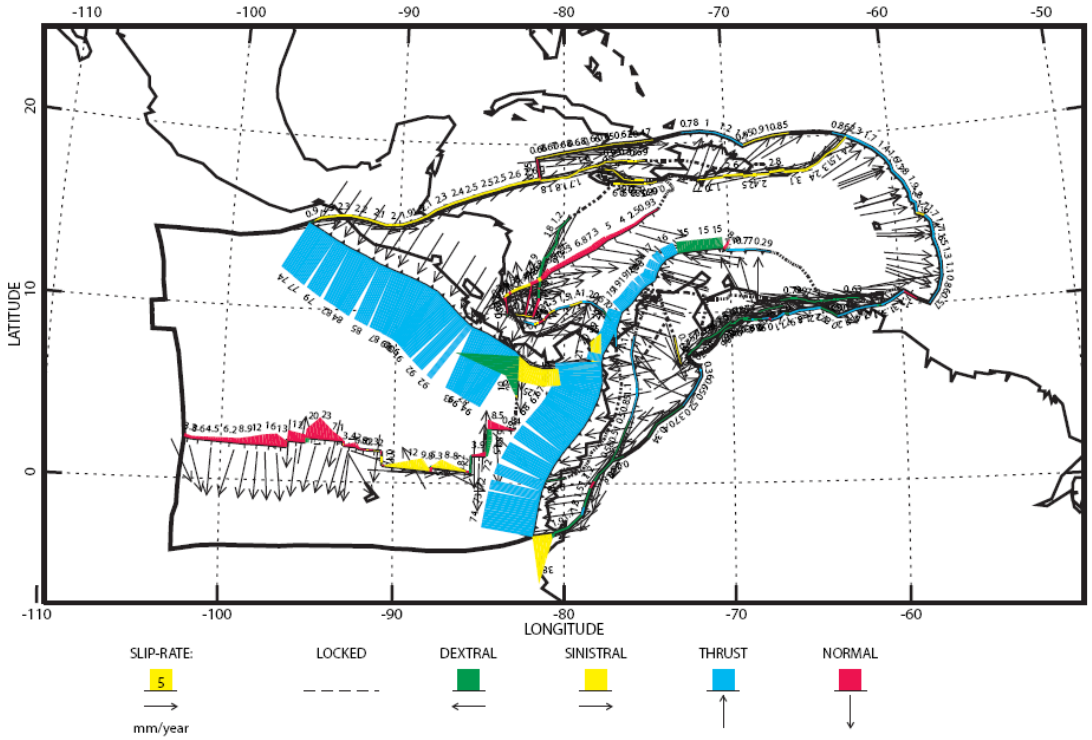

Figure 50. Fault slip rates for model SUB3.

6.4.4 SUMMARY OF MODELS SUB1 THROUGH SUB3

The concept of subduction zones being the primary driving force for plate motion was tested in the three models described above. The first model, SUB1, was designed to test whether or not the forces from the fast moving Cocos and Nazca plates could be responsible for the movement of both the Caribbean and North Andes plates. The nodes along the subduction zones adjacent to Central and South America were the only nodes that had velocities applied to them; all other nodes were initialized to zero. In addition, the base of the model (lithosphere) was traction free. The results were such that the surface velocities and fault slip rates were rather good within the Cocos and Nazca plates, but both the Caribbean and North Andes moved only marginally, and all of the faults were locked. The second model, SUB2, was designed to address the lack of movement within the Caribbean and North Andes plates by applying velocity conditions to the subduction zone directly adjacent to the North Andes plate. The results for this model were an improvement over SUB1, such that the Caribbean and North Andes plates both moved at rates higher than those in SUB1, yet still nearly 10 mm/yr too slow in the Caribbean. In addition, the velocity field in the western portion of the Caribbean plate moved south-southeast, directly toward the subduction zone where the velocity conditions were applied, and resumed an eastward movement directly past the subduction zone. This south-southeast velocity movement is contrary to the current observations of the Caribbean plate which is predominantly east to northeast. The fault slip rates along the boundary between the Caribbean and North America plates were also substantially slower then the observed slip rates. These poor results are likely due to both the southeast

direction of the surface velocity field in the western portion of the model along with the overall slow movement of the Caribbean plate in general. Model SUB3 was identical to model SUB2 with the exception that basal traction was applied to it. The results were not too dissimilar to those of SUB2 with respect to velocities and fault slip rates in the Caribbean. However, the results significantly varied within the Cocos and Nazca plates where the velocities drastically decreased away from the subduction zones. In addition, the stress field results for these two plates indicated that under these conditions, the state of stress for both the Cocos and Nazca plates would be predominantly extensional, which is inconsistent with the tectonic conditions of these two plates.

7. DISCUSSION

Historically, the measurements of relative motions between tectonic plates have largely been based on geologic observations. However, over the past two decades, the use of highly accurate GPS data has begun to supplement and or replace geologic data used for estimating plate motions. The regional model used here has the advantage of having a large number of GPS measurements within it, as well as geologic complexity, such that velocity misfits output from the model can primarily be attributed to inaccuracies of the model and not the field measurements. Therefore, based on the small velocity misfits presented here between the model results and GPS measurements, there is strong support for an eastward mantle flow beneath most of the modeled area.

However, GPS data is sparse in the Cocos and Nazca plates which make the results in these regions of the model the least certain. The subduction zone along the MAT is the portion of the model where the lack of GPS data hinders the evaluation of the model results the most. Estimates of the subduction rate of the Cocos plate beneath Central America are primarily based on seafloor magnetic reversal data. These measurements are less accurate than GPS measurements which make it more difficult to ascertain the accuracy of the subduction rate misfit from the model.

While the rate of subduction between the Cocos and Caribbean plate along the MAT is too slow in most of the eastward flow based models, the discrepancies can be easily accounted for by either errors in the plate kinematic models used for comparison, or slight errors in the total lithosphere thickness calculated for the

subducting slab of the Cocos plate. However, the angle at which the Cocos plate approaches the MAT is consistently very large in nearly all of the eastward basal models where all other comparative values had small misfit errors good (surface velocity and direction, spreading rate of the Cayman Trough, and stress directions). On average, most of these models have a maximum approach angle of 75 degrees azimuth, which is considerably more than the estimated 26.6 degrees azimuth (DeMets et al., 1990). The 26.6 degrees azimuth was determined through reexamination of the slip-vector data used by DeMets et al. (1990), such that only the Harvard CMT data were used. This discrepancy can not be easily overlooked. However, several authors suggest that subduction of the Cocos plate is oblique to the MAT (DeMets, 2001; Guzman-Speziale, 1995; Harlow and White, 1985; Fitch, 1972). In addition, Giner-Robles et al. (2008) evaluated 488 focal mechanisms within the Caribbean, Cocos, and North American convergence zone. Their findings revealed at least three slip trajectories within the region. The slip trajectory of the Central American Volcanic Arc has a lateral movement towards the ESE. Between the Motagua-Polochic fault zone in Guatemala and Lake Managua in Nicaragua, there were two different depth-dependent slip trajectories. For shallow earthquakes, the slip trajectory was determined to be N30E. For earthquakes deeper than 70 km, the slip trajectory was determined to be N50E, which is significantly closer to the 75 degrees azimuth predicted by the eastward basal flow finite element models.

The wide variation in slip directions determined from earthquake focal mechanisms can similarly be seen in the surface velocity results of the eastward basal flow model of run number 48 (figure 51). In these particular results, the surface

velocities of “both” the continental crust of Central America and the oceanic crust of the Cocos Plate move oblique to the MAT. The directional component of surface velocities for the continental crust of Central America varies substantially from west to east relative to the MAT. Directly adjacent to the MAT, the predominant velocity direction is to the southeast. The velocity direction rapidly rotates to the northeast away from the MAT to the east though Guatemala, Honduras, and Nicaragua and into the Caribbean Sea. The large changes in velocity direction observed in the model for Central America are not observed in the Cocos plate. In general, the velocity direction of the Cocos plate changes from due east directly adjacent to the MAT in the north and gradually rotates to northeast along the trench down to the Panama Fracture. The magnitude of the Cocos surface velocity is roughly 30 mm/yr faster than the surface velocity in Central America and the Caribbean Sea, which supports the argument for subduction along the MAT.

Additional evidence for oblique motion between the Cocos plate and Central America is also seen in a close-up view of the ocean floor along the MAT illustrated in figure 52. The sub-parallel lineations in the ocean floor directly adjacent to the MAT can be interpreted as wrench faults that would be typical of strike-slip motion between two plates, whereas, for comparison, the parallel lineations in the ocean floor directly adjacent to the Japan Trench are consistent with reverse faults that occur in compressional environments such as the one there, where the Pacific Plate converges with the Eurasian Plate in a direction perpendicular to the trench (figure 53).

One final observation with respect to the surface velocity results of the eastward basal velocity model directly adjacent to the MAT is that the movement of the Cocos plate over time may very well be a function of both its reaction to an underlying mantle flow direction and its interaction with the movement of the continental crust of the southern portion of Mexico and Central America. A simple graphical experiment is illustrated in figure 54 where the outline of the MAT was digitized and copied several times. Each copy of the trench was pivoted clockwise about a point just west of Guadalajara Mexico. Many of the distinctive kinks in the trench tracked well with several curvilinear features within the Cocos plate. In addition, the final projection of the trench lined up rather well with the subtle features and bends along the East Pacific Rise. While admittedly this method does not account for projection distortion, such distortion was deemed minor due to the relatively small area covered. These observations could suggest that the features observed in the ocean floor of the Cocos plate are a record of the movement of the continental crust of southern Mexico and Central America that result from the Cocos plate moving faster then the continental crust, but in a path of least resistance which would be in the direction the continental blocks move.

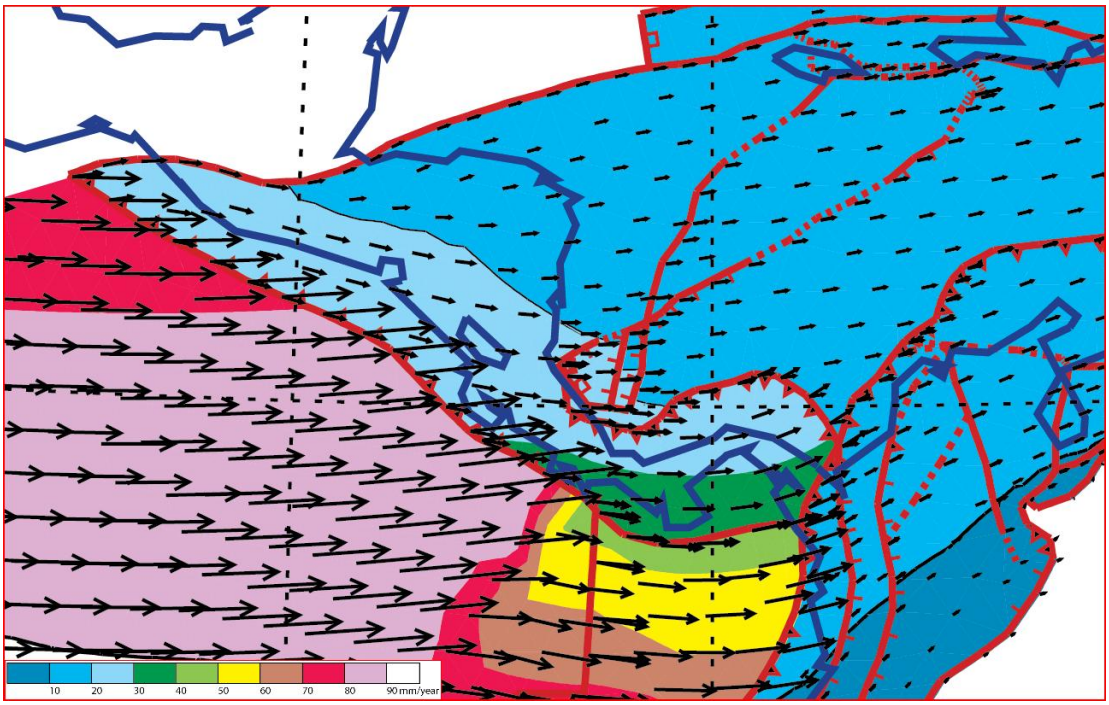

Figure 51. Surface velocity results from a successful eastward basal velocity model. There are two prominent velocity directions directly west and east of the MAT such that both directions are oblique to the strike of the MAT. Central America predominantly moves to the ESE, whereas the Cocos moves in a direction slightly NE, but at a greater magnitude that that of Central America.

Figure 52. Close-up view of MAT where the striations in the oceanic crust that are oblique to the trench, are interpreted as potential reverse faults created by oblique motion between the Central American continental crust and the Cocos oceanic plate. This would be consistent with the model results illustrated in figure 51.

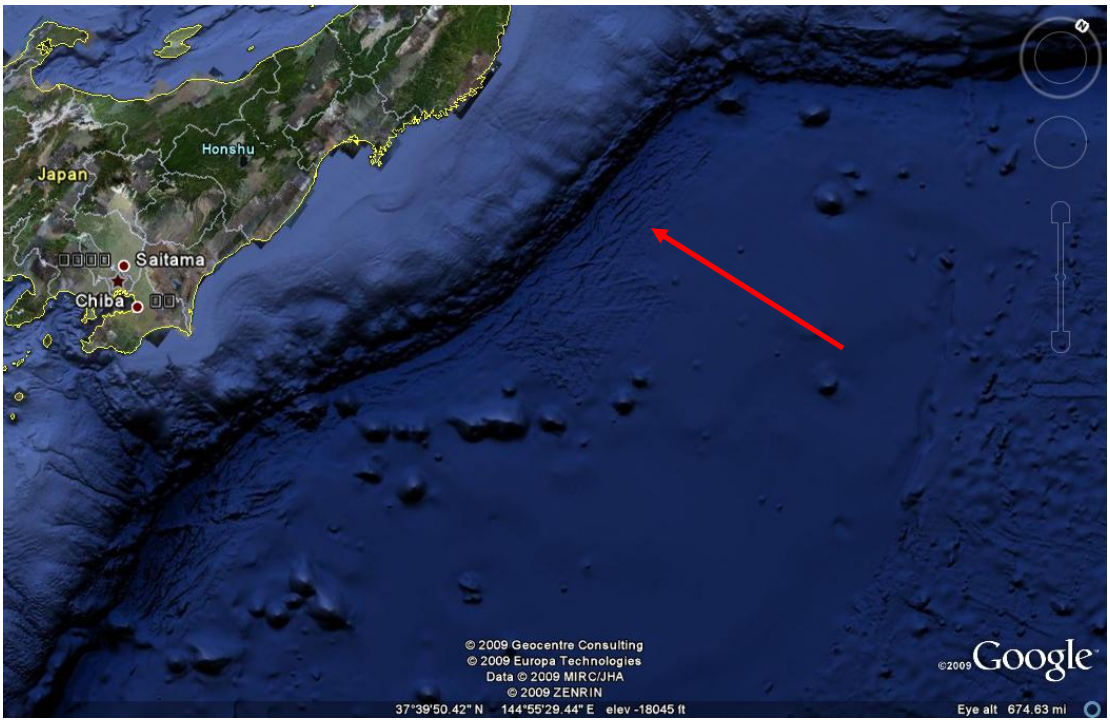

Figure 53. Close-up view of the Japan Trench where the striations in the oceanic crust, parallel to the trench, are interpreted as potential reverse faults caused by compression that results from the convergence of the Pacific Plate perpendicular to the trench.

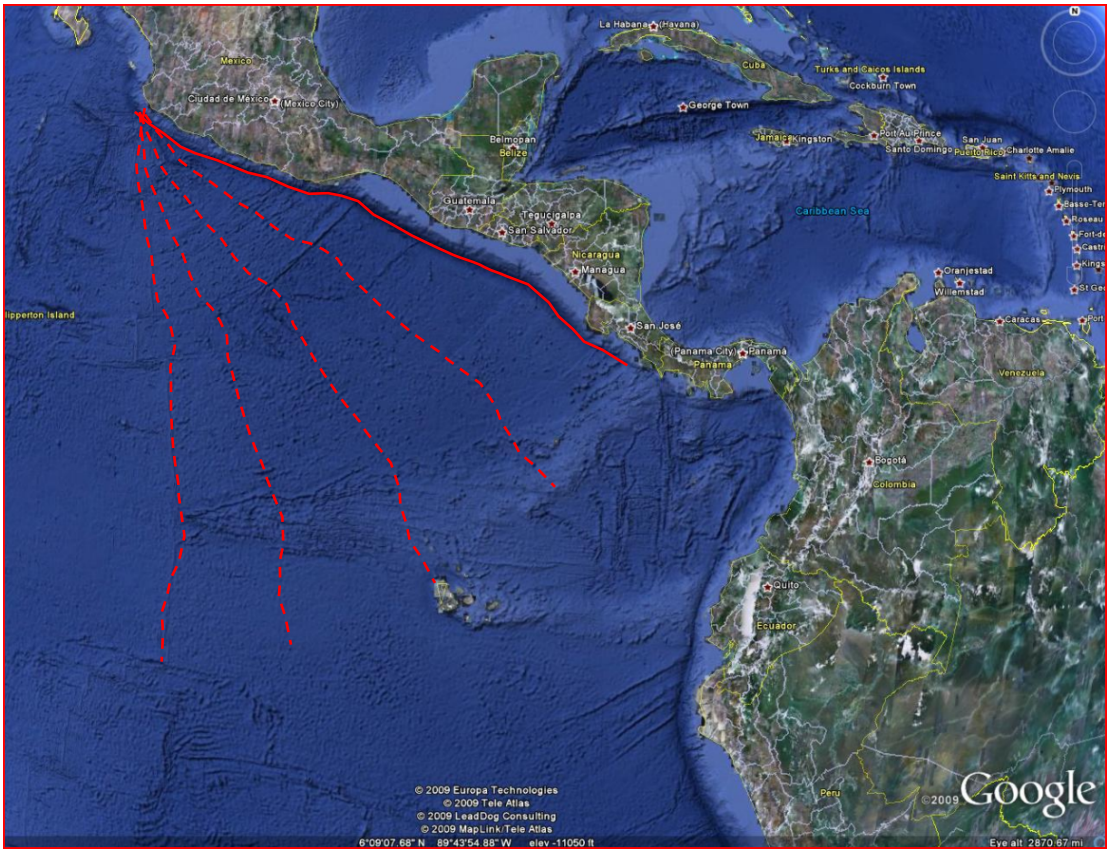

Figure 54. The shape of the MAT closely approximates the shape of the East Pacific Rise as seen by the transposition of the copied red line along the MAT to the dashed lines that pivot about a point west of Guadalajara Mexico (image does not account for possible projection distortion). This may suggest a possible relationship between the movement of the continental crust of Mexico and Central America and the oceanic crust of the Cocos plate.

SHELLS accounts for subducting slabs down to a depth of 100 km. Beyond this depth the slab is truncated and it is unknown what possible affects on a model are left out when slabs that extend deeper than 100 km are truncated. This is particularly important with respect to the model tested here, where a predominant eastward mantle flow is imposed on the asthenosphere. Burbach et al. (1984) describe the Cocos slab beneath Central America as having three major segments. The southern segment extends north from the Panama Fracture to the Nicoya Peninsula and is poorly defined. The middle segment consists of two sections and is the best defined of all three segments; the first section extends north from the Nicoya Peninsula to

western Guatemala, and the second section extends from western Guatemala to Orizaba, Mexico. The third segment extends from Orzaba to the Rivera Fracture Zone. The southern and northern segments of the plate subduct to a depth less than 100 km with a shallow dip angle of roughly 30 degrees or less. The middle segment subducts to depths between 210 and 240 km with a dip angle around 60 degrees. Only the southern and middle segments of the plate were included in the finite element model. The contrast in surface velocities on either side of the Cocos and Nazca plates in the model can be used to some extent to investigate what effects on the model a subducting slab has on the eastward flowing asthenosphere. While only half of the total depth of the Cocos slab is accounted for in the model, there is a strong surface velocity contrast in the model on opposite sides of the MAT, where velocities in the Cocos plate average between 70 and 80 mm/yr but only 20 mm/yr in the Caribbean plate. This might suggest significant slab interference with the eastward mantle flow. However, the maximum depth of the subducting Nazca slab adjacent to Colombia and Ecuador is only 50 km (White et al., 2003). If the slab interference was truly significant in the model, the shallow depth of the Nazca slab should provide less interference to an eastward basal velocity field and therefore result in an even higher surface velocity for the North Andes plate compared to the Caribbean plate. This is not the case. The surface velocity results for the North Andes plate are lower than those for the Caribbean plate by about 10 mm/yr on average. Therefore, the concept of a subducting slab potentially blocking an eastward mantle flow appears negligible in this case.

The structural variability of the Negredo et al. (2004) model was considerably limited as most of the model was comprised east-west strike-slip faults. In addition, the fault friction coefficient was set so low (0.03) in the model that resistance to the forces applied by the plates adjacent to the Caribbean plate were essentially negated. These features made it inevitable that an eastward flowing mantle will move the surface of this model to the east. Negredo et al. (2004) also concluded that a basal velocity of 20 mm/yr, set at 400 km below the surface of Caribbean plate, provided the lowest overall misfits to observed data, including the surface velocity. This raises a significant question regarding the validity of their model and results because the surface velocity of the Caribbean plate is also 20 mm/yr to the east. These results would suggest complete coupling from the base of the model at 400 km to the surface, and thus imply that no shear occurs through the entire 400 km vertical section; something that would seem unlikely.

While the Negredo et al. (2004) model encompasses approximately fifty percent of the model tested here (figures 55 and 56 respectively), there were several significant differences between the two models. The first major difference is the purpose for building and testing each model. The Negredo et al. (2004) model was built primarily to test what, if any, mantle conditions were necessary to move the Caribbean plate at the rate and direction currently determined by GPS data. The results from this model indicated that an eastward mantle flow of 20 mm/yr beneath the Caribbean plate was necessary in order to agree with the GPS data. While these results are somewhat questionable, the area covered by the model served as a good starting point for building the model to be tested here. The purpose of the model built

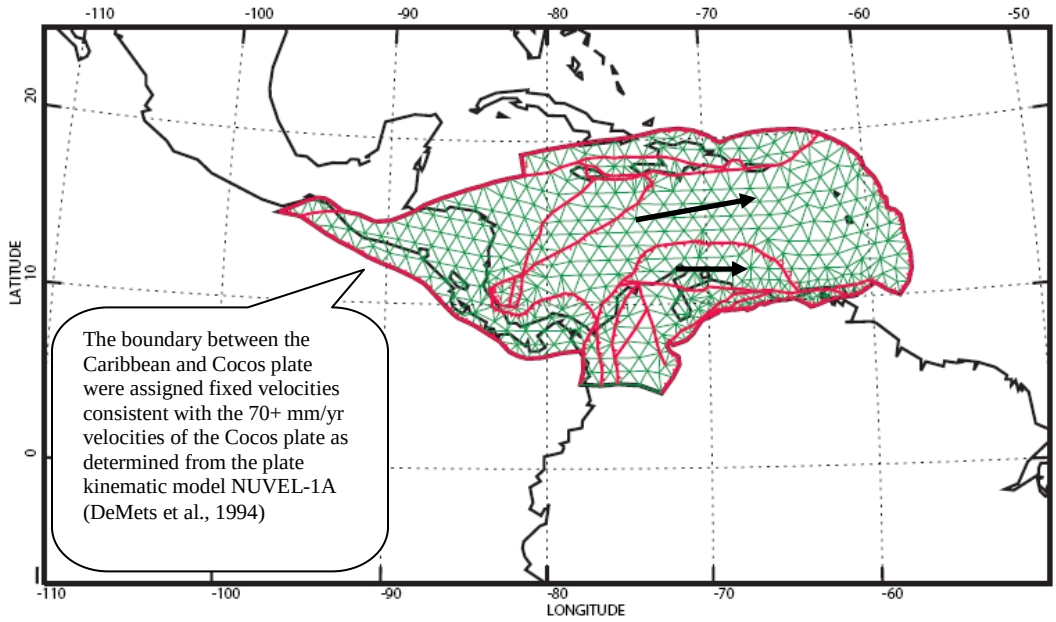

Figure 55. Rough approximation of model tested by Negredo et al. (2004). The black arrows represent generalized plate motions relative to SA and do not represent vectors.

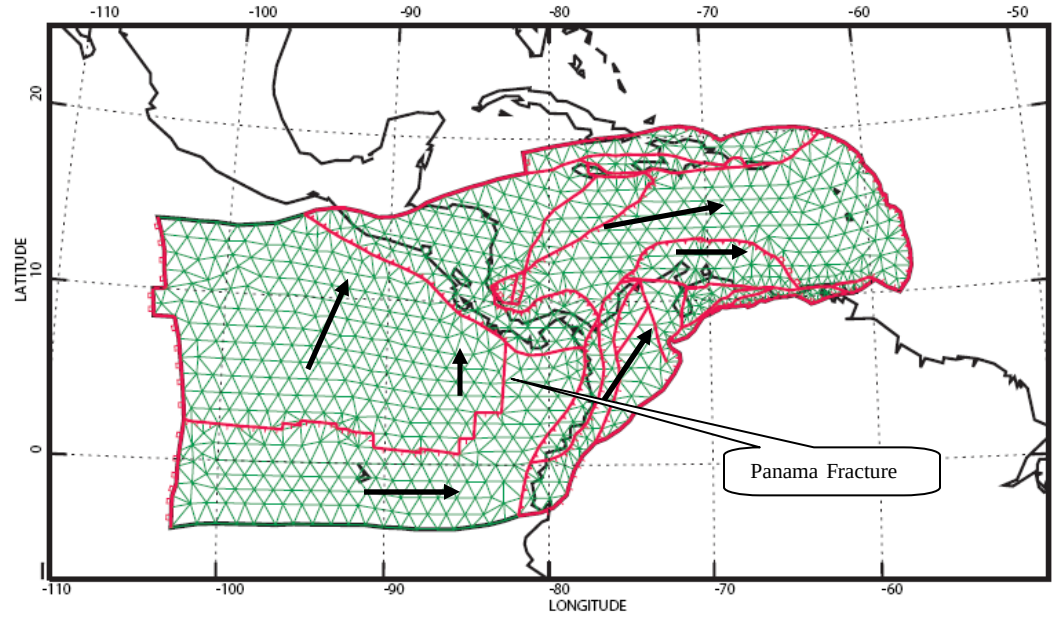

Figure 56. Finite element model used this study. The black arrows represent generalized plate motions relative to SA and do not represent vectors.

for this study was to test whether or not a *global* eastward mantle flow is a viable explanation for the multitude of varying plate geometries, sizes, velocities, and direction of movement. The model was limited to the size of a regional model in order to simplify the problem while at the same time maintaining many of the complexities that exist in a global model.

The second major difference between the two models was the size and number of plates included in the model. While the Negredo et at. (2004) model served as a good base for the model tested here, it lacked the complexities listed above to test the global eastward mantle flow concept as it was comprised of only one complete plate, the Caribbean plate, and a partial plate, the northernmost section of the North Andes plate. This required significant expansion of the model in order to include and test the necessary variety of plate geometries, sizes, velocities, and direction of movement. The addition of all of the North Andes plate, most of the Cocos plate, and a portion of the Nazca plate significantly distinguished the model tested here from the Negredo et al. (2004) model.

The significant extension to the south of the model tested here, relative to the Negredo et al. (2004) model, made the test more comprehensive with respect to the North Andes plate. The southernmost portion of the North Andes plate directly abuts against South America with only north-south trending faults and no east-west faults. Therefore, it provided a more robust test ~~to~~ of the eastward basal flow concept than

the Negredo et al. (2004) model by testing whether or not an eastward mantle flow could move the complete North Andes plate both north and east as indicated by GPS data.

The extension of the model to the west was the most significant difference between the Negredo et al. (2004) model and the model tested here. This extension added nearly all of the Cocos plate, which moves north-northeast, and a portion of the Nazca plate, which moves nearly due east. It also included both the north-south spreading rift and north-south moving Panama Fracture that separate the Cocos and Nazca plates. These additional features added significant complexity to the model that the Negredo et al. (2004) model lacked, and provided a robust means to test the ability of a simple eastward mantle flow to recreate such surface complexities. In this expanded portion of the model, an eastward mantle flow would have to move the surface simultaneously in three different directions. The extension of the model to the west also tested the uniqueness of the 20 mm/yr mantle flow beneath the Caribbean plate determined by Negredo et al. (2004). The Cocos and Nazca plates move at rates between 70 plus and 55 mm/yr respectively, whereas the Caribbean and North Andes plates move at 20 and 10 mm/yr respectively. These velocity magnitudes and contrasts raised an additional question to the viability of a 20 mm/yr mantle flow being able to account for such plate motions.

There were both similarities and dissimilarities between the results of the overlapping sections of the model tested here and that presented by Negredo et al. (2004). The results of both models suggest that an eastward basal flow is necessary

within the mantle beneath the Caribbean plate in order for it to move in a manner consistent with GPS observations of the region. However, this is where the similarities end. The results presented by Negredo et al. (2004) were only given with respect to a base of lithosphere temperature of 1150° C (1423 K). The model tested here included five different basal temperatures; including 1423K. The sensitivity analysis presented in figure 17 clearly demonstrates that there are several combinations of basal temperature, basal velocity, and fault friction coefficients that can produce low misfit values to surface velocities determined from GPS data in the region. The reason for this non-uniqueness can be explained using the following examples. A model where the surface velocity results are faster than the geodetic data can be compensated for by an increase of the basal temperature for the model. The increase in temperature reduces the shear in the model and thereby reduces the energy transmitted to the surface from the basal velocity field set for the model. Likewise, a model that produces surface velocity results that are too slow can be compensated for by increasing the basal velocity of the model.

The discrimination of the model parameters can better be determined by examining whether or not a specific set of parameters can account for both the velocity of the Caribbean plate and the subduction rate of the Cocos plate along the MAT. The subduction rate of the Cocos plate is estimated to be roughly 50 mm/yr faster than the surface velocity of the Caribbean plate. This analysis could not be done on the model tested by Negredo et al. (2004) because the MAT was a boundary for the model, and therefore all the nodes along this segment of the model were assigned fixed velocities that were calculated by the same Euler poles used to

estimate the rate of subduction for the Cocos plate. Therefore, the subduction rate along the MAT for the Negredo et al. (2004) model was predetermined. This problem was eliminated for the model tested here by extending the model boundary out to the East Pacific Rise. This enabled the nodes along the MAT to respond freely to the parameters being tested. The results of these changes are shown in figure 18a, which illustrates the misfit between subduction rates generated from the model along the MAT compared to those estimated by kinematic models. Only a very narrow range of base of lithosphere temperature and basal velocity yielded satisfactory results for the subduction rate along the MAT. These parameters also fell within the range of possible parameters combinations that produced good results for the Caribbean only model.

The inclusion of a wider range of basal lithosphere temperatures and the removal of the MAT as a boundary for the model resulted in parameters that significantly differed from those used by Negredo et al. (2004), with the exception of eastward mantle flow direction. Their best model results came from using a base of lithosphere temperature of 1423 K, a basal velocity of 20 mm/yr, and a fault friction coefficient of 0.03. The best results from the model tested here used a base of lithosphere temperature of 1380 K, a basal velocity of 100 mm/yr, and a fault friction coefficient of 0.12. A 20 mm/yr mantle flow failed to generate even moderate subduction rates along the MAT. The most interesting observation with respect to the parameter differences between the two models is that while there was only a 43 K difference in base of lithosphere temperature (3%), there was an 80 mm/yr difference

in basal velocity (80%), yet the misfit results for the Caribbean plate were very similar. This would suggest that the model is particularly sensitive to the base of lithosphere temperature.

One of the more problematic issues related to the finite element model is the use of surface heat flow to determine the total lithosphere thickness. Data in the region is sparse and/or biased. An incorrect heat flow value can lead to an incorrect positioning of the brittle/ductile transitions in the crust and in the mantle lithosphere. This can make the plate either weaker or stronger and can result in either an overestimation or underestimation of the surface velocity field. The misfits in the model subduction rates along Central and South America were likely due to these inaccuracies; this is particularly obvious with respect the excessive rates of subduction along South America. This area is perpendicular to the spreading ridge between the Cocos and Nazca plates. As such, the heat flow values were very high, which resulted in the calculation of a very weak lithosphere which resulted in surface velocities very close to the basal velocity field imposed on the model. Modification of these heat flow values can often times make this problem worse. A more recent version of SHELLS has been developed, whereby in addition to elevation and heat flow, the age of seafloor, thickness of crust, and s-wave travel time anomaly in the upper mantle, above 400 km depth, are now incorporated into the program (Dr. Peter Bird, personal communication). This program was not available when this study was carried out.

Jardetzkey (1948) clearly illustrated the relative motion problem with his physical model. Separate plates can appear to be moving in opposite directions when in fact they are moving in the same direction, just at different speeds. Therefore, relative plate velocities can easily obscure our conjectures with respect to the drive mechanism behind plate tectonics. For example, one could say that the relative motion between North America and Eurasia is a function of Eurasia moving faster to the east than North America, instead of the two plates moving in opposite directions relative to each other as theorized today. This might explain why primarily only passive margins exist on either side of the Mid-Atlantic Ridge. A more complex example can involve a scenario such as the one primarily used in this study where North and South America are fixed, and the Caribbean, Cocos, and Nazca plates are permitted to move. Based on geologic and GPS measurements, the relative motion between the North and South American plates and the Caribbean plate suggests that both the North and South American plates move to the west while the Caribbean plate moves to the east. However, it is equally plausible to suggest that all three plates move to the east, with the Caribbean plate moving faster to the east than the North and South American plates at a velocity that still preserves the relative motion of the system. The problem becomes increasingly more complex at the global scale. However, continued modeling with the use of finite elements offers us a simpler means of solving this complex problem.

8. CONCLUSIONS

In addition to eastward mantle flow, the model was run to test the affects of slab pull from subduction zones. The models were based on velocity conditions being placed only on nodes along the subduction zones relative to South America, whereas the basal velocity field was set to zero. The model was run with and without basal traction. For the most part, neither of these models were able to move the Caribbean plate at an adequate velocity and/or direction. In addition, the fault slip rates along the boundary between the North America and Caribbean plates were significantly too slow relative to geodetic measurements. The most successful of these models included the subduction zone directly adjacent to the North Andes plate and was able to move the Caribbean plate (unlike the model where this subduction zone was left out). However, it became clear from the south-southeast surface velocity results in the western portion of the model that if the Caribbean plate was driven by this subducting slab, the western half of the Caribbean plate would move directly towards the subduction zone, whereas the eastern half moved nearly due east. This is contrary to the geodetic evidence that indicates that all of the Caribbean plate is moving predominantly east to slightly northeast. The results in the Cocos and Nazca plates were particularly good for the subduction based models; provided traction was not applied to the base lithosphere. When basal traction was applied, surface velocities rapidly decreased away from the subduction zones, and the stress regime became predominantly extensional throughout both plates. In general, the subduction based models provided reasonable results in some areas, and very poor results in others. It is important to note that the eastward mantle flow models gave low overall misfits to the

complex surface motions in the modeled area, using a flow pattern that was much more simple and uniform than the subduction zone based models which imposed velocities of varying directions and magnitudes.

The finite element model that used the parameters of 1380 K for a basal temperature, a due east basal velocity field at 100 mm/yr, and a fault friction coefficient value of 0.10, produced results very close to the observed motions and neotectonics of the Caribbean and North Andes plates. Three results from the model were particularly interesting. The first is with respect to the large surface velocity contrast between the Cocos and Caribbean plates. The entire model had a uniform basal velocity field applied of 100 mm/yr due east. However, the surface velocity results for the Cocos plate were on the order 70 to 80 mm/yr, whereas the surface velocity of the Caribbean plate averages only 20 mm/yr. In addition, the Middle America Trench, which separates the two plates, yielded subduction rates and directions that were reasonably close to the values estimated by global kinematic models. The second interesting result is with respect to the North Andes plate. The surface velocity results for the North Andes suggest that its interaction with the South American plate, in conjunction with the underlying mantle flow, determine its movement. The third, and most interesting result, is with respect to the fault slip on the Panama Fracture. While the slip rate of the fault fell far short of the estimated geologic rates, the fault motion is north-south in a right-lateral strike-slip manner, which is consistent with geologic observations. The significance of this result relates to the fact that the fault moves in a direction that is directly perpendicular to the basal velocity field applied beneath it. The movements of the North Andes plate, in

conjunction with that of the Panama Fracture, support the concept that a simple eastward directed basal velocity field in the mantle is capable of producing complex surface plate motions. Therefore, it is reasonable to consider that the plate geometries and motions observed today are not solely representative of the basal velocity field below them. Rather, the plate motions are likely a combination of both the mantle flow beneath the plate, and the collision of the plates with each other. The use of finite elements to model these complex interactions is ideal. However, due to the relative small scale of the model presented here, future studies should involve both larger regional finite element models, as well as global models, to determine if an eastward mantle flow is a global occurrence.

REFERENCES

Bird, P. (1989) New finite element techniques for modeling deformation histories of continents with stratified temperature-dependent Rheologies. *J. Geophys. Res*. 94: 3967-90

Bird, P., and X. Kong (1994) Computer simulations of California tectonics confirm very low strength of major faults, *Geol. Soc. Am. Bull*., 106, 159-174.

Bird, P. (1996) Computer simulations of the Alaskan neotectonics, *Tectonics*, 15, 235-236.

Bird, P. (1998) Testing hypotheses on plate-driving mechanisms with global lithosphere models including topography, thermal structure, and faults, *J. Geophys. Res.*, 103, 10,115-10,129.

Bird, P. (1999) Thin-plate and thin-shell finite-element programs for forward dynamic modeling of plate deformation and faulting, *Comput. Geosci*., 25, 383-394.

Bird, P., and Z. Liu (1999) global finite-element model makes a small contribution to intraplate seismic hazard, Bull. *Seismol. Soc. Am*., 89, 1642-1647.

Burbach, G. V., Frohlich, C., Pennington, W. D., Matumoto, T., (1984) Seismicity and Tectonics of the Subducted Cocos Plate. J. Geophys. Res. Vol 89, No. B9, 7719-7735

Burbidge, D. R., (2004), Thin plate neotectonics models of the Australian plate, *J. Geophys. Res*., 109, B10405, doi: 10.1029/2004JB003156, 2004

Caceres, D., Monterroso, D., Tavakoli, B., (2005) Crustal deformation in northern Central America. Tectonophysics 404 p. 119-131

Carlson, R.L., Hilde, T.W.C., Uyeda, S., (1983). The driving mechanism of plate tectonics: relation to age of the lithosphere at trenches. Geophys. Res. Lett. 10, 297 – 300.

Chaisson, E., and McMillan, S., 1993. Astronomy Today. Englewood Cliffs, 199 pp.

Cowan, H. (1998), Map of Quaternary faults and folds of Panama and its offshore regions, U.S. Geol. Surv. Open File Rep. 98-779.

DeMets, C., R. G. Gordon, F. Argus and S. Stein, (1990) Current plate motions, *Geophys. J. Int*., 101, 425-478

DeMets, C., R. G. Gordon, D. F. Argus, and Stein, S., (1994) Effect of recent revisions to the geomagnetic time scale on estimates of current plate motions, *Geophys. Res. Lett.,* 21, 2191-2194.

DeMets, C., P. E. Jansma, G. S. Mattioli, T. H. Dixon, F. Farina, R. Bilham, E. Calais and P. Mann (2000), GPS geodetic constraints on Caribbean-North American plate motion, *Geophys. Res. Lett*., 27, 437-440

DeMets, C., (2001), A new estimate for present-day Cocos-Caribbean plate motion: implications for slip along the Central American volcanic arc. Geophys. Res. Lett. 28, 4043-4046.

Doglioni, C., Carminati, E., Cuffaro, M., Scrocca, D., (2007) Subduction kinematics and dynamic constraints. Earth-Science Reviews 83, p. 125-175, doi: 10.1016/j.earthscirev.2007.04.001.

Doglioni, C., Carminati, E., Bonatti, E., (2003). Rift asymmetry and continental uplift. Tectonics 22 (3), 1024.

Doglioni, C., (1993) Geological evidence for a global tectonic polarity: Journal of the Geological Society of London, v. 150, p. 991-1002.

Fitch, T. J., (1972), Plate convergence, transcurrent faults, and internal deformation adjacent to southeast Asia and the western Pacific. J. Geophys. Res. 77, 4432-4460

Freymueller, J. T., J. N. Kellogg, and V. Vega, (1993), Plate motions in the north Andean region, *J. Geophys. Res*., 98, 21,853-21,863.

Giner-Robles, J. L., Martinez-Diaz, J. J., Rodriguez-Pascua, M. A., Gonzalez-Casado, M. J., Cluster analysis of the 3D instrumental seismicity within a subduction zone (Caribbean, Cocos and North American tectonic convergence): Implications for a kinematical tectonic model, 33rd International Geological Congress (33IGC), Oslo, Norway, 6-14 August, 2008

Guzman-Speziale, M., (1995), Relative motioin of the Central America forearc sliver (abstract), EOS Transact. Am. Geophys. Union 76, F547 (suppl.)

Hammond, W.C., Toomey, D.R., (2003). Seismic velocity anisotropy and heterogeneity beneath the Mantle Electromagnetic and Tomography Experiment (MELT) region of East Pacific Rise from analysis of P and S body waves. J. Geophys. Res. 108 (B4), 2176.

Harlow, D. H., White, R. A., (1985), Shallow earthquakes along the volcanic chain in Central America: evidence for oblique subduction (abstract). Earthq. Notes 55, 28.

Harvard Centroid-Moment-Tensor (CMT) http://www.globalcmt.org/

Hassani, R., Jongmans, D., and Chery, J. (1997), Study of plate deformation and stress in subduction processes using two-dimensional numerical models: *Journal of Geophysical Research*, v. 102, p. 17951-17965, doi: 10.1029/97JB01354.

Heidbach, O., Tingay, M., Barth, A., Reinecker, J., Kurfeß, D., and Müller, B.(2008): The 2008 release of the World Stress Map (available online at www.world-stress-map.org)

Hickman, S. H. (1991), Stress in the lithosphere and strength of active faults: *Reviews of Geophysics*, v. 29, p. 759-775.

Jardetzky, W., 1948. On the Dynamics of the Earth's Crust: Soc. Amis. Sci. Pozan, B., Lv. 9, p. 3-24.

Jimenez-Munt, I., Bird, P., and M. Fernandez (2001), Thin-shell modeling of neotectonics in the Azores-Gibraltar region, *Geophys. Ress. Lett*., 28, 1083-1086.

Keary, P., Vine, F.J. (1996) Global Tectonics, Second Edition, Blackwell Science p.333

Kellogg, J. N.,R. Trenkamp, and J. T. Freymueller (1996) Transect of the southern Caribbean plate boundary: 8 years of CASA GPS results, Eos Trans. AGU, 77(46), Fall Meet. Suppl., F142

Kellogg, J.N. and Vega, V., (1995) Tectonic development of Panama, Costa Rica, and the Colombian Andes: Constraints from global positioning system geodetic studies and gravity. In: P. Mann (Editor), Geologic and tectonic development of the Caribbean plate boundary in southern Central America. *Geological Society of America Special Paper. Geological Society of America*, *Boulder*, CO, pp. 75-90.

Kellogg, J. N.,I. J. Ogujjofor, and D. R. Kansakar, (1985) Cenozoic tectonics of the Panama and North Andes blocks, Mem. Congr. Latinoam. Geol., 6, 40-59.

Kirby, S. H. (1983), Rheology of the lithosphere, *Rev. Geophys*., 21, 1458-1487.

Kong, X., and P. Bird (1995), SHELLS: A thin-shell program for modeling neotectonics of regional or global lithosphere with faults., *J. Geophys. Res*., 100, 22,129-22,131.

Kong, X. (1995) Numerical modeling of the neotectonics of Asia: A new spherical shell finite element method with faults, Ph.D. thesis, Univ. of Calif., Los Angeles.

Kong, X., and P. Bird, (1996) Neotectonics of Asia: Thin-shell finite element models with faults, in Tectonic Evolution of Asia, edited by A. Yin and T. M Harrison, pp. 18-34, Cambridge Univ. Press, New York,.

Kreemer, C., W.E. Holt, and A.J. Haines (2003) An integrated global model of present-day plate motions and plate boundary deformation, *Geophys. J. Int.*, *154*, 8-34, http://gsrm.unavco.org/data/

Leroy, S., Mauffret, A., Patriat, P. and Mercier de Lepinay, B. (2000), an alternative interpretation of the Cayman Trough evolution from a reidentification of magnetic anomalies, *Geophys. J. Int*., 141, 539-557.

Liu, Z., and Bird, P. (2002), North America is driven westward by lower mantle flow, *Geophys. Res. Lett*., 29(24), 2164, doi: 10.1029/2002GL016002.

Liu, Z., and Bird, P., (2002), Finite element modeling of neotectonics in New Zealand, *J. Geophys. Res*., 107(B12), 2328, doi:10.1029/2001JB001075.

Lowrie, W. Fundamentals of Geophysics, Cambridge Univ. Press, New York, 2004.

Macdonald, K. C. and Holcombe, T. L.,(1978), Inversion of magnetic anomalies and sea-floor spreading in the Cayman Trough, *Earth and Planet. Sci. Lett*., 40, 407-414.

Mann, P., Calis, E., Ruegg, J.C., Demets, C., Jansma., P. E., Mattioli, G. S., (2002) Oblique collision in the northeastern Caribbean from GPS measurements and geological observations.

Margheriti, L., Lucente, F.P., Pondrelli, S., (2003). SKS splitting measurements in the Apenninic-Tyrrhenian domain (Italy) and their relation with lithospheric subduction and mantle convection. J.Geophys. Res. 108 (B4), 2218. doi: 10.1029/2002JB001793

McNally, K.C., Minister, B., (1981) Nonuniform seismic slip rates along the Middle America trench. J. Geophys. Res. 86, 4949 – 4959.

National Geophysical Data Center (NGDC), NOAA Satellite and Information Service, http://www.ngdc.noaa.gov/mgg/bathymetry/relief.html

Negredo, A. M., Jimenez-Munt, I., and Villasenor, A. (2004) Evidence for eastward mantle flow beneath the Caribbean plate from neotectonics modeling, *Geophys. Res Lett.* 31, L06615:doi:10/1029/2003GL019315

Negredo, A. M., Bird, P., Galdeano, C. S de., and Buforn, E. (2002) Neotectonic modeling of the Ibero-Maghrebian region, *J. Geophys. Res*., 107, B11, 2292, doi: 10.1029/2001JB000743

Pollack, H. N., S. J. Hurter, and J. R. Johnson (1993), Heat flow from the Earth's interior: Analysis of global data set, *Rev Geophys*., 31, 267-280

Rosencrantz, E., and Sclater, J. G. (1986), depth and age in the Cayman Trough, *Earth Planet. Sci. Lett*., 79, 133-144.

Russo, R.M., Silver, P.G., (1994). Trench-parallel flow beneath the Nazca plate from seismic anisotropy. Science 263, 1105-1111.

Schubert, G., Turcotte L. D., Olson P., (2001) Mantle Convection in the earth and Planets, Cambridge University Press.

Silver, P.G., Hold, W.E., (2002). The mantle flow field beneath western North America. Science 295, 1054-1057.

Sobolev, S.V., and Babeyko, A.Y. (2005), What drives orogeny in the Andes?: *Geology*, v. 33, p. 617-620, doi: 10.1130/G21557.1

Sperner, B., Mueller, B., Heidbach,O., Delvaux, D., Reinecker, J., Fuchs, K., (2003) Tectonic stress in the Earth's crust; advances in the World Stress Map project. Geological Society Special Publications, vol. 2`12, pp. 101-116.

TECTONIC MAP OF THE WORLD. Copyright © by the American Association of Petroleum Geologists Foundation. All Rights Reserved.

TECTONIC MAP OF SOUTH AMERICA (1978) Commission for the Geological Map of the World. Authors: Nacional da Producao Mineral, Brazil. Divisao de Geologia e Mineralogia, Servicos Aerofotogrametricos Cruzeiro do Sul

Trenkamp, R., J. N. Kellog, and J. T. Freymueller (1996), Transect of Nazca-South America plate boundary in Ecuador and Combia: 8 years of CASA GPS results (abstract), EOS Trans. AGU, 77(46) Fall Meet. Suppl., F142

Van Hunen, J., van den Berg, A.P., Vlaar, N.J., (2002). The impact of the South-American plate motion and the Nazca Ridge subduction on the flat subduction below South Peru. Geophys. Res. Lett. 29, 14

Weber, J. C., T. H. Dixon, C. DeMets, W. B. Ambeh, P. Jansma, G. Mattioli, J. Saleh, G. Sella, R. Bilham, and O. Perez (2001), GPS estimate of relative motion between the Caribbean and south American plates, and geologic implications for Trinidad and Venezuela, *Geology*, 29, 75-78.

Wei, T., Han-jing, H., Pei-xun, L. (2000), Finite element modeling for formation of major regions of great earthquakes in the Chinese mainland and its vicinity, Acta Seismologica Sinica, Vol 13, no. 3, 288-294.

White, S.M., Trenkamp, R., Kellog, J.N., (2003) Recent crustal deformation and the earthquake cycle along the Ecuador-Colombia subduction zone. Earth and Planetary Science Letters, v. 216 (3) p 231-242.

Zoback, M. L., Zoback, M. D., (1989) Tectonic stress field of the continental United States Memoir – Geological Society of America, vol. 172, pp. 523-539.

Appendix A

ADDITIONAL DISCUSSION OF SHELLS METHODOLGY

A detailed description of the SHELLS methodology is provided by Kong (1995), Kong and Bird (1995), and Kong and Bird (1996). The methodology evolved from a flat-Earth modeling method for continua of realistic nonlinear rheology described by Bird (1989), as well as methods for adding faults detailed by Bird and Kong (1994). A more general description of the SHELLS methodology is provided by Bird (1998) and Burbidge (2004), and is incorporated together in the following description for the purpose of this paper.

The method assumes that the lithosphere can be represented by a thin spherical shell, whereby it can account for the curvature of the Earth for large regional models, as well as global models. The total thickness of the shell is controlled by the depth to a given isotherm, whereas the base of the lithosphere is defined to be the point at which there is a transition from conduction to an adiabatic geotherm. The method uses a two-dimensional finite element grid in a manner that only the horizontal components of the momentum equation are solved and only the horizontal components of velocity are predicted; the inertia term in the momentum equation is ignored. The radial component of the momentum equation is represented by the isostatic approximation and the vertical normal stress at any point is assumed to be equal to the weight of overburden per unit area. The strength of the lithosphere is vertically integrated, and the velocity vectors are assumed to be independent of depth.

While the program operates in two dimensions, there are certain functions the program performs whereby it can be considered a pseudo 3-dimensonal program. For example, the volume integrals of density and strength are performed numerically on a lithosphere model with laterally varying topography and heat flow, as well as laterally varying crust and mantle lithosphere layer thicknesses. Vertical integrals are performed using 1-km depth steps at all seven Gauss integration points within each element, figure A-1. The Gauss integration formula to these selected vertical integrals gives a good approximation of three dimensional integrals, and thus gives a partial 3-dimensional solution.

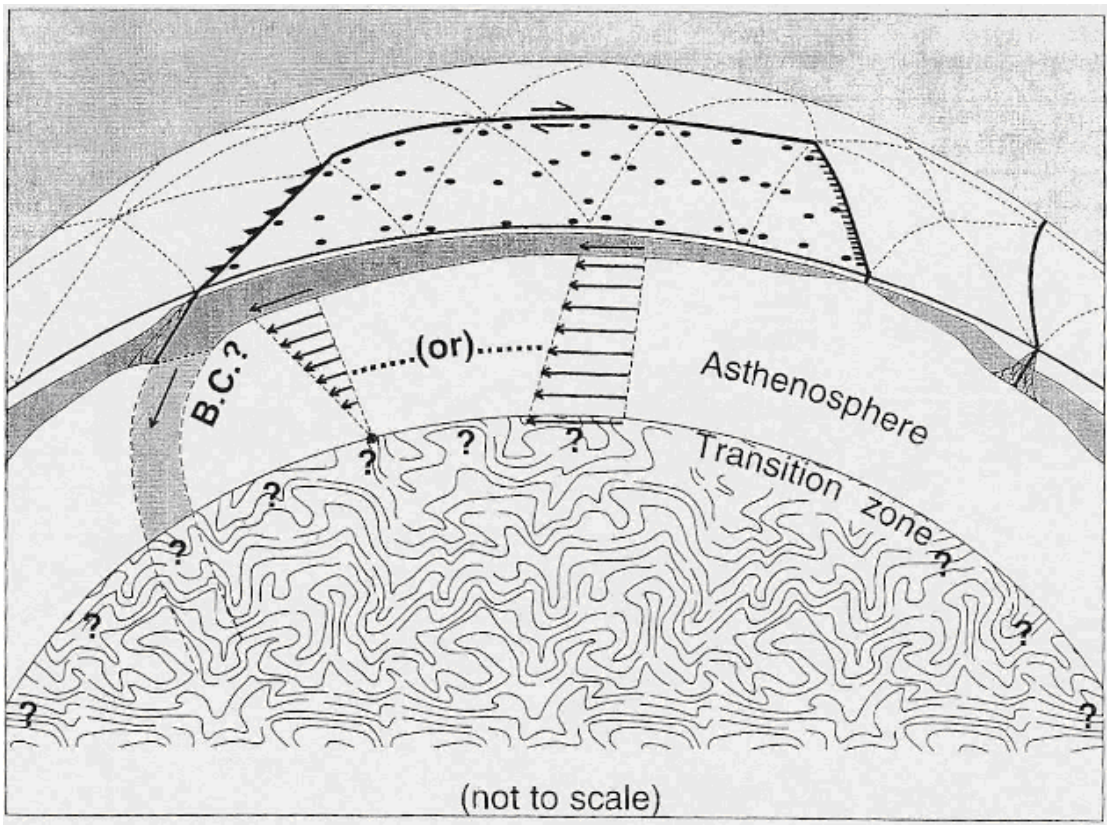

Figure A-1. Cartoon of the geometry assumed in program SHELLS. Crust (white) is bonded to the mantle lithosphere (shaded) and their joint strength is represented by 2D grid of spherical triangles on surface. Within each triangle, vertical integrals of strength are performed at 7 G integration points (black dots). Fault elements are used to represent plate boundaries. Because subducting slabs deeper than 100 km are not included in model, their 'cut' ends require boundary conditions (either velocity or traction specified.) Whether lower mantle is assumed to be fast-moving or sluggish, velocity differences between lower mantle and lithosphere cause simple shear in asthenosphere, which applies horizontal shear tractions to base of model. (Figure taken from Bird, 1999; Note: the required boundary conditions for subducting slabs refers to global models only and not regional models such as those tested here.)

The rheology at a given depth is assumed to be either anelastic brittle (Mohr-Coulomb frictional plasticity) or ductile (dislocation creep). The crustal rheology is based on California models of Bird and Kong (1994), whereas mantle rheology is based on olivine deformation studies evaluated by Kirby (1983). For each strain rate tensor, the software calculates the deviatoric stress tensor using each of three flow laws: cohesionless frictional faulting, dislocation (power law) creep, and Newtonian (linear creep). The flow law giving the lowest maximum shear stress is presumed to

dominate at that point. Once the deviatoric stress is determined, the total stress tensor is found by adding pressure to the deviatoric stress until the vertical stress becomes lithostatic.

SHELLS also provides for the use of faults within the model. This includes normal, thrust, and strike-slip faults, which are placed at the continuum element boundaries. Each fault can be assigned a dip angle as well as a dip direction. In addition, the program accounts for fault stresses within the continuum elements (or intra-plate segments of the model that comprise the crust-lithosphere-mantle layers). Fault stresses are considered frictional, and are calculated based on the assumption of hydrostatic pore pressure. The fault elements also have brittle/ductile transitions, and have dislocation creep below their transitions. Sometimes there are two brittle/ductile transitions; one in the crust, and another in the mantle lithosphere. However, in other places there is only one. The coefficient of friction within the continuum elements are consistently set to a value of: 0.85 in all models based on studies by Bird and Kong, 1994; Kong, 1995; Bird, 1996; Kong and Bird, 1996. The coefficient of friction for boundary faults varies from model to model, but is constant for all faults within each particular model as the software is currently unable to vary this value with respect to individual faults or fault types.

Appendix B

FURTHER DISCUSSION ON FINITE ELEMENT GRID CONSTRUCTION

There are several supporting applications to the SHELLS program that are used to build the input model. ORBWEAVE is the primary utility to do this, and is a graphical user interface application (GUI). The first step in the process is to import a digitized base map file. This map is used to define the boundaries that the finite elements will conform to, such as faults and coastlines. Any map can be digitized and imported into the application, but must comply with a specific format described by a supporting text file. A very useful global coastline map is provided (Worldmap.dig) which consists of a reformatted version of coastline data by NOAA (http://rimmer.ngdc.noaa.gov/coast/getcoast.html). Once the map of interest is displayed, the finite elements can be added. Each element consists of three nodes which can be interactively repositioned along the desired features of the model. An automated feature of the program can "tile" a region with elements of constant size that range from 72 degrees in width to 1 degree. Elements can also be manually added or subtracted, and made smaller or larger depending on the needs of the model. Once the elements are in their desired position, faults with angle of dip and dip direction are added. After the faults are added, the software checks for completeness of the model by making sure that all nodes are assigned to an element and that no elements overlap. At this stage, the model is primarily spatial, consisting of nodes with latitude and longitude, elements and faults.

To build the physical aspects of the model, a second supporting application, called ORBDATA, is used. This application computes the structure of the lithosphere (thickness of the crust and upper mantle lithosphere) based on three assumptions and thee file inputs. The four assumptions (based on the guide provided by Dr. Bird, (http://element.ess.ucla.edu/guide) are: that the base of the lithosphere is an isothermal surface; heat conduction though the lithosphere is in steady state; all lithosphere is isostatic with respect to the mid-ocean ridges; and the crust and mantle lithosphere are approximated as laterally homogeneous. A parameter file containing various values of temperature, temperature gradient, conductivity, radioactivity and densities (see appendix C) is used in conjunction with two other files containing grids of topography/bathymetry and heat-flow (figures B1 and B2 respectively).

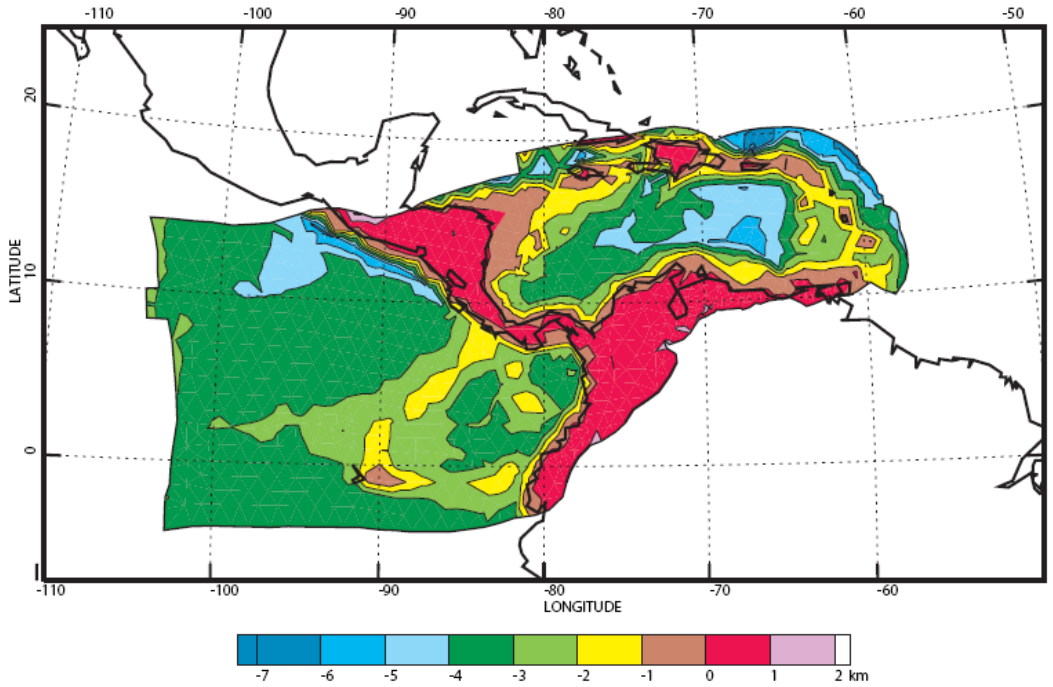

Figure B-1. Illustration of topographic and bathymetry data from ETOPO2v2 (National Geophysical Data Center, June 2006) that was used as input for model. The data was used at the maximum of 2 minute resolution.

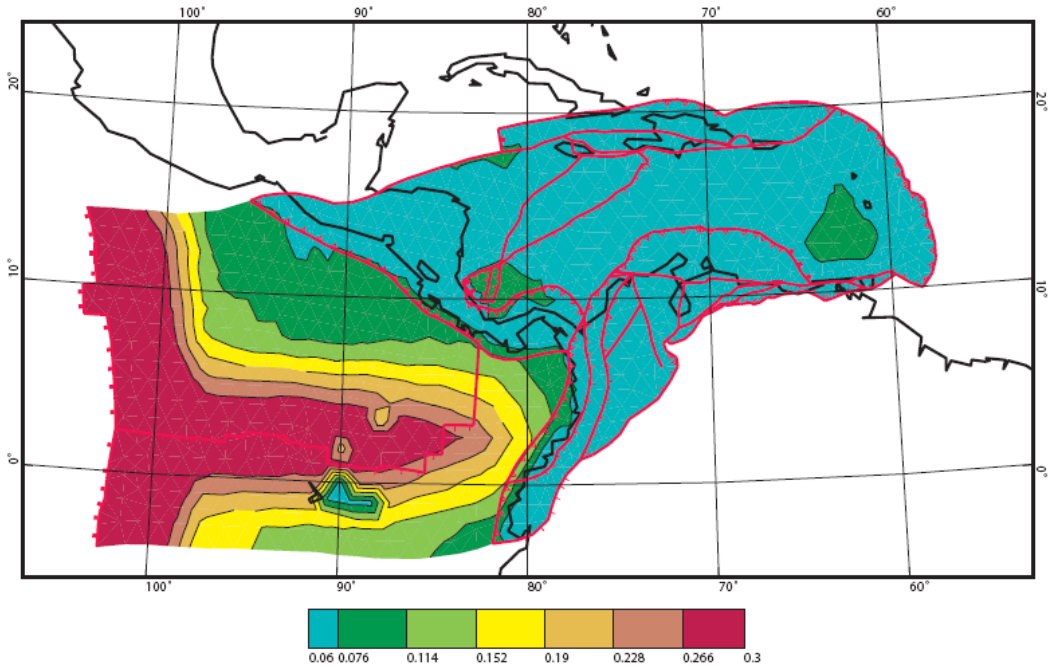

Figure B-2. Illustration of heat flow data that were used as input into all 3 models based on the 5 degree heat flow data in SI units of (W/m^2) of Pollack et al. (1993). The data along the ridges were truncated at 0.3 W/m^2 to prevent artifacts.

Through a personal communication with Dr. Peter Bird, the process by which ORBDATA computes the crust and lithosphere is as follows. The temperatures within the asthenosphere, which for practical purposes can be considered as the entire upper mantle below the base of the lithosphere, lie along an adiabat. For simplicity, the adiabatic gradient is approximated as constant, and is typically specified as 6.14E-4 K/m for most models. An intercept value, which represents an isothermal surface that forms the base of the lithosphere is also given, and is a parameter frequently modified during model testing. The intercept value along with the adiabatic gradient, determine the total lithosphere thickness. Temperature values along this linear adiabatic geotherm are used to compute the strength of coupling between the lithosphere and asthenosphere, relative to the assigned velocity of mantle flow at the base of the model, or basal boundary condition. Dr. Bird (personal communication) suggests that

intercept values much below 1412 K result in models such that the strength of coupling between the lithosphere and bottom boundary condition become so strong that that all plates essentially move together as driven by below. Additionally, values much above 1412 K reduce the coupling to such an extent that the bottom boundary condition has little effect in driving the plates.

The upper mantle thickness is found by assuming the base of the lithosphere to be an isothermal surface that marks the transition in the model between rigid and viscous behavior. The isotherm is arbitrarily determined at a depth of 100 km in a laterally homogeneous model based on the adiabatic gradient and intercept values described above. The depth of this isotherm becomes laterally varying depending on the surface heat-flow and crustal thickness as well as the contrast between crust and mantle thermal conductivities. The program iteratively adjusts the crust and upper mantle thicknesses relative to the isotherm in order to ensure that the model is isostatic.

Appendix C

EXAMPLE PARAMETER FILE

USED BY VARIOUS APPLICATIONS ASSOCIATED WITH SHELLS

```
1380K; 100MM MANTLE VELOCITY; FAULT 0.1; TAUMAX 2.0E12
0.1        FAULT     FRICTION COEFFICIENT     <*********** !
0.85       CONTINUUM FRICTION COEFFICIENT
1.00       BIOT COEFFICIENT (EFFICACY OF PORE PRESSURE)
0.00       BYERLY (0.-.99); FRACTIONAL STRENGTH REDUCTION OF MASTER FAULT
2.3E9,9.5E4  ACREEP (SHEAR STRESS COEFFICIENT OF CREEP LAW) <**** !
4000.,18314. BCREEP (ACTIVATION ENERGY/N/GAS-CONSTANT) (IN KELVIN) <** !
   0.,0.0171 CCREEP (DERIVITIVE OF BCREEP WITH RESPECT TO DEPTH; CRUST/MANTLE)
 5.E8,5.E8   DCREEP (MAXIMUM SHEAR STRESS; CRUST/MANTLE)
0.333333   ECREEP (EXPONENT ON STRAIN-RATE IN CREEP-STRESS LAWS)=(1/N)
1380.      6.1E-4 INTERCEPT AND SLOPE OF UPPER MANTLE ADIABAT (K, K/M)
400.E3     ZBASTH: DEPTH OF BASE OF ASTHENOSPHERE
SA         PLTREF: PLATE WHICH DEFINES VELOCITY REFERENCE FRAME (AF,EU, NA, ...)
 6  1.10   ICONVE:0=NONE;1=HAGER/O'CONNELL;2=BAUMGARDNER;3=NV1;4=CONTINENTAL NV1
1.E8       TRHMAX (LIMIT ON BASAL TRACTION)
2.0E+12    TAUMAX (DOWN-DIP INTEGRAL OF SUBDUCTION ZONE TRACTION)
1032.      RHOH2O (DENSITY OF WATER, AT P=0 AND T=SURFACE TEMPERATURE)
2889.,3332. RHOBAR (MEAN DENSITY AT P=0 AND T=0; CRUST/MANTLE)
3125.      RHOAST (DENSITY OF ASTHENOSPHERE, AT P=0 AND AMBIENT T)
9.8        GRAVITATIONAL ACCELERATION
1000.      ONE KILOMETER, EXPRESSED IN CURRENT LENGTH UNITS
6371000.   RADIUS OF THE PLANET
2.4E-5,3.94E-5 VOLUMETRIC THERMAL EXPANSION COEFFICIENT; CRUST/MANTLE
2.7,3.20   THERMAL CONDUCTIVITY; CRUST/MANTLE
3.5E-7,3.2E-8 RADIOACTIVE HEAT PRODUCTION, ON VOLUME (NOT MASS) BASIS
273.       SURFACE TEMPERATURE, IN KELVIN
1223.,1673. UPPER TEMPERATURE LIMITS, IN KELVIN; CRUST/MANTLE-LITHOSPHERE
100         MAXIMUM NUMBER OF ITERATIONS
0.0001     ACCEPTABLE CONVERGENCE LEVEL (FRACTIONAL VELOCITY CHANGE)
 50.E6     REFERENCE LEVEL OF SHEAR STRESS
1.00E-11   ACCEPTABLE LEVEL OF VELOCITY ERRORS (1 MM/A = 3.17E-11 M/S)
F          OUTPUT NODE VELOCITIES EVERY ITERATION? (FOR CONVERGENCE STUDIES)
===== POST-PROCESSING PLOT CONTROL PARAMETERS (NOT USED BY SHELLS) =====
       999 PLOTFILE # ON INPUT DATASET (OR 999 FOR LAST, OR 0 FOR ALL)
         F ---------------------- PLOT GRID OF ELEMENTS
         F     1000.    -2000.+1 PLOT ELEVATIONS
         F    10.E-3    80.E-3+1 PLOT HEAT-FLOW
         F     5.E+3          +1 PLOT CRUSTAL THICKNESS
         F    20.E+3    80.E+3-1 PLOT TOTAL LITHOSPHERE THICKNESS
         F                   +1 PLOT TEMPERATURE OF MOHO
         F                   +1 PLOT TEMPERATURE OF BASE OF PLATE
         F                   +1 PLOT NONLITHOSTATIC PRESSURE ANOMALY AT BASE
         F                   +1 PLOT VELOCITY VECTORS BELOW PLATE
         F                   +1 PLOT SHEAR TRACTION ON BASE OF PLATE
         T                   +1 PLOT SURFACE VELOCITY VECTORS
         F                   +1 PLOT VELOCITY CHANGES SINCE LAST TIME
         F                   +1 PLOT GREATEST PRIN. STRAIN RATE
         F ---------------------- PLOT HORIZONTAL-VELOCITY DISCONTINUITY
         F ---------------------- PLOT SLIP-RATE OF FAULTS
         F 3.169E-10   1.0E-15+1 PLOT CRUSTAL THICKENING RATE
         F                   +1 PLOT VERTICAL INTEGRAL OF STRESS ANOMALY
         F ---------------------- PLOT MOST COMPRESSIVE STRESS AXES
         F ---------------------- PLOT NET EXTERNAL FORCE ON NODES
         F    1.00            2 PLOT Log10[Viscosity Integral]&LIMITS(1 or 2)
        10 APPROXIMATE NUMBER OF CONTOURS IN EACH PLOT (FOR DEFAULT)
         1 COASTLINES? (0=NONE, 1=PRESENT, 2=USER DATA)
      12.  RMS LENGTH OF VECTORS AND SYMBOLS, IN DEGREES (12. OR 4.)
 60.      WIDTH OF MAP, IN DEGREES (.LE.360.), E.G., 360. OR 60.
  -80.,    0.    (LON,LAT) OF PLOT CENTER
         1 PEN WEIGHT FOR LIGHT LINES
         2 PEN WEIGHT FOR MEDIUM LINES
         3 PEN WEIGHT FOR HEAVY LINES
         T COLOR? (F GIVES BLACK-AND-WHITE)
```

Appendix D
TEST PARAMETER RESULTS
SORTED FROM LOWEST VELOCITY MISFIT TO HIGHEST VELOCITY MISFIT
WITH BOUNDARY CONDITIONS SET TO ZERO ALONG NA, SA, AND FREE AT NZ
("DNC" refers to models that did not converge)

RUN No.	TEMP K	TEMP ℃	VEL MM/YR	FRIC COEFF.	VEL MISFIT MM/YR	CAYMAN TROUGH SPREADING MISFIT	STRESS MISFIT °	MAT SUBDUCTION RATE	MAT SUBDUCTION ANGLE MISFIT
8	1323	1050	40	0.12	8.4	2.0	29.5	14.2	48.5
37	1373	1100	60	0.08	8.5	4.9	29.2	28.8	47.8
15	1323	1050	60	0.02	8.5	3.4	27.9	31.4	51.7
42	1373	1100	80	0.08	8.9	1.5	29.9	37.1	49.1
14	1323	1050	60	0.16	8.9	1.6	28.6	25.6	51.1
43	1373	1100	80	0.12	9.3	6.8	29.2	44.3	49.5
48	1373	1100	100	0.12	9.3	2.7	28.9	55.6	50.6
9	1323	1050	40	0.16	9.7	6.2	28.0	18.7	49.6
49	1373	1100	100	0.16	10.3	8.7	28.1	61.8	50.7
38	1373	1100	60	0.12	11.1	10.1	28.4	32.6	48.1
44	1373	1100	80	0.16	11.1	10.9	28.1	48.4	49.5
10	1323	1050	40	0.02	11.2	9.2	27.4	22.1	50.1
50	1373	1100	100	0.02	11.5	11.7	27.4	65.3	50.7
20	1323	1050	80	0.02	11.6	3.6	28.7	39.4	52.7
45	1373	1100	80	0.02	12.3	12.8	26.8	50.6	49.6
13	1323	1050	60	0.12	12.5	8.1	29.1	18.8	49.9
39	1373	1100	60	0.16	12.7	12.6	27.3	34.6	48.0
73	1423	1150	100	0.12	13.2	13.5	26.7	43.5	44.7
3	1323	1050	20	0.12	13.3	10.3	28.0	8.2	45.8
40	1373	1100	60	0.02	13.6	13.7	26.5	35.8	48.0
33	1373	1100	40	0.12	13.9	12.6	27.6	20.2	45.7
74	1423	1150	100	0.16	14.0	14.1	25.5	42.1	44.0
68	1423	1150	80	0.12	14.3	13.9	26.3	30.1	43.1
75	1423	1150	100	0.02	14.4	14.2	25.3	40.8	43.4
4	1323	1050	20	0.16	14.5	12.1	27.4	10.0	46.5
121	1523	1250	100	0.04	14.5	14.2	31.3	30.8	32.4
125	1523	1250	100	0.02	14.5	14.2	31.3	30.8	32.4
34	1373	1100	40	0.16	14.8	13.7	26.5	20.8	45.6
69	1423	1150	80	0.16	14.9	14.2	25.4	28.7	42.4
35	1373	1100	40	0.02	15.2	14.1	25.7	21.2	45.6
70	1423	1150	80	0.02	15.2	14.3	25.6	27.6	41.8
5	1323	1050	20	0.02	15.2	13.3	26.5	11.2	47.1
116	1523	1250	80	0.04	15.3	14.2	31.0	22.0	30.7
120	1523	1250	80	0.02	15.3	14.2	31.0	22.0	30.7
47	1373	1100	100	0.08	15.4	9.0	30.0	44.7	50.1
63	1423	1150	60	0.12	15.5	14.1	25.8	17.7	40.9
97	1473	1200	100	0.08	15.8	14.2	27.3	15.5	36.9
64	1423	1150	60	0.16	15.9	14.2	25.9	16.3	40.3
65	1423	1150	60	0.02	16.1	14.3	26.2	15.5	39.7
111	1523	1250	60	0.04	16.2	14.3	30.5	14.1	28.6
115	1523	1250	60	0.02	16.2	14.3	31.0	10.8	35.7

RUN No.	TEMP K	TEMP ℃	VEL MM/YR	FRIC COEFF.	VEL MISFIT MM/YR	CAYMAN TROUGH SPREADING MISFIT	STRESS MISFIT °	MAT SUBDUCTION RATE	MAT SUBDUCTION ANGLE MISFIT
92	1473	1200	80	0.08	16.4	14.2	27.2	8.9	35.2
28	1373	1100	20	0.12	16.4	14.0	26.0	7.7	41.1
19	1323	1050	80	0.16	16.5	10.8	28.5	31.4	52.0
58	1423	1150	40	0.12	16.6	14.2	26.1	7.3	37.9
98	1473	1200	100	0.12	16.7	14.3	26.9	7.1	37.0
29	1373	1100	20	0.16	16.7	14.2	25.8	7.5	40.9
59	1423	1150	40	0.16	16.9	14.3	26.3	6.1	37.4
87	1473	1200	60	0.08	16.9	14.3	26.8	4.3	33.3
106	1523	1250	40	0.04	16.9	14.3	30.0	7.5	25.8
110	1523	1250	40	0.02	16.9	14.3	30.0	7.5	25.8
99	1473	1200	100	0.16	17.0	14.3	26.5	4.9	36.5
60	1423	1150	40	0.02	17.0	14.3	26.2	5.7	36.9
93	1473	1200	80	0.12	17.0	14.3	26.6	3.5	36.0
100	1473	1200	100	0.02	17.1	14.3	26.4	4.1	35.9
94	1473	1200	80	0.16	17.2	14.3	26.5	2.1	35.5
95	1473	1200	80	0.02	17.3	14.3	26.2	1.6	34.8
88	1473	1200	60	0.12	17.3	14.3	26.5	1.4	34.4
122	1523	1250	100	0.08	17.4	14.3	27.4	1.0	49.1
82	1473	1200	40	0.08	17.4	14.3	26.9	1.3	31.0
89	1473	1200	60	0.16	17.5	14.3	26.4	0.7	33.8
117	1523	1250	80	0.08	17.5	14.3	27.4	0.5	48.5
53	1423	1150	20	0.12	17.5	14.3	26.1	1.1	33.4
123	1523	1250	100	0.12	17.6	14.3	27.8	0.2	33.1
101	1523	1250	20	0.04	17.6	14.3	30.4	2.7	21.2
105	1523	1250	20	0.02	17.6	14.3	30.4	2.7	21.2
54	1423	1150	20	0.16	17.6	14.3	26.0	0.6	33.0
83	1473	1200	40	0.12	17.6	14.3	27.1	0.4	32.2
124	1523	1250	100	0.16	17.6	14.3	27.8	0.1	34.2
55	1423	1150	20	0.02	17.6	14.3	26.1	0.5	32.5
112	1523	1250	60	0.08	17.6	14.3	27.2	0.2	30.4
118	1523	1250	80	0.12	17.6	14.3	27.8	0.1	34.2
119	1523	1250	80	0.16	17.6	14.3	27.8	0.0	35.4
84	1473	1200	40	0.16	17.6	14.3	27.1	0.2	32.6
85	1473	1200	40	0.02	17.7	14.3	27.0	0.1	32.6
77	1473	1200	20	0.08	17.7	14.3	27.0	0.2	29.8
113	1523	1250	60	0.12	17.7	14.3	27.6	0.0	35.8
107	1523	1250	40	0.08	17.7	14.3	26.6	0.1	31.8
114	1523	1250	60	0.16	17.7	14.3	27.6	0.0	34.9
78	1473	1200	20	0.12	17.8	14.3	27.1	0.0	34.5
79	1473	1200	20	0.16	17.8	14.3	27.0	0.0	33.5
80	1473	1200	20	0.02	17.8	14.3	27.0	0.0	32.9
108	1523	1250	40	0.12	17.8	14.3	26.4	0.0	32.6
109	1523	1250	40	0.16	17.8	14.3	26.1	0.0	31.3
102	1523	1250	20	0.08	17.8	14.3	26.4	0.0	27.6
103	1523	1250	20	0.12	17.9	14.3	25.9	0.0	25.5
104	1523	1250	20	0.16	17.9	14.3	25.6	0.0	24.7

RUN No.	TEMP K	TEMP ℃	VEL MM/YR	FRIC COEFF.	VEL MISFIT MM/YR	CAYMAN TROUGH SPREADING MISFIT	STRESS MISFIT °	MAT SUBDUCTION RATE	MAT SUBDUCTION ANGLE MISFIT
12	1323	1050	60	0.08	17.9	14.5	30.7	12.3	49.5
18	1323	1050	80	0.12	22.2	19.3	28.7	22.4	51.0
24	1323	1050	100	0.16	26.7	21.1	27.9	36.4	52.8
23	1323	1050	100	0.12	34.7	31.2	28.5	25.5	51.9
22	1323	1050	100	0.08	41.9	39.6	30.9	16.3	52.0
1	1323	1050	20	0.04	DNC				
2	1323	1050	20	0.08	DNC				
6	1323	1050	40	0.04	DNC				
7	1323	1050	40	0.08	DNC				
11	1323	1050	60	0.04	DNC				
16	1323	1050	80	0.04	DNC				
17	1323	1050	80	0.08	DNC				
21	1323	1050	100	0.04	DNC				
25	1323	1050	100	0.02	DNC				
26	1373	1100	20	0.04	DNC				
27	1373	1100	20	0.08	DNC				
30	1373	1100	20	0.02	DNC				
31	1373	1100	40	0.04	DNC				
32	1373	1100	40	0.08	DNC				
36	1373	1100	60	0.04	DNC				
41	1373	1100	80	0.04	DNC				
46	1373	1100	100	0.04	DNC				
51	1423	1150	20	0.04	DNC				
52	1423	1150	20	0.08	DNC				
56	1423	1150	40	0.04	DNC				
57	1423	1150	40	0.08	DNC				
61	1423	1150	60	0.04	DNC				
62	1423	1150	60	0.08	DNC				
66	1423	1150	80	0.04	DNC				
67	1423	1150	80	0.08	DNC				
71	1423	1150	100	0.04	DNC				
72	1423	1150	100	0.08	DNC				
76	1473	1200	20	0.04	DNC				
81	1473	1200	40	0.04	DNC				
86	1473	1200	60	0.04	DNC				
90	1473	1200	60	0.02	DNC				
91	1473	1200	80	0.04	DNC				
96	1473	1200	100	0.04	DNC				

Appendix E
UNSORTED TEST PARAMETER RESULTS FOR MODEL
WITH BOUNDARY CONDITIONS SET TO ZERO ALONG NA, SA AND FREE AT NZ
("DNC" refers to models that did not converge)

RUN No.	TEMP K	TEMP ℃	VEL MM/YR	FRIC COEFF.	VEL MISFIT MM/YR	CAYMAN TROUGH SPREADING MISFIT	STRESS MISFIT °	MAT SUBDUCTION RATE	MAT SUBDUCTION ANGLE MISFIT
1	1323	1050	20	0.04	DNC				
2	1323	1050	20	0.08	DNC				
3	1323	1050	20	0.12	13.3	10.3	28.0	8.2	45.8
4	1323	1050	20	0.16	14.5	12.1	27.4	10.0	46.5
5	1323	1050	20	0.02	15.2	13.3	26.5	11.2	47.1
6	1323	1050	40	0.04	DNC				
7	1323	1050	40	0.08	DNC				
8	1323	1050	40	0.12	8.4	2.0	29.5	14.2	48.5
9	1323	1050	40	0.16	9.7	6.2	28.0	18.7	49.6
10	1323	1050	40	0.02	11.2	9.2	27.4	22.1	50.1
11	1323	1050	60	0.04	DNC				
12	1323	1050	60	0.08	17.9	14.5	30.7	12.3	49.5
13	1323	1050	60	0.12	12.5	8.1	29.1	18.8	49.9
14	1323	1050	60	0.16	8.9	1.6	28.6	25.6	51.1
15	1323	1050	60	0.02	8.5	3.4	27.9	31.4	51.7
16	1323	1050	80	0.04	DNC				
17	1323	1050	80	0.08	DNC				
18	1323	1050	80	0.12	22.2	19.3	28.7	22.4	51.0
19	1323	1050	80	0.16	16.5	10.8	28.5	31.4	52.0
20	1323	1050	80	0.02	11.6	3.6	28.7	39.4	52.7
21	1323	1050	100	0.04	DNC				
22	1323	1050	100	0.08	41.9	39.6	30.9	16.3	52.0
23	1323	1050	100	0.12	34.7	31.2	28.5	25.5	51.9
24	1323	1050	100	0.16	26.7	21.1	27.9	36.4	52.8
25	1323	1050	100	0.02	DNC				
26	1373	1100	20	0.04	DNC				
27	1373	1100	20	0.08	DNC				
28	1373	1100	20	0.12	16.4	14.0	26.0	7.7	41.1
29	1373	1100	20	0.16	16.7	14.2	25.8	7.5	40.9
30	1373	1100	20	0.02	DNC				
31	1373	1100	40	0.04	DNC				
32	1373	1100	40	0.08	DNC				
33	1373	1100	40	0.12	13.9	12.6	27.6	20.2	45.7
34	1373	1100	40	0.16	14.8	13.7	26.5	20.8	45.6
35	1373	1100	40	0.02	15.2	14.1	25.7	21.2	45.6
36	1373	1100	60	0.04	DNC				
37	1373	1100	60	0.08	8.5	4.9	29.2	28.8	47.8
38	1373	1100	60	0.12	11.1	10.1	28.4	32.6	48.1
39	1373	1100	60	0.16	12.7	12.6	27.3	34.6	48.0
40	1373	1100	60	0.02	13.6	13.7	26.5	35.8	48.0
41	1373	1100	80	0.04	DNC				

RUN No.	TEMP K	TEMP ℃	VEL MM/YR	FRIC COEFF.	VEL MISFIT MM/YR	CAYMAN TROUGH SPREADING MISFIT	STRESS MISFIT °	MAT SUBDUCTION RATE	MAT SUBDUCTION ANGLE MISFIT
42	1373	1100	80	0.08	8.9	1.5	29.9	37.1	49.1
43	1373	1100	80	0.12	9.3	6.8	29.2	44.3	49.5
44	1373	1100	80	0.16	11.1	10.9	28.1	48.4	49.5
45	1373	1100	80	0.02	12.3	12.8	26.8	50.6	49.6
46	1373	1100	100	0.04	DNC				
47	1373	1100	100	0.08	15.4	9.0	30.0	44.7	50.1
48	1373	1100	100	0.12	9.3	2.7	28.9	55.6	50.6
49	1373	1100	100	0.16	10.3	8.7	28.1	61.8	50.7
50	1373	1100	100	0.02	11.5	11.7	27.4	65.3	50.7
51	1423	1150	20	0.04	DNC				
52	1423	1150	20	0.08	DNC				
53	1423	1150	20	0.12	17.5	14.3	26.1	1.1	33.4
54	1423	1150	20	0.16	17.6	14.3	26.0	0.6	33.0
55	1423	1150	20	0.02	17.6	14.3	26.1	0.5	32.5
56	1423	1150	40	0.04	DNC				
57	1423	1150	40	0.08	DNC				
58	1423	1150	40	0.12	16.6	14.2	26.1	7.3	37.9
59	1423	1150	40	0.16	16.9	14.3	26.3	6.1	37.4
60	1423	1150	40	0.02	17.0	14.3	26.2	5.7	36.9
61	1423	1150	60	0.04	DNC				
62	1423	1150	60	0.08	DNC				
63	1423	1150	60	0.12	15.5	14.1	25.8	17.7	40.9
64	1423	1150	60	0.16	15.9	14.2	25.9	16.3	40.3
65	1423	1150	60	0.02	16.1	14.3	26.2	15.5	39.7
66	1423	1150	80	0.04	DNC				
67	1423	1150	80	0.08	DNC				
68	1423	1150	80	0.12	14.3	13.9	26.3	30.1	43.1
69	1423	1150	80	0.16	14.9	14.2	25.4	28.7	42.4
70	1423	1150	80	0.02	15.2	14.3	25.6	27.6	41.8
71	1423	1150	100	0.04	DNC				
72	1423	1150	100	0.08	DNC				
73	1423	1150	100	0.12	13.2	13.5	26.7	43.5	44.7
74	1423	1150	100	0.16	14.0	14.1	25.5	42.1	44.0
75	1423	1150	100	0.02	14.4	14.2	25.3	40.8	43.4
76	1473	1200	20	0.04	DNC				
77	1473	1200	20	0.08	17.7	14.3	27.0	0.2	29.8
78	1473	1200	20	0.12	17.8	14.3	27.1	0.0	34.5
79	1473	1200	20	0.16	17.8	14.3	27.0	0.0	33.5
80	1473	1200	20	0.02	17.8	14.3	27.0	0.0	32.9
81	1473	1200	40	0.04	DNC				
82	1473	1200	40	0.08	17.4	14.3	26.9	1.3	31.0
83	1473	1200	40	0.12	17.6	14.3	27.1	0.4	32.2
84	1473	1200	40	0.16	17.6	14.3	27.1	0.2	32.6
85	1473	1200	40	0.02	17.7	14.3	27.0	0.1	32.6
86	1473	1200	60	0.04	DNC				

RUN No.	TEMP K	TEMP ℃	VEL MM/YR	FRIC COEFF.	VEL MISFIT MM/YR	CAYMAN TROUGH SPREADING MISFIT	STRESS MISFIT °	MAT SUBDUCTION RATE	MAT SUBDUCTION ANGLE MISFIT
87	1473	1200	60	0.08	16.9	14.3	26.8	4.3	33.3
88	1473	1200	60	0.12	17.3	14.3	26.5	1.4	34.4
89	1473	1200	60	0.16	17.5	14.3	26.4	0.7	33.8
90	1473	1200	60	0.02	DNC				
91	1473	1200	80	0.04	DNC				
92	1473	1200	80	0.08	16.4	14.2	27.2	8.9	35.2
93	1473	1200	80	0.12	17.0	14.3	26.6	3.5	36.0
94	1473	1200	80	0.16	17.2	14.3	26.5	2.1	35.5
95	1473	1200	80	0.02	17.3	14.3	26.2	1.6	34.8
96	1473	1200	100	0.04	DNC				
97	1473	1200	100	0.08	15.8	14.2	27.3	15.5	36.9
98	1473	1200	100	0.12	16.7	14.3	26.9	7.1	37.0
99	1473	1200	100	0.16	17.0	14.3	26.5	4.9	36.5
100	1473	1200	100	0.02	17.1	14.3	26.4	4.1	35.9
101	1523	1250	20	0.04	17.6	14.3	30.4	2.7	21.2
102	1523	1250	20	0.08	17.8	14.3	26.4	0.0	27.6
103	1523	1250	20	0.12	17.9	14.3	25.9	0.0	25.5
104	1523	1250	20	0.16	17.9	14.3	25.6	0.0	24.7
105	1523	1250	20	0.02	17.6	14.3	30.4	2.7	21.2
106	1523	1250	40	0.04	16.9	14.3	30.0	7.5	25.8
107	1523	1250	40	0.08	17.7	14.3	26.6	0.1	31.8
108	1523	1250	40	0.12	17.8	14.3	26.4	0.0	32.6
109	1523	1250	40	0.16	17.8	14.3	26.1	0.0	31.3
110	1523	1250	40	0.02	16.9	14.3	30.0	7.5	25.8
111	1523	1250	60	0.04	16.2	14.3	30.5	14.1	28.6
112	1523	1250	60	0.08	17.6	14.3	27.2	0.2	30.4
113	1523	1250	60	0.12	17.7	14.3	27.6	0.0	35.8
114	1523	1250	60	0.16	17.7	14.3	27.6	0.0	34.9
115	1523	1250	60	0.02	16.2	14.3	31.0	10.8	35.7
116	1523	1250	80	0.04	15.3	14.2	31.0	22.0	30.7
117	1523	1250	80	0.08	17.5	14.3	27.4	0.5	48.5
118	1523	1250	80	0.12	17.6	14.3	27.8	0.1	34.2
119	1523	1250	80	0.16	17.6	14.3	27.8	0.0	35.4
120	1523	1250	80	0.02	15.3	14.2	31.0	22.0	30.7
121	1523	1250	100	0.04	14.5	14.2	31.3	30.8	32.4
122	1523	1250	100	0.08	17.4	14.3	27.4	1.0	49.1
123	1523	1250	100	0.12	17.6	14.3	27.8	0.2	33.1
124	1523	1250	100	0.16	17.6	14.3	27.8	0.1	34.2
125	1523	1250	100	0.02	14.5	14.2	31.3	30.8	32.4

Appendix F
TEST PARAMETER RESULTS
SORTED FROM LOWEST VELOCITY MISFIT TO HIGHEST VELOCITY MISFIT
WITH NA AND NZ BOUNDARY CONDITIONS SET RELATIVE TO SA
("DNC" refers to models that did not converge)

RUN No.	TEMP K	TEMP ℃	VEL MM/YR	FRIC COEFF.	VEL MISFIT MM/YR	CAYMAN TROUGH SPREADING MISFIT	STRESS MISFIT °	MAT SUBDUCTION RATE	MAT SUBDUCTION ANGLE MISFIT
139	1323	1050	60	0.16	8.7	0.1	37.5	30.9	43.4
132	1323	1050	40	0.08	8.7	2.9	40.1	14.0	32.7
167	1373	1100	80	0.08	8.9	0.9	35.8	40.0	43.3
162	1373	1100	60	0.08	9.0	5.6	36.0	33.0	40.9
140	1323	1050	60	0.20	9.2	5.6	30.4	36.8	45.0
173	1373	1100	100	0.12	9.2	4.3	31.3	58.1	46.0
168	1373	1100	80	0.12	10.0	8.1	29.0	47.8	44.6
145	1323	1050	80	0.20	10.2	1.2	32.9	44.7	47.0
134	1323	1050	40	0.16	10.5	8.0	31.5	24.4	40.0
174	1373	1100	100	0.16	11.1	10.6	28.7	64.7	46.5
127	1323	1050	20	0.08	11.9	8.7	39.2	11.4	24.1
163	1373	1100	60	0.12	12.0	11.4	29.6	37.2	41.9
135	1323	1050	40	0.20	12.3	11.3	30.5	27.6	41.3
138	1323	1050	60	0.12	12.3	7.6	36.7	23.4	40.9
157	1373	1100	40	0.08	12.3	10.8	31.8	23.9	36.8
169	1373	1100	80	0.16	12.3	12.4	27.7	52.1	45.0
175	1373	1100	100	0.20	12.5	13.2	27.7	67.7	46.8
170	1373	1100	80	0.20	13.3	13.9	27.1	53.7	45.2
198	1423	1150	100	0.12	13.6	14.0	27.5	45.3	40.4
164	1373	1100	60	0.16	13.7	13.7	28.2	39.3	42.2
246	1523	1250	100	0.04	13.7	14.2	33.0	37.1	28.4
250	1523	1250	100	0.20	13.7	14.3	33.0	37.1	28.4
128	1323	1050	20	0.12	13.9	11.8	31.6	13.9	29.1
172	1373	1100	100	0.08	14.0	8.2	35.1	46.9	44.5
199	1423	1150	100	0.16	14.1	14.2	28.3	44.7	40.0
165	1373	1100	60	0.20	14.2	14.2	28.5	39.9	42.3
241	1523	1250	80	0.04	14.2	14.3	33.5	30.8	26.6
245	1523	1250	80	0.20	14.2	14.3	33.5	30.8	26.6
193	1423	1150	80	0.12	14.3	14.1	26.5	35.2	38.0
200	1423	1150	100	0.20	14.3	14.3	29.0	44.6	39.6
158	1373	1100	40	0.12	14.4	13.6	29.0	24.9	37.5
194	1423	1150	80	0.16	14.7	14.2	27.4	34.7	37.5
195	1423	1150	80	0.20	14.9	14.3	27.9	34.8	37.1
236	1523	1250	60	0.04	14.9	14.3	36.0	24.1	24.3
240	1523	1250	60	0.20	14.9	14.3	36.0	24.1	24.3
144	1323	1050	80	0.16	15.0	9.5	35.3	36.4	45.5
159	1373	1100	40	0.16	15.0	14.2	30.4	25.3	37.7
222	1473	1200	100	0.08	15.0	14.2	29.5	21.5	31.8
129	1323	1050	20	0.16	15.2	13.6	29.7	15.5	31.1
160	1373	1100	40	0.20	15.2	14.2	31.0	25.4	37.6
188	1423	1150	60	0.12	15.2	14.2	31.1	24.0	35.0
189	1423	1150	60	0.16	15.5	14.3	32.0	23.1	34.5
152	1373	1100	20	0.08	15.6	14.0	30.3	13.4	27.3
190	1423	1150	60	0.20	15.6	14.3	32.4	23.5	34.0
231	1523	1250	40	0.04	15.6	14.3	38.8	17.6	20.8
235	1523	1250	40	0.20	15.6	14.3	38.8	17.6	20.8

RUN No.	TEMP K	TEMP ℃	VEL MM/YR	FRIC COEFF.	VEL MISFIT MM/YR	CAYMAN TROUGH SPREADING MISFIT	STRESS MISFIT °	MAT SUBDUCTION RATE	MAT SUBDUCTION ANGLE MISFIT
130	1323	1050	20	0.20	15.6	14.1	30.0	16.0	238.3
217	1473	1200	80	0.08	15.7	14.3	30.0	14.5	29.8
153	1373	1100	20	0.12	16.0	14.2	32.5	12.5	27.8
223	1473	1200	100	0.12	16.0	14.3	31.1	12.5	31.5
183	1423	1150	40	0.12	16.1	14.2	32.6	13.4	30.5
154	1373	1100	20	0.16	16.2	14.2	33.0	12.3	27.8
155	1373	1100	20	0.20	16.3	14.2	33.0	12.3	27.5
184	1423	1150	40	0.16	16.3	14.3	33.4	12.4	30.0
212	1473	1200	60	0.08	16.3	14.3	33.0	8.5	27.1
224	1473	1200	100	0.16	16.3	14.3	31.5	11.3	31.0
185	1423	1150	40	0.20	16.4	14.3	33.8	12.4	29.4
225	1473	1200	100	0.20	16.4	14.3	31.4	11.3	30.1
226	1523	1250	20	0.04	16.4	14.3	42.8	11.0	14.4
230	1523	1250	20	0.20	16.4	14.3	42.8	11.0	14.4
150	1323	1050	100	0.20	16.5	9.1	34.2	52.4	48.5
218	1473	1200	80	0.12	16.5	14.3	30.6	7.6	29.9
219	1473	1200	80	0.16	16.7	14.3	30.3	6.3	29.4
178	1423	1150	20	0.12	16.8	14.3	35.5	6.1	22.0
207	1473	1200	40	0.08	16.8	14.3	34.7	4.2	23.3
213	1473	1200	60	0.12	16.8	14.3	34.4	4.2	27.8
220	1473	1200	80	0.20	16.8	14.3	31.6	6.6	28.4
247	1523	1250	100	0.08	16.8	14.3	32.7	2.5	23.9
179	1423	1150	20	0.16	17.0	14.3	37.1	5.6	21.1
180	1423	1150	20	0.20	17.0	14.3	37.9	5.4	19.8
202	1473	1200	20	0.08	17.0	14.3	37.0	2.8	17.3
208	1473	1200	40	0.12	17.0	14.3	36.6	2.1	24.1
209	1473	1200	40	0.16	17.0	14.3	38.5	1.8	23.0
214	1473	1200	60	0.16	17.0	14.3	35.5	3.4	27.2
215	1473	1200	60	0.20	17.0	14.3	36.6	3.2	25.8
237	1523	1250	60	0.08	17.0	14.3	35.7	1.0	20.8
242	1523	1250	80	0.08	17.0	14.3	32.2	1.7	22.5
248	1523	1250	100	0.12	17.0	14.3	33.5	0.9	25.7
210	1473	1200	40	0.20	17.1	14.3	40.0	1.8	21.1
232	1523	1250	40	0.08	17.1	14.3	40.8	0.5	18.4
243	1523	1250	80	0.12	17.1	14.3	36.5	0.6	24.3
203	1473	1200	20	0.12	17.2	14.3	44.0	1.8	16.6
204	1473	1200	20	0.16	17.2	14.3	46.0	1.7	14.5
205	1473	1200	20	0.20	17.2	14.3	46.5	1.8	12.6
227	1523	1250	20	0.08	17.2	14.3	46.7	0.3	13.6
233	1523	1250	40	0.12	17.2	14.3	45.7	0.1	19.3
238	1523	1250	60	0.12	17.2	14.3	43.8	0.3	22.3
239	1523	1250	60	0.16	17.2	14.3	44.0	0.3	20.4
244	1523	1250	80	0.16	17.2	14.3	40.5	0.5	22.9
249	1523	1250	100	0.16	17.2	14.3	37.0	0.7	24.7
228	1523	1250	20	0.12	17.3	14.3	49.2	0.2	11.6
229	1523	1250	20	0.16	17.3	14.3	50.4	0.2	8.9
234	1523	1250	40	0.16	17.3	14.3	47.0	0.1	17.1
137	1323	1050	60	0.08	17.7	15.6	38.5	16.1	37.4
143	1323	1050	80	0.12	22.0	19.2	32.8	26.9	43.4
149	1323	1050	100	0.16	24.0	19.6	34.2	42.0	47.2
142	1323	1050	80	0.08	29.0	28.4	34.7	18.1	40.8

RUN No.	TEMP K	TEMP ℃	VEL MM/YR	FRIC COEFF.	VEL MISFIT MM/YR	CAYMAN TROUGH SPREADING MISFIT	STRESS MISFIT °	MAT SUBDUCTION RATE	MAT SUBDUCTION ANGLE MISFIT
148	1323	1050	100	0.12	33.1	31.2	33.3	30.4	45.4
147	1323	1050	100	0.08	41.6	41.4	36.3	19.9	43.2
126	1323	1050	20	0.04	DNC				
131	1323	1050	40	0.04	DNC				
133	1323	1050	40	0.12	DNC				
136	1323	1050	60	0.04	DNC				
141	1323	1050	80	0.04	DNC				
146	1323	1050	100	0.04	DNC				
151	1373	1100	20	0.04	DNC				
156	1373	1100	40	0.04	DNC				
161	1373	1100	60	0.04	DNC				
166	1373	1100	80	0.04	DNC				
171	1373	1100	100	0.04	DNC				
176	1423	1150	20	0.04	DNC				
177	1423	1150	20	0.08	DNC				
181	1423	1150	40	0.04	DNC				
182	1423	1150	40	0.08	DNC				
186	1423	1150	60	0.04	DNC				
187	1423	1150	60	0.08	DNC				
191	1423	1150	80	0.04	DNC				
192	1423	1150	80	0.08	DNC				
196	1423	1150	100	0.04	DNC				
197	1423	1150	100	0.08	DNC				
201	1473	1200	20	0.04	DNC				
206	1473	1200	40	0.04	DNC				
211	1473	1200	60	0.04	DNC				
216	1473	1200	80	0.04	DNC				
221	1473	1200	100	0.04	DNC				

Appendix G
TEST PARAMETER RESULTS
UNSORTED FOR MODEL WITH NA AND NZ BOUNDARY CONDITIONS
SET RELATIVE TO SA
("DNC" refers to models that did not converge)

RUN No.	TEMP K	TEMP ℃	VEL MM/YR	FRIC COEFF.	VEL MISFIT MM/YR	CAYMAN TROUGH SPREADING MISFIT	STRESS MISFIT °	MAT SUBDUCTION RATE	MAT SUBDUCTION ANGLE MISFIT
126	1323	1050	20	0.04	DNC				
127	1323	1050	20	0.08	11.9	8.7	39.2	11.4	24.1
128	1323	1050	20	0.12	13.9	11.8	31.6	13.9	29.1
129	1323	1050	20	0.16	15.2	13.6	29.7	15.5	31.1
130	1323	1050	20	0.20	15.6	14.1	30.0	16.0	31.7
131	1323	1050	40	0.04	DNC				
132	1323	1050	40	0.08	8.7	2.9	40.1	14.0	32.7
133	1323	1050	40	0.12	DNC				
134	1323	1050	40	0.16	10.5	8.0	31.5	24.4	40.0
135	1323	1050	40	0.20	12.3	11.3	30.5	27.6	41.3
136	1323	1050	60	0.04	DNC				
137	1323	1050	60	0.08	17.7	15.6	38.5	16.1	37.4
138	1323	1050	60	0.12	12.3	7.6	36.7	23.4	40.9
139	1323	1050	60	0.16	8.7	0.1	37.5	30.9	43.4
140	1323	1050	60	0.20	9.2	5.6	30.4	36.8	45.5
141	1323	1050	80	0.04	DNC				
142	1323	1050	80	0.08	29.0	28.4	34.7	18.1	40.8
143	1323	1050	80	0.12	22.0	19.2	32.8	26.9	43.4
144	1323	1050	80	0.16	15.0	9.5	35.3	36.4	45.0
145	1323	1050	80	0.20	10.2	1.2	32.9	44.7	47.0
146	1323	1050	100	0.04	DNC				
147	1323	1050	100	0.08	41.6	41.4	36.3	19.9	43.2
148	1323	1050	100	0.12	33.1	31.2	33.3	30.4	45.4
149	1323	1050	100	0.16	24.0	19.6	34.2	42.0	47.2
150	1323	1050	100	0.20	16.5	9.1	34.2	52.4	48.5
151	1373	1100	20	0.04	DNC				
152	1373	1100	20	0.08	15.6	14.0	30.3	13.4	27.3
153	1373	1100	20	0.12	16.0	14.2	32.5	12.5	27.8
154	1373	1100	20	0.16	16.2	14.2	33.0	12.3	27.8
155	1373	1100	20	0.20	16.3	14.2	33.0	12.3	27.5
156	1373	1100	40	0.04	DNC				
157	1373	1100	40	0.08	12.3	10.8	31.8	23.9	36.8
158	1373	1100	40	0.12	14.4	13.6	29.0	24.9	37.5
159	1373	1100	40	0.16	15.0	14.2	30.4	25.3	37.7
160	1373	1100	40	0.20	15.2	14.2	31.0	25.4	37.6
161	1373	1100	60	0.04	DNC				
162	1373	1100	60	0.08	9.0	5.6	36.0	33.0	40.9
163	1373	1100	60	0.12	12.0	11.4	29.6	37.2	41.9
164	1373	1100	60	0.16	13.7	13.7	28.2	39.3	42.2
165	1373	1100	60	0.20	14.2	14.2	28.5	39.9	42.3
166	1373	1100	80	0.04	DNC				
167	1373	1100	80	0.08	8.9	0.9	35.8	40.0	43.3
168	1373	1100	80	0.12	10.0	8.1	29.0	47.8	44.6
169	1373	1100	80	0.16	12.3	12.4	27.7	52.1	45.0
170	1373	1100	80	0.20	13.3	13.9	27.1	53.7	45.2
171	1373	1100	100	0.04	DNC				

RUN No.	TEMP K	TEMP ℃	VEL MM/YR	FRIC COEFF.	VEL MISFIT MM/YR	CAYMAN TROUGH SPREADING MISFIT	STRESS MISFIT °	MAT SUBDUCTION RATE	MAT SUBDUCTION ANGLE MISFIT
172	1373	1100	100	0.08	14.0	8.2	35.1	46.9	44.5
173	1373	1100	100	0.12	9.2	4.3	31.3	58.1	46.0
174	1373	1100	100	0.16	11.1	10.6	28.7	64.7	46.5
175	1373	1100	100	0.20	12.5	13.2	27.7	67.7	46.8
176	1423	1150	20	0.04	DNC				
177	1423	1150	20	0.08	DNC				
178	1423	1150	20	0.12	16.8	14.3	35.5	6.1	22.0
179	1423	1150	20	0.16	17.0	14.3	37.1	5.6	21.1
180	1423	1150	20	0.20	17.0	14.3	37.9	5.4	19.8
181	1423	1150	40	0.04	DNC				
182	1423	1150	40	0.08	DNC				
183	1423	1150	40	0.12	16.1	14.2	32.6	13.4	30.5
184	1423	1150	40	0.16	16.3	14.3	33.4	12.4	30.0
185	1423	1150	40	0.20	16.4	14.3	33.8	12.4	29.4
186	1423	1150	60	0.04	DNC				
187	1423	1150	60	0.08	DNC				
188	1423	1150	60	0.12	15.2	14.2	31.1	24.0	35.0
189	1423	1150	60	0.16	15.5	14.3	32.0	23.1	34.5
190	1423	1150	60	0.20	15.6	14.3	32.4	23.5	34.0
191	1423	1150	80	0.04	DNC				
192	1423	1150	80	0.08	DNC				
193	1423	1150	80	0.12	14.3	14.1	26.5	35.2	38.0
194	1423	1150	80	0.16	14.7	14.2	27.4	34.7	37.5
195	1423	1150	80	0.20	14.9	14.3	27.9	34.8	37.1
196	1423	1150	100	0.04	DNC				
197	1423	1150	100	0.08	DNC				
198	1423	1150	100	0.12	13.6	14.0	27.5	45.3	40.4
199	1423	1150	100	0.16	14.1	14.2	28.3	44.7	40.0
200	1423	1150	100	0.20	14.3	14.3	29.0	44.6	39.6
201	1473	1200	20	0.04	DNC				
202	1473	1200	20	0.08	17.0	14.3	37.0	2.8	17.3
203	1473	1200	20	0.12	17.2	14.3	44.0	1.8	16.6
204	1473	1200	20	0.16	17.2	14.3	46.0	1.7	14.5
205	1473	1200	20	0.20	17.2	14.3	46.5	1.8	12.6
206	1473	1200	40	0.04	DNC				
207	1473	1200	40	0.08	16.8	14.3	34.7	4.2	23.3
208	1473	1200	40	0.12	17.0	14.3	36.6	2.1	24.1
209	1473	1200	40	0.16	17.0	14.3	38.5	1.8	23.0
210	1473	1200	40	0.20	17.1	14.3	40.0	1.8	21.1
211	1473	1200	60	0.04	DNC				
212	1473	1200	60	0.08	16.3	14.3	33.0	8.5	27.1
213	1473	1200	60	0.12	16.8	14.3	34.4	4.2	27.8
214	1473	1200	60	0.16	17.0	14.3	35.5	3.4	27.2
215	1473	1200	60	0.20	17.0	14.3	36.6	3.2	25.8
216	1473	1200	80	0.04	DNC				
217	1473	1200	80	0.08	15.7	14.3	30.0	14.5	29.8
218	1473	1200	80	0.12	16.5	14.3	30.6	7.6	29.9
219	1473	1200	80	0.16	16.7	14.3	30.3	6.3	29.4
220	1473	1200	80	0.20	16.8	14.3	31.6	6.6	28.4
221	1473	1200	100	0.04	DNC				
222	1473	1200	100	0.08	15.0	14.2	29.5	21.5	31.8

RUN No.	TEMP K	TEMP ℃	VEL MM/YR	FRIC COEFF.	VEL MISFIT MM/YR	CAYMAN TROUGH SPREADING MISFIT	STRESS MISFIT °	MAT SUBDUCTION RATE	MAT SUBDUCTION ANGLE MISFIT
223	1473	1200	100	0.12	16.0	14.3	31.1	12.5	31.5
224	1473	1200	100	0.16	16.3	14.3	31.5	11.3	31.0
225	1473	1200	100	0.20	16.4	14.3	31.4	11.3	30.1
226	1523	1250	20	0.04	16.4	14.3	42.8	11.0	14.4
227	1523	1250	20	0.08	17.2	14.3	46.7	0.3	13.6
228	1523	1250	20	0.12	17.3	14.3	49.2	0.2	11.6
229	1523	1250	20	0.16	17.3	14.3	50.4	0.2	8.9
230	1523	1250	20	0.20	16.4	14.3	42.8	11.0	14.4
231	1523	1250	40	0.04	15.6	14.3	38.8	17.6	20.8
232	1523	1250	40	0.08	17.1	14.3	40.8	0.5	18.4
233	1523	1250	40	0.12	17.2	14.3	45.7	0.1	19.3
234	1523	1250	40	0.16	17.3	14.3	47.0	0.1	17.1
235	1523	1250	40	0.20	15.6	14.3	38.8	17.6	20.8
236	1523	1250	60	0.04	14.9	14.3	36.0	24.1	24.3
237	1523	1250	60	0.08	17.0	14.3	35.7	1.0	20.8
238	1523	1250	60	0.12	17.2	14.3	43.8	0.3	22.3
239	1523	1250	60	0.16	17.2	14.3	44.0	0.3	20.4
240	1523	1250	60	0.20	14.9	14.3	36.0	24.1	24.3
241	1523	1250	80	0.04	14.2	14.3	33.5	30.8	26.6
242	1523	1250	80	0.08	17.0	14.3	32.2	1.7	22.5
243	1523	1250	80	0.12	17.1	14.3	36.5	0.6	24.3
244	1523	1250	80	0.16	17.2	14.3	40.5	0.5	22.9
245	1523	1250	80	0.20	14.2	14.3	33.5	30.8	26.6
246	1523	1250	100	0.04	13.7	14.2	33.0	37.1	28.4
247	1523	1250	100	0.08	16.8	14.3	32.7	2.5	23.9
248	1523	1250	100	0.12	17.0	14.3	33.5	0.9	25.7
249	1523	1250	100	0.16	17.2	14.3	37.0	0.7	24.7
250	1523	1250	100	0.20	13.7	14.3	33.0	37.1	28.4